NEAR INFRARED SPECTROSCOPY: A STUDY OF CEREBRAL HEMODYNAMICS DURING BREATHHOLDING AND DEVELOPMENT OF A SYSTEM FOR HOTFLASH MEASUREMENT

by

VIKRANT SHARMA

Presented to the Faculty of the Graduate School of

The University of Texas at Arlington in Partial Fulfillment

of the Requirements

for the Degree of

MASTERS OF SCIENCE IN BIOMEDICAL ENGINEERING

THE UNIVERSITY OF TEXAS AT ARLINGTON

August 2005

ACKNOWLEDGEMENTS

I take this opportunity to acknowledge all the people who helped me through the course of my thesis.

First, I express my sincere gratitude to Dr. Hanli Liu for acknowledging my skill and providing me the opportunity to work on this project. She has been a source of constant inspiration for me.

I would also like to thank Dr. Anna Ratka for helping me with all the reading materials and giving me all the information and support that was required. I also express my thanks to Dr. Digant Dave for accepting to be a committee member.

I would like to thank all my lab members especially Raghavendra Ranga and Jae Kim for their suggestions and cooperation from time to time during the project.

Finally, I would like to thank my parents who have been a constant support and inspiration at all times. It is because of their love and encouragement that I have reached this stage.

July 25, 2005

ABSTRACT

NEAR INFRARED SPECTROSCOPY: A STUDY OF CEREBRAL HEMODYNAMICS DURING BREATHHOLDING AND DEVELOPMENT OF A SYSTEM FOR HOTFLASH MEASUREMENT

Publication No. _____

Vikrant Sharma, M.S.

The University of Texas at Arlington
and
The University of Texas Southwestern Medical Center at Dallas, 2005

Supervising Professor: Dr. Hanli Liu

Near Infrared (NIR) spectroscopy and imaging has become popular in research fields for the past 2-3 decades. My research focuses on the continuous wave near infrared imaging technique. The work consists of two main parts. In the first part, an existing commercial system, an LEDI (Light Emitting Diode Imager), is used to study the cerebral hemodynamics during breath holding. The aim was to evaluate the ability

of an LED-based continuous wave imager to capture changes in hemodynamics occurring inside the skull induced by breath holding. The study involved 15 human subjects. It was found that the total hemoglobin concentration (in proportion to blood volume) within the detected region increases during the breath hold period, reaches a peak after the start of re-breathing, and comes back to normal gradually.

In the second part, the near infrared spectroscopy (NIRS) was employed to measure hot flashes, one of the most common and troublesome symptoms of menopause. During this application, I realized that it is desirable to design and build a new NIR system with a more compact and convenient probe for hot flash measurements. Thus, a low-cost, compact NIRS (LCC-NIRS) system consisting of a probe with single source and four detectors was built. The hardware consisted of a probe, a control board, a power supply, and a DAQ card which is connected to a laptop. The LABVIEW interface was used to control the hardware and to acquire data. The new LCC-NIRS system was tested for its functions by conducting two sets of experiments using both static and dynamic blood phantoms with horse blood mixed with intralipid solutions. The results obtained were found to be satisfactory to support the functions of the system.

Further development can be done to add many features to this LCC-NIRS system so as to make it more compact and eventually a wireless system, which can be very helpful for clinical uses.

TABLE OF CONTENTS

LIST OF ILLUSTRATIONS

LIST OF TABLES

CHAPTER 1

INTRODUCTION

1.1 Background of Near Infra-Red Spectroscopy

Infrared light is composed of a broad range of electromagnetic waves with wavelengths longer than the visible light and shorter than microwaves and millimeter-waves (about 770 nm to 1 mm). Infrared light is further classified as “near infrared” (770 nm – 1400 nm) and “far infrared” (1400 nm – 1 mm) [1, 2].

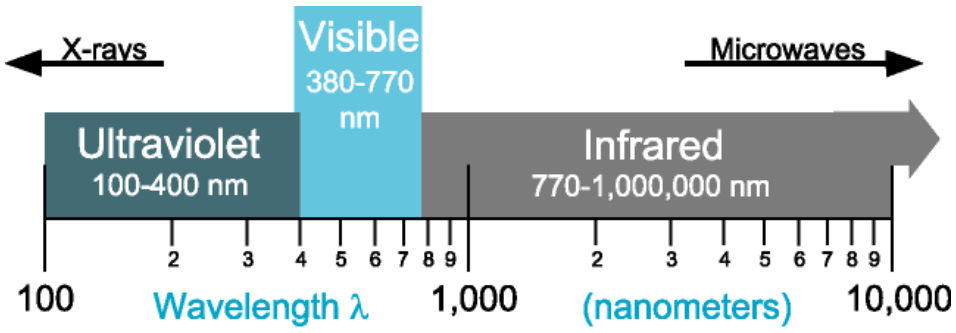

Figure 1.1 Optical Portion of the electromagnetic spectrum [1]

Near Infrared Spectroscopy was first introduced by F.F. Jobsis in 1977 in his paper, entitled "Noninvasive, infrared monitoring of cerebral and myocardial oxygen sufficiency and circulatory parameters". His study was based on the fact that relatively good transparency of biological materials in the near infrared region of the spectrum permits sufficient photon transmission through tissues. Oxygen sufficiency, average

oxy- and deoxy-hemoglobin equilibrium, and changes in tissue blood volume could be determined [3, 4].

Interests were built up in this technique in the early eighties, and more studies were done by Jobsis and other groups to validate and explore more usages of this technique. In late eighties, time- and frequency- resolved techniques were developed which will be discussed later in detail. Till then, the continuous light was also being used. During the nineties, hundreds of studies were published. Monitoring of changes during occlusion of carotid artery and during cardiopulmonary bypass were some examples of reported studies. Since late nineties, NIRS has been increasingly applied in the brain mapping studies and breast cancer screening and diagnosis. Due to its non invasive nature and the information that NIRS can provide, NIRS becomes more accepted in the research fields, particularly for the brain function mapping. Recently, in the past few years, near infrared imaging has been introduced, utilizing multiple source-detector separations to image the hemodynamic activities [3].

1.1.1 Behavior of light inside the tissue

When light enters a tissue, its propagation is mainly governed by two physical phenomena, i.e., light absorption and scattering. There are certain substances in human tissues for which the spectra within the NIR wavelengths are well defined. Some of these absorbers such as water, melanin, and bilirubin do not change in concentration with time. But concentrations of some other absorbers such as oxygenated hemoglobin (HbO_2) and deoxy hemoglobin (Hb) are strongly related to the tissue oxygenation and

metabolism. Thus the absorption changes can provide clinically useful physiological information [5, 6]. Figure 1.2 shows absorption spectra of water, and figure 1.3 shows absorption spectra of Hb and HbO_2 [5]. As can be seen from these two spectra, water absorption dominates at wavelengths above 1000 nm, and below 650 nm, there is a dominant absorption by Hb.

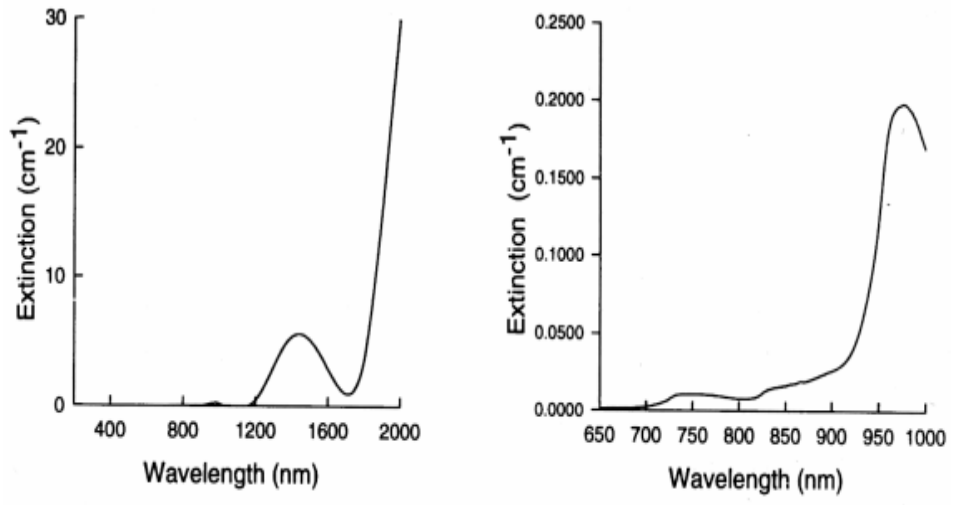

Figure 1.2 Absorption Spectra of pure Water [5]

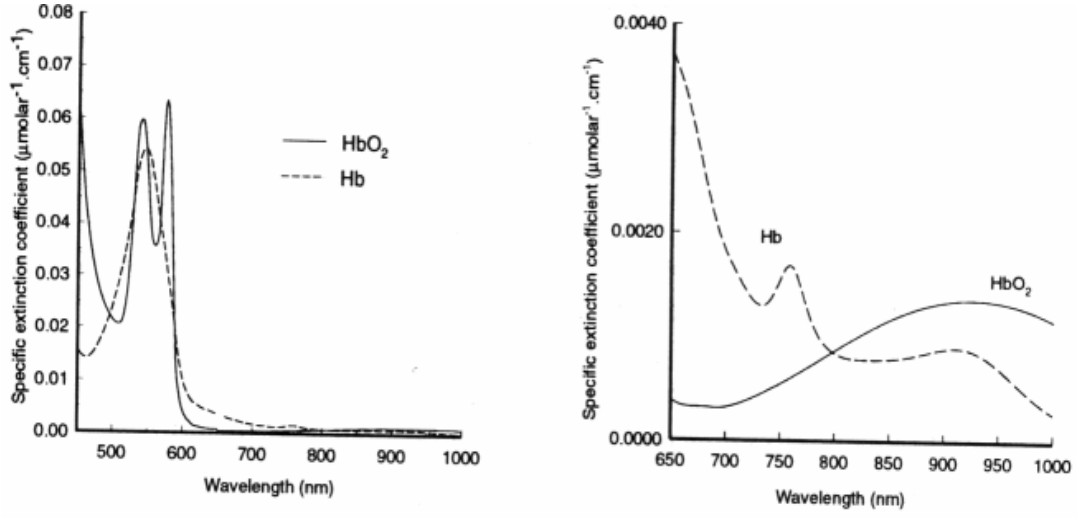

Figure 1.3 Absorption Spectra for Hb and HbO_2 [5]

Thus a so called 'near infrared window' is defined in the range from 650 nm to 1000 nm, which is considered useful for the non-invasive NIR measurements.

1.2 Types of Instruments for NIRS

There are different ways in which diffuse light can be used for excitation. Three different sources are: 1) illumination by sub-nanosecond light pulses, 2) amplitude modulated light at a radio frequency (RF), and 3) continuous wave (CW) illumination. Thus there exist three kinds of instruments based on these different types of illuminations. Each method consists of a completely different set up and principle of calculation [6, 7].

1.2.1 Time Resolved Systems

A time resolved instrument delivers sub-nanosecond laser pulses and measures temporal responses of a tissue. The detectors receive the 'temporal point spread function' (TPSF) which is the temporal distribution of photons as they leave the tissue. The shape of this point spread function provides information about the tissue optical properties. The detection is commonly done using either a synchroscan streak camera or time correlated single photon counting (TCSPC) system which utilizes a photomultiplier tube (PMT). When a complete TPSF is recorded at a fixed source detector separation, values for absorption coefficient (μ_a) and scattering coefficient (μ_s') can be calculated from light transport model, i.e., the diffusion approximation. Figure 1.4(a) shows the TPSF after an impulse passes through the tissue [8].

Though the time-domain systems provide most amount of information per source detector pair, these systems have long acquisition time, which makes them slow, due to relatively low signal to noise ratio (SNR). These kinds of instruments are expensive and relatively bulky [7].

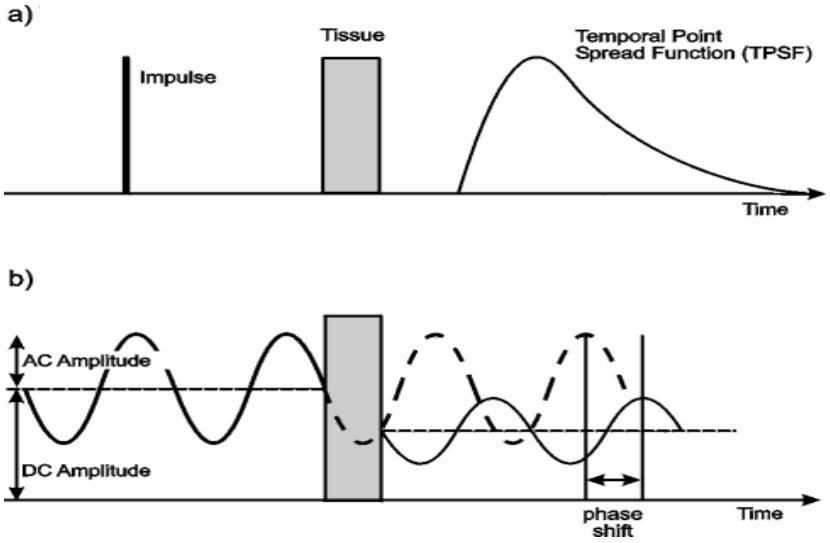

Figure 1.4 An illustration of working principles of a) the time-domain and b) the frequency-domain NIRS instruments [8]

1.2.2 Frequency Domain Systems

Frequency domain systems use intensity modulation of light source at frequencies of tens to hundreds of megahertz. At the detector side, by recording the amplitude attenuation and phase shift with respect to the source light, information about the absorption and scattering properties of the tissue can be obtained. Figure 1.4(b) shows the working principle of such a system. The frequency domain systems acquire data faster than the time domain system and provide quantitative characterization of absorption and scattering as well. However, being fast and quantitative, these systems

require complex electronics and are still relatively expensive [6, 7]. An example of such kind of systems is the ISS oximeter which is widely used in research laboratories.

1.2.3 Continuous Wave Systems

In most of continuous wave (CW) systems, light is emitted at constant amplitude. In some cases, light is modulated at a few kilohertz to reduce the low frequency noise. Light coming out from the tissue is collected by a detector or detectors. If more than one wavelength is used, a relative change of chromophore concentrations can be calculated. CW systems are comparatively easy to build and acquire data fast, but due to lack of temporal information, they cannot provide absolute quantification of concentration changes, which the frequency domain and time domain systems can do, and provide only relative changes.

1.3 Theory of Continuous Wave Measurement

In case of absorptive media, where there is no scattering, the absorption of light obeys Beer-Lambert's law. The law states that for an absorbing compound dissolved in a non-absorbing medium, the attenuation (*A*) is proportional to the concentration of the compound in the solution (*c*) and the optical pathlength (*d*):

$$A = OD = \log_{10} [I_0/I] = \varepsilon.c.d \qquad (1.1)$$

where, OD is the attenuation measured in optical densities, I_0 is the intensity of the incident light, I is the intensity of the transmitted light, ε ($mMol^{-1}$ cm^{-1}) is the specific extinction coefficient of the absorber, c (mMol) is the concentration of absorbing compound in solution, d is the distance between the points where light enters and leaves

the medium. For a medium having more than one absorbing compounds, overall attenuation is the linear sum of individual contributions:

$$OD = \log_{10} [I_0/I] = [\varepsilon_1.c_1 + \varepsilon_2.c_2 + \ldots. + \varepsilon_n.c_n].d. \quad (1.2)$$

For human tissues, however, absorption is not the only phenomena. Light scattering also exists and is rather a dominant phenomenon. As scattering changes the optical path length of the light propagation, absorption characteristics of the medium are difficult to quantify due to light scattering. Figure 1.5 shows the path of light inside the brain [9]. Thus, Beer Lambert's law was modified to be applicable in the human tissue. The modified Beer Lambert's Law is given by:

$$OD = \log_{10} [I_o/I] = \varepsilon.c.d.\ DPF + G \quad (1.3)$$

where G is the term added to compensate for scattering losses, and DPF is the differential path length factor. Thus, the modified Beer Lambert law can be rewritten as:

$$OD = \log_{10} [I_o/I] = \mu_a.L + G \quad (1.4)$$

where $\mu_a = \varepsilon.c$ is the absorption coefficient, and L = d.DPF is the optical path length. In case of relative measurements, a change in OD from the baseline condition to transient condition at wavelength λ is calculated as:

$$\Delta OD^{\lambda} = OD^{\lambda}\ (\text{transient}) - OD^{\lambda}\ (\text{baseline})$$

$$= \log_{10}(I_b/I_t)^{\lambda} = \Delta\mu_a{}^{\lambda}.L^{\lambda} \quad (1.5)$$

Path length was assumed to be constant for all wavelengths [10]. The two main chromophores in tissue for the NIR window are Hb and HbO_2. Thus the absorption coefficients at two wavelengths can be given by:

$$\mu_a{}^{\lambda 1} = \varepsilon_{Hb}{}^{\lambda 1}Hb + \varepsilon_{HbO2}{}^{\lambda 1}HbO_2 \quad (1.6)$$

$$\mu_a{}^{\lambda 2} = \varepsilon_{Hb}{}^{\lambda 2} Hb + \varepsilon_{HbO2}{}^{\lambda 2} HbO_2 \qquad (1.7)$$

If $\Delta\mu_a$ values at two different wavelengths are calculated, it is possible to obtain ΔHb and ΔHbO_2 based on the above two equations [10].

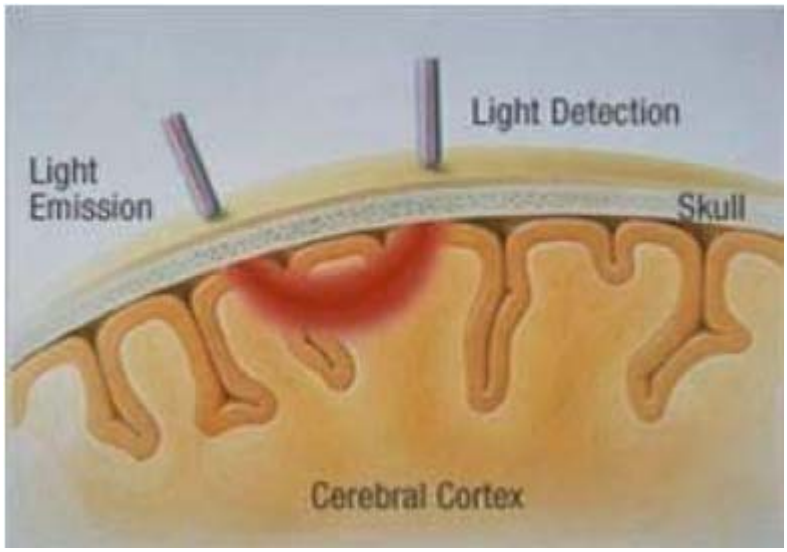

Figure 1.5 Light propagation through brain [9]

1.4 Research Outline

The focus of my project is on the continuous wave system using more than one wavelength so as to calculate changes in Hb, HbO_2 and Hb_{total}. The project consists of three parts: firstly, a commercial system, LEDI, which is a continuous wave LED based imager, was used to map temporal cerebral hemodynamics and to test the ability of the system to be able to measure hemodynamic changes occurring inside the human skull. Cerebral hemodynamics was studied using this system during the breath holding protocol, and the study was successfully completed with 15 human subjects. This part

of study will be described in chapter 2. Next, in order to explore a new application of NIRS, I conducted a preliminary study to apply the LEDI for hot flash measurement in women. Details for this portion of the project will be reported in chapter 3. While the results support the feasibility to use NIRS for hot flash identification and monitoring, it was discovered that the probe of the existing LEDI system was not suitable for sternal measurements. There was a need to develop a low-cost, compact, NIR (LCC-NIR) system to provide flexibility in hot flash measurements to be used in the future. Thus, in the third part of my thesis (Chapter 4), I designed and built a prototype of LCC-NIR system with a single source and four detector chips. Then the LCC-NIR system was tested using laboratory phantoms and was able to record similar changes when compared with the LEDI system. Furthermore, this LCC-NIR system can be modified to become a wireless monitor, and more source detector pairs can be added to make different kinds of probes that can be suitable for broader clinical and physiological applications.

CHAPTER 2

BRAIN STUDY

2.1 Background of LEDI System

The LEDI machine is a continuous wave Near Infrared Imager manufactured by NIM (Near Infrared Monitor) Inc. (Philadelphia, PA). The system consists of a probe, a base control unit, and a power supply unit. The base control unit is connected to the Laptop using a PCMCIA NIDAQ card. Power supply unit provides power (+/- 8V) to the base control unit. Figure 2.1 shows the block diagram of the whole system [11].

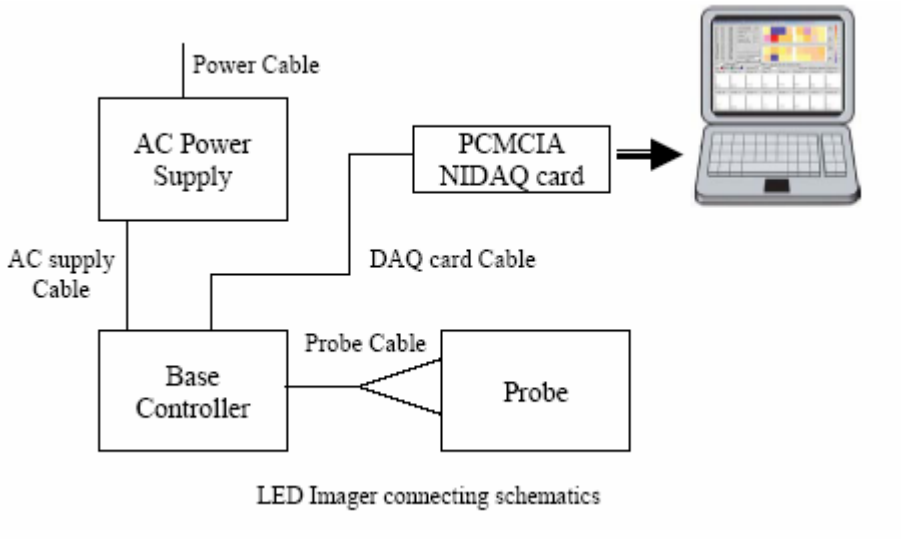

Figure 2.1 Block Diagram of LEDI [11]

2.1.1 Probe

The probe consists of 4 dual-wavelength LEDs (each emitting at 730 nm and 850 nm) and ten photodetectors (OPT101) as shown in figure 2.2. The 4 LEDs at the

two wavelengths are switched on in a sequence, and the four detectors surrounding each of the LEDs collect the data simultaneously when a wavelength is emitted. Thus, 4 sources and 10 detectors lead to 16 recording channels. One set of data points consists of 16 points at each wavelength, and there are total 48 data points, 32 for two wavelengths and 16 for the background. The frequency of data acquisition per image, i.e., a complete cycle to collect 48 points is around 3 Hz.

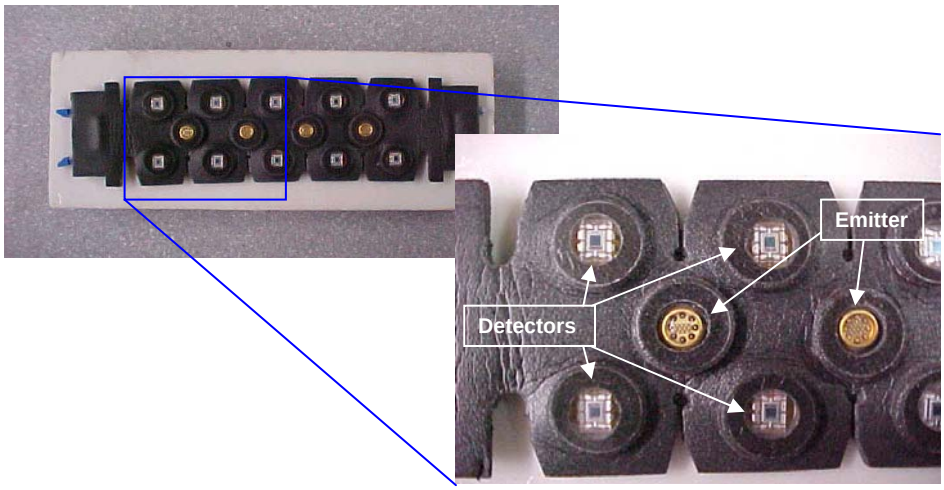

Figure 2.2 LEDI Probe

2.1.2 Software

Figure 2.3 shows the user interface of LEDI. It displays raw data from all the 16 channels. The value of current in the LEDs is variable and 35 mA was used for this experiment. The gain of each detector is adjustable in 256 steps through the software control 'balance'. If the value of the gain is too high, meaning the signal is too low, either the LED current should be increased or the position/location of the detectors needs to be checked to ensure that there is no hair blocking the light to the detector.

For analysis there is a MATLAB code provided by NIM Inc. which utilizes modified Beer Lambert's Law (as explained in chapter 1) to calculate changes in oxy-hemoglobin, deoxy-hemoglobin and blood volume. However, in this study I developed a different MATLAB code for data analysis to provide more flexibility in analysis, allowing different wavelengths to be used.

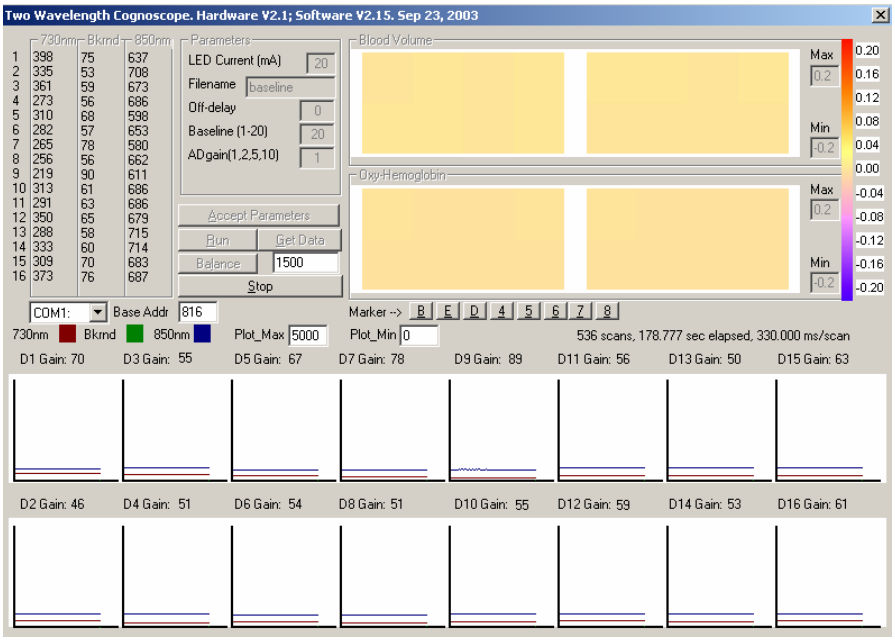

Figure 2.3 LEDI Program User Interface

2.2 Why Breath-holding?

The aim of this study was to examine the ability of the LEDI system to measure changes in the concentrations of oxy-hemoglobin and deoxy-hemoglobin occurring inside the human skull during an induced condition. If the system proves successful in measuring such changes, it is possible to design protocols to study individual parts of the cortex under various test conditions.

The oxygen that is bound to hemoglobin comes from the air that we breathe in during respiration. The blocking of the source of oxygen supply will cause changes in oxygenation in the brain tissue as well as other tissues in the body. This was the assumption which led us to the use of "Breath Holding" as a protocol for this study. Such a protocol is non-invasive, harmless, and easy to induce physiological changes in a human subject.

Forehead is the only place where the measurement can be easily taken considering the limitation of the LEDI probe design. The current design of the probe makes the placement of the probe on the forehead very convenient.

2.3 Experimental Protocol

The experimental protocol was designed as follows:

1. The human subjects taken the experiment were notified for the detailed procedures, and a consent form was signed by the participants.
2. The LEDI probe was placed on the forehead of the human participant. The room was dark during the experiment to reduce interference due to ambient light.
3. The participant was instructed to keep the eyes closed for the entire experiment and to minimize any kind of motor activity like moving hands or talking.
4. The participant was instructed to relax for first ~100 sec, when the baseline was obtained.

5. The participant was asked to hold the breath, after exhalation, as long as possible before re-breathing.
6. The participant was asked to breathe normally for a period of about 2 minutes after the breath hold.

The protocol did not specify the time for the breath hold since everyone has a different capacity of holding breath. The breath hold time ranged from 18 seconds to 90 seconds. The study was done for 15 participants, including 12 males and 3 females; all of them were volunteer students from UTA. An IRB approval was obtained from the office of research for this study. The approval form is attached in the Appendix B.

2.4 Method

The data were obtained as a '.dat' file consisting of data from all of the 16 channels and a time stamp. The data file was read into an array (N X 49), where N denotes the number of sample points obtained, and 49 = 3 x 16 +1 represents the 16 channels, each having three readings (at 730 nm, 850 nm and background without any LED light) and a time stamp. Equations 1.4 to 1.7 were used to arrive at the following expressions which were used for the calculation:

$$\Delta \mathrm{HbO}_2 = \frac{\log \frac{\mathrm{I}^{\mathrm{b}}(\lambda_{730\mathrm{nm}})}{\mathrm{I}^{\mathrm{s}}(\lambda_{730\mathrm{nm}})} \varepsilon_{\mathrm{deoxy}}(\lambda_{850\mathrm{nm}}) - \log \frac{\mathrm{I}^{\mathrm{b}}(\lambda_{850\mathrm{nm}})}{\mathrm{I}^{\mathrm{s}}(\lambda_{850\mathrm{nm}})} \varepsilon_{\mathrm{deoxy}}(\lambda_{730\mathrm{nm}})}{\mathrm{L}[\varepsilon_{\mathrm{oxy}}(\lambda_{730\mathrm{nm}})\varepsilon_{\mathrm{deoxy}}(\lambda_{850\mathrm{nm}}) - \varepsilon_{\mathrm{oxy}}(\lambda_{850\mathrm{nm}})\varepsilon_{\mathrm{deoxy}}(\lambda_{730\mathrm{nm}})]} \qquad (2.1)$$

$$\Delta \mathrm{Hb} = \frac{\log \frac{\mathrm{I}^{\mathrm{b}}(\lambda_{850\mathrm{nm}})}{\mathrm{I}^{\mathrm{s}}(\lambda_{850\mathrm{nm}})} \varepsilon_{\mathrm{oxy}}(\lambda_{730\mathrm{nm}}) - \log \frac{\mathrm{I}^{\mathrm{b}}(\lambda_{730\mathrm{nm}})}{\mathrm{I}^{\mathrm{s}}(\lambda_{730\mathrm{nm}})} \varepsilon_{\mathrm{oxy}}(\lambda_{850\mathrm{nm}})}{\mathrm{L}[\varepsilon_{\mathrm{oxy}}(\lambda_{730\mathrm{nm}})\varepsilon_{\mathrm{deoxy}}(\lambda_{850\mathrm{nm}}) - \varepsilon_{\mathrm{oxy}}(\lambda_{850\mathrm{nm}})\varepsilon_{\mathrm{deoxy}}(\lambda_{730\mathrm{nm}})]} \qquad (2.2)$$

$$\Delta Hb_{total} = (\Delta Hb + \Delta HbO_2) \tag{2.3}$$

where

ΔHbO_2 ⟶ change in oxy hemoglobin concentration,

ΔHb ⟶ change in deoxy hemoglobin concentration,

ΔHb_{total} ⟶ change in total hemoglobin concentration,

$I^s(\lambda_x)$ ⟶ intensity of light at wavelength 'x' during stimulus,

$I^b(\lambda_x)$ ⟶ intensity of light at wavelength 'x' during baseline,

$\varepsilon_{oxy}(\lambda_x)$ ⟶ extinction coefficient for oxy-hemoglobin at wavelength 'x',

$\varepsilon_{deoxy}(\lambda_x)$ ⟶ extinction coefficient for deoxy-hemoglobin at wavelength 'x',

L ⟶ optical path length.

$\varepsilon_{oxy}(\lambda_{730}) = 0.4383 mM^{-1}cm^{-1}$ $\varepsilon_{deoxy}(\lambda_{730}) = 1.3029 mM^{-1}cm^{-1}$

$\varepsilon_{oxy}(\lambda_{850}) = 1.1596 mM^{-1}cm^{-1}$ $\varepsilon_{deoxy}(\lambda_{850}) = 0.7861 mM^{-1}cm^{-1}$

$\varepsilon_{oxy}(\lambda_x)$ and $\varepsilon_{deoxy}(\lambda_x)$ are constants and were obtained from Mark Cope's dissertation [12]. $I^s(\lambda_x)$ and $I^b(\lambda_x)$ can be obtained from the collected data. Thus ΔHbO_2 and ΔHb are the only unknowns and can be calculated. Substituting the values of extinction coefficients in Eqs. (2.1) & (2.2), we get:

$$\Delta HbO_2 = [\, - 0.6740 \log(\frac{I^b(\lambda_{850nm})}{I^s(\lambda_{850nm})}) + 1.1171 \log(\frac{I^b(\lambda_{730nm})}{I^s(\lambda_{730nm})}) \,]/L \tag{2.4}$$

$$\Delta Hb = [- 0.3758 \log(\frac{I^b(\lambda_{850nm})}{I^s(\lambda_{850nm})}) + 0.9943 \log(\frac{I^b(\lambda_{730nm})}{I^s(\lambda_{730nm})})]/L \qquad (2.5)$$

Note that since the optical path length, L, is an unknown parameter, I am including it in the unit for both ΔHbO_2 and ΔHb, as a scaling factor. Now, the units for both ΔHbO_2 and ΔHb are mM/L.

A MATLAB code was written to analyze the data. The code is attached in Appendix A. Hb, HbO_2 and Hbt were plotted against time. The data from 16 detectors were interpolated to obtain a spatial map of the forehead at different instants of time. I^b (baseline intensity) was obtained by averaging out the values from the start to the end of baseline. Then ΔHbO_2 and ΔHb were calculated for each data point using the expression given in Eqs. (2.4) and (2.5). ΔHb_{total}, which is calculated as a sum of ΔHbO_2 and ΔHb, also gives a close approximation to total change in the blood volume. Maximum values of ΔHb, ΔHbO_2 and ΔHb_{total} after the breath hold were calculated. Moreover, the period of breath hold was calculated using the difference between the starting and ending time of breath hold, and the time to reach maximum value of Hbt after breath hold was also recorded.

A flow chart for the software code to calculate the parameters mentioned above is given on the next page.

Program Flow Chart:

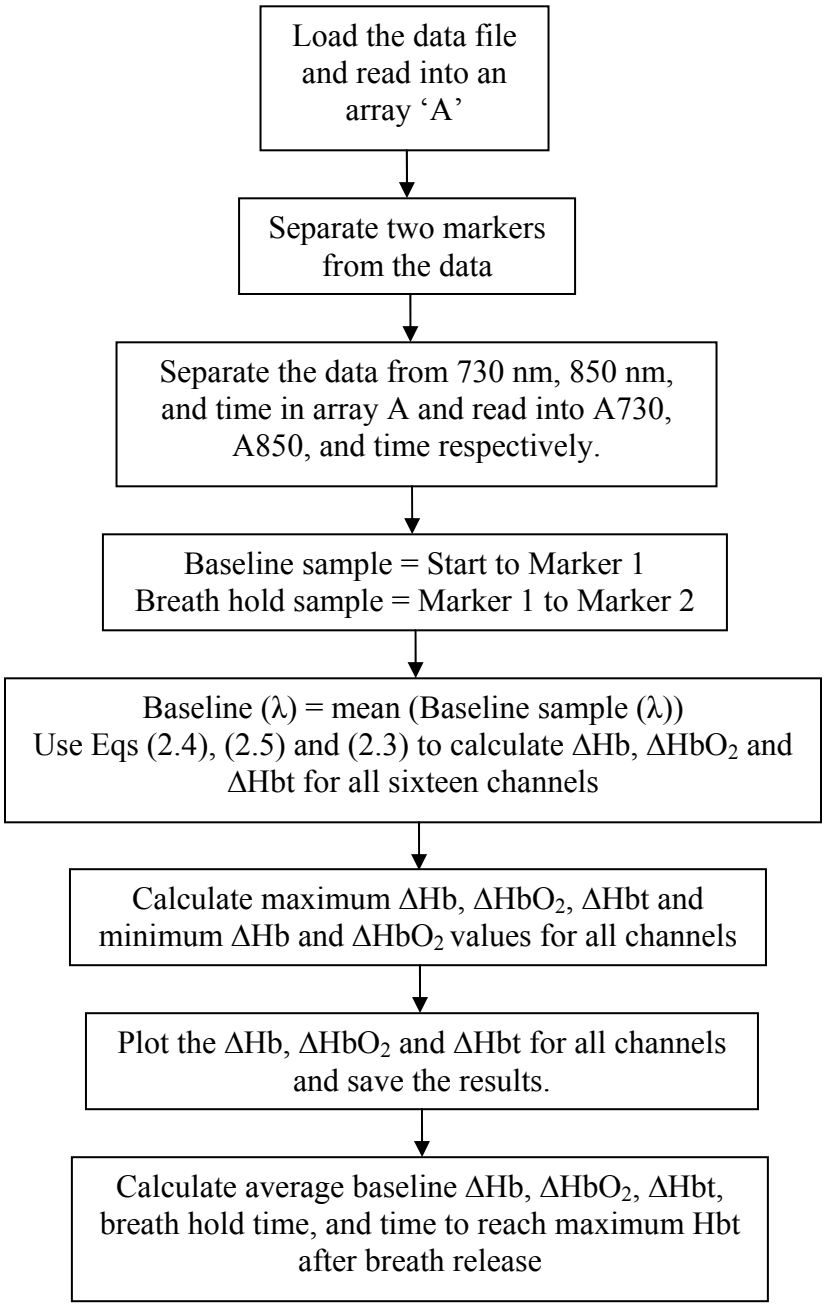

Figure 2.4 Flow chart for MATLAB program used for processing data

2.5 Results

Fifteen participants were recruited for the study. Figure 2.5 shows the plot of Hb, HbO_2 and Hbt for Channel 1 for the first participant. The first marker represents the time when the participant exhaled and started holding the breath. The second marker represents the time when participant resumes breathing. As seen in the figure, all the three parameters start to increase as breath hold continues, and the increase continues even after the participant resumes breathing. Some time after normal breathing, the values of Hb, HbO2 and Hbt come back gradually (but not as fast as they increased) towards the baseline.

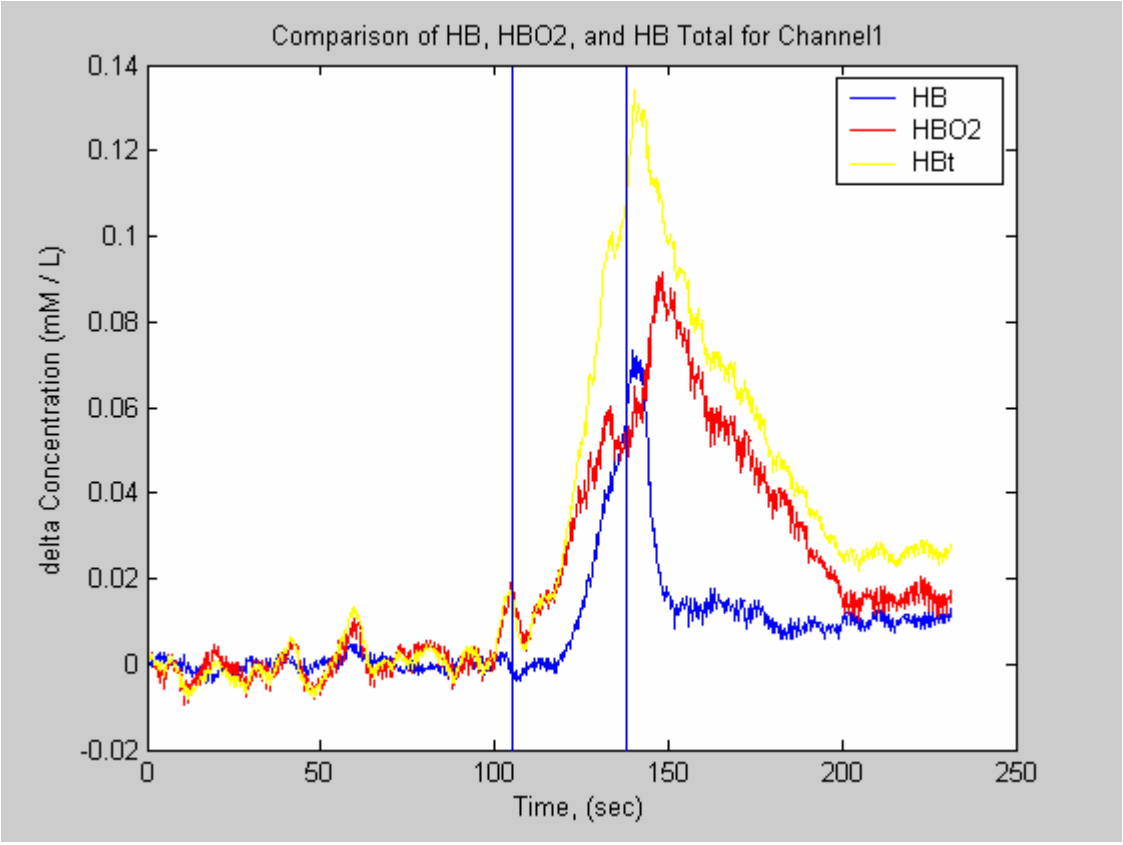

Figure 2.5 Participant 1- Plot of Hb, HbO2 and Hbt for Channel 1

Figures 2.6 to 2.20 show the data from rest of the 15 channels. All the channels record nearly similar changes. In some channels, a few peaks temporally apart from each other were seen, and they can be attributed to the noise due to motion during the measurement. A downward peak at around 130 sec in channel 2 is an example of such noise. As seen in the subsequent figures, the changes in all channels follow almost the same pattern except that there are differences in amplitudes i.e. the concentration changes. The Blood volume (Hbt), Hb and HbO_2 increase during the breath hold and continue to increase till sometime after the participant resumes breathing before the respective values start coming down to the baseline.

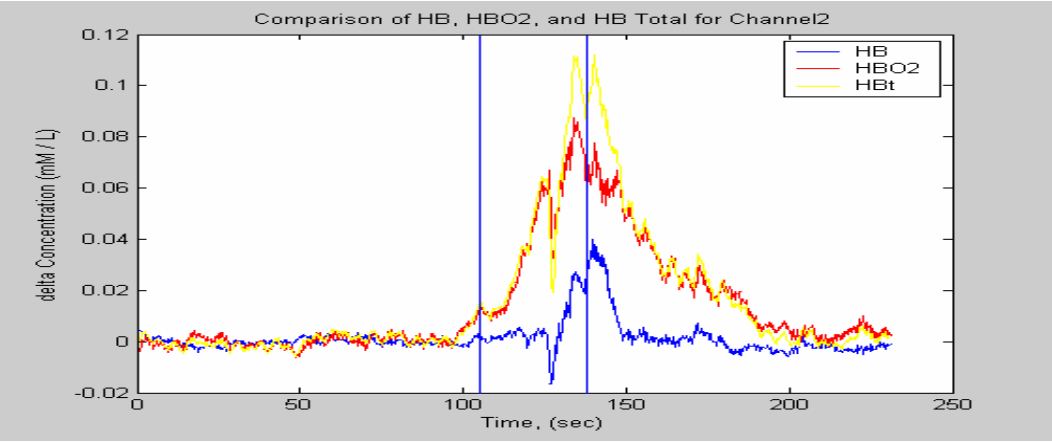

Figure 2.6 Participant 1- Plot of Hb, HbO2 and Hbt for Channel 2

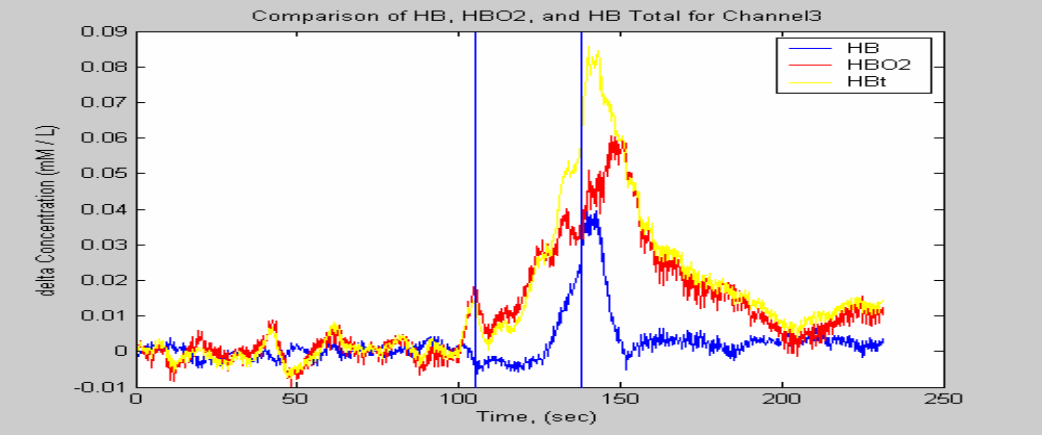

Figure 2.7 Participant 1- Plot of Hb, HbO2 and Hbt for Channel 3

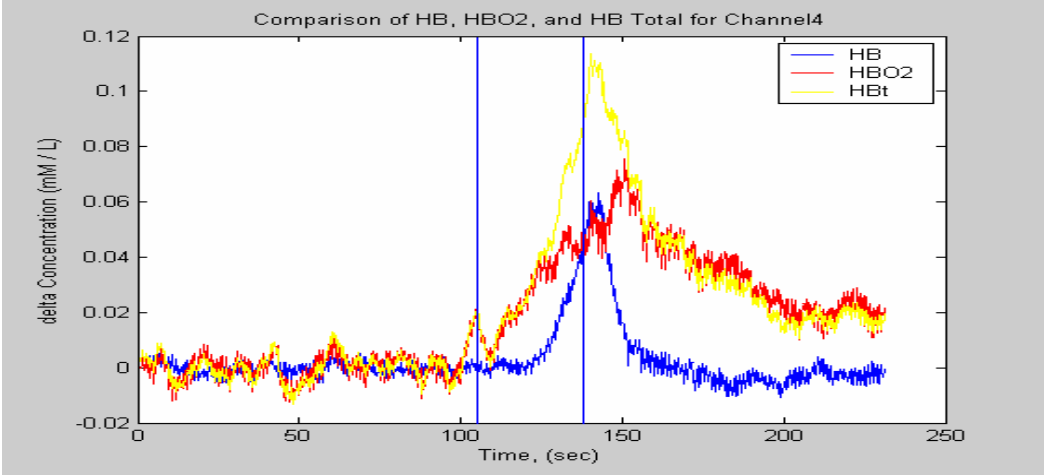

Figure 2.8 Participant 1- Plot of Hb, HbO2 and Hbt for Channel 4

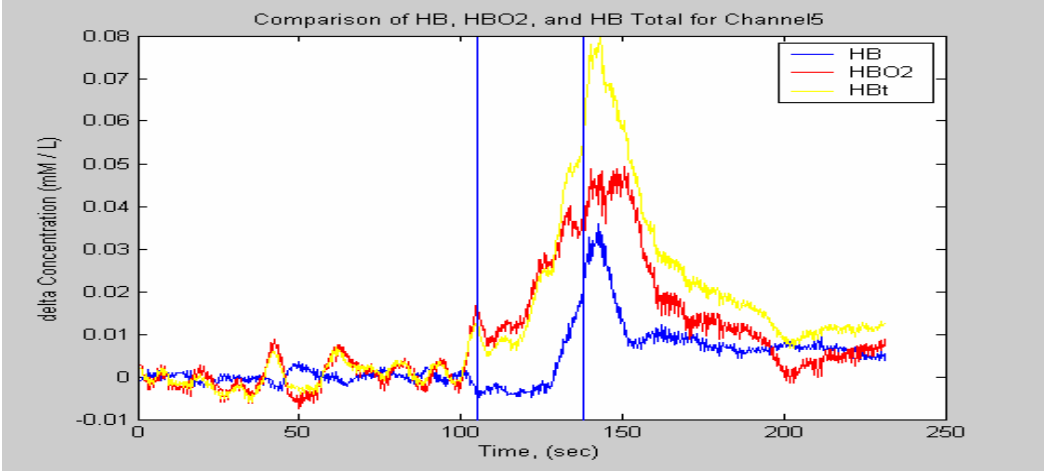

Figure 2.9 Participant 1- Plot of Hb, HbO2 and Hbt for Channel 5

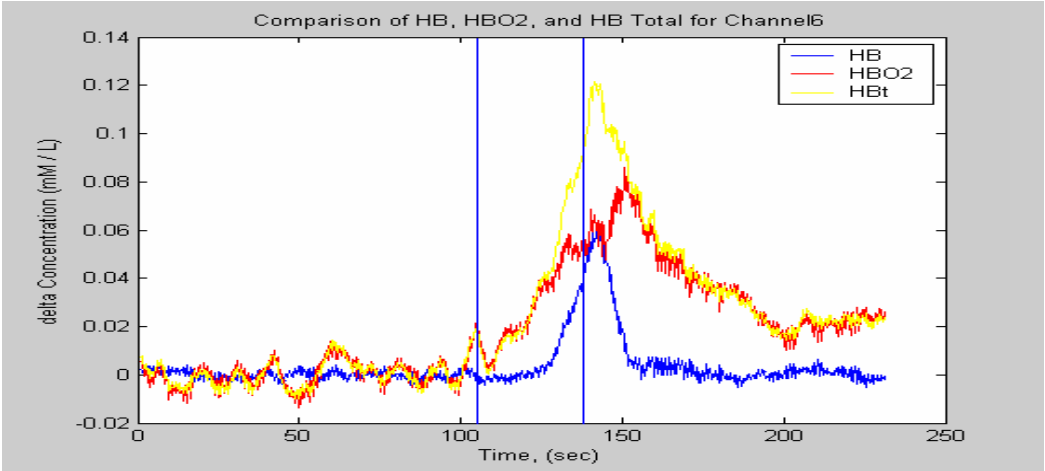

Figure 2.10 Participant 1- Plot of Hb, HbO2 and Hbt for Channel 6

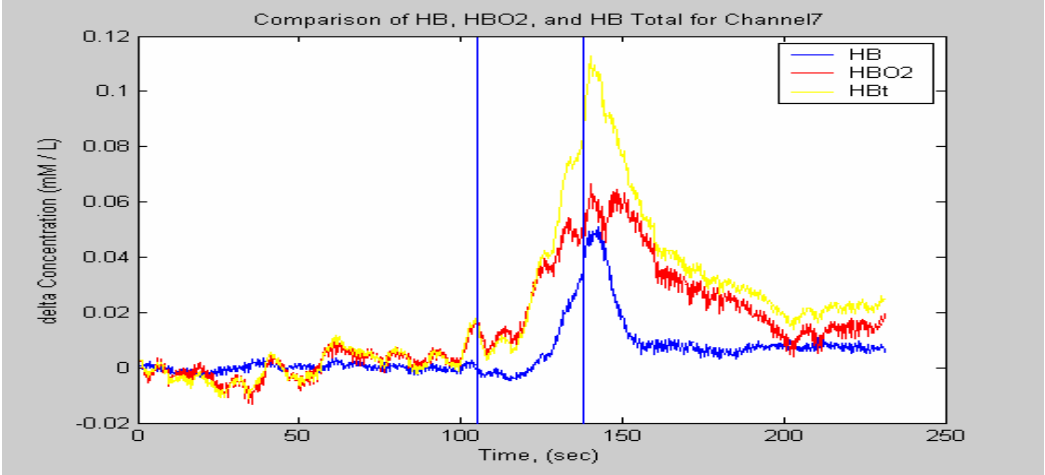

Figure 2.11 Participant 1- Plot of Hb, HbO2 and Hbt for Channel 7

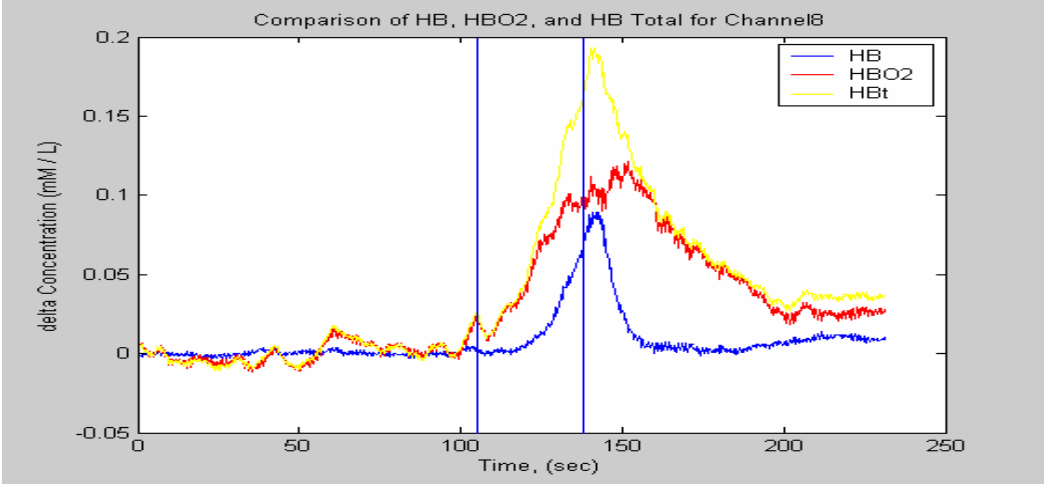

Figure 2.12 Participant 1- Plot of Hb, HbO2 and Hbt for Channel 8

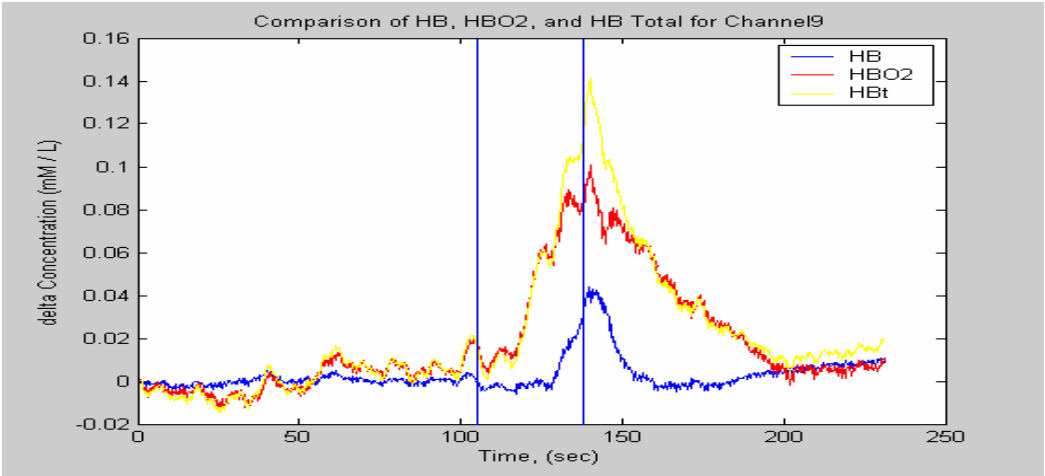

Figure 2.13 Participant 1- Plot of Hb, HbO2 and Hbt for Channel 9

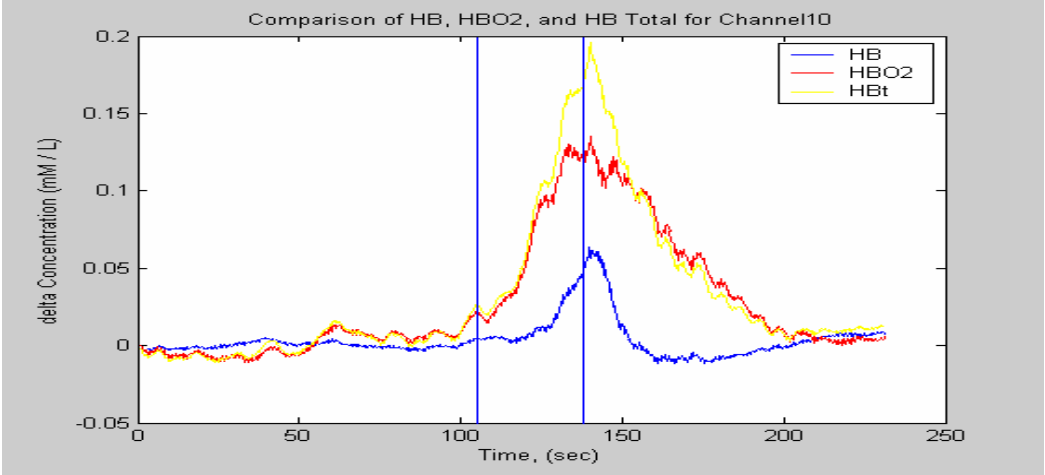

Figure 2.14 Participant 1- Plot of Hb, HbO2 and Hbt for Channel 10

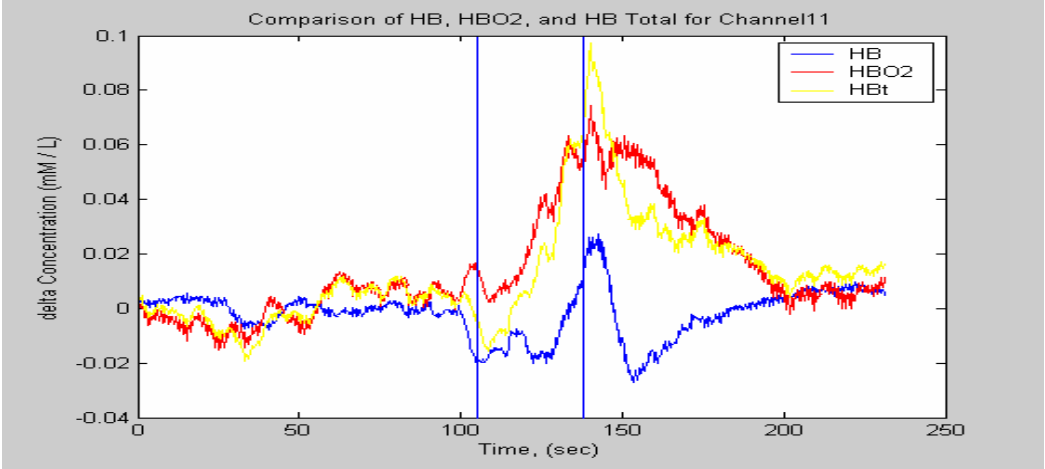

Figure 2.15 Participant 1- Plot of Hb, HbO2 and Hbt for Channel 11

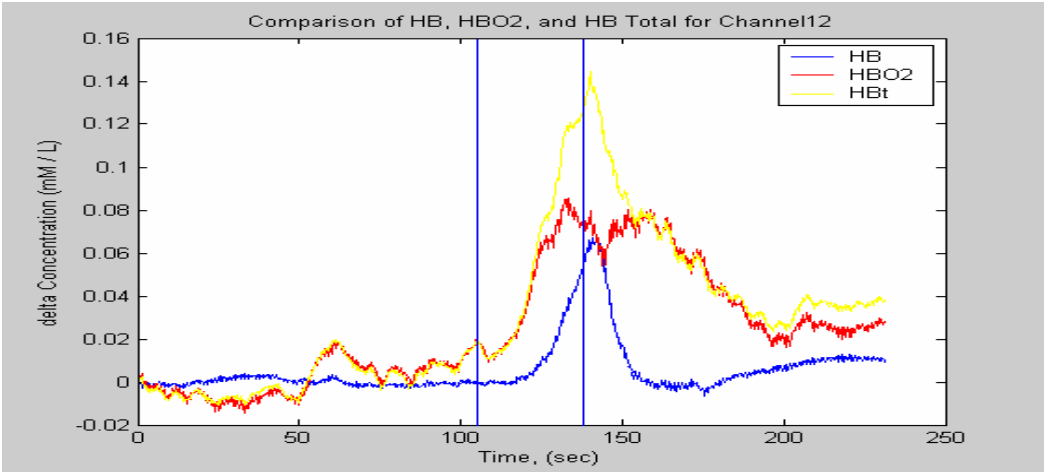

Figure 2.16 Participant 1- Plot of Hb, HbO2 and Hbt for Channel 12

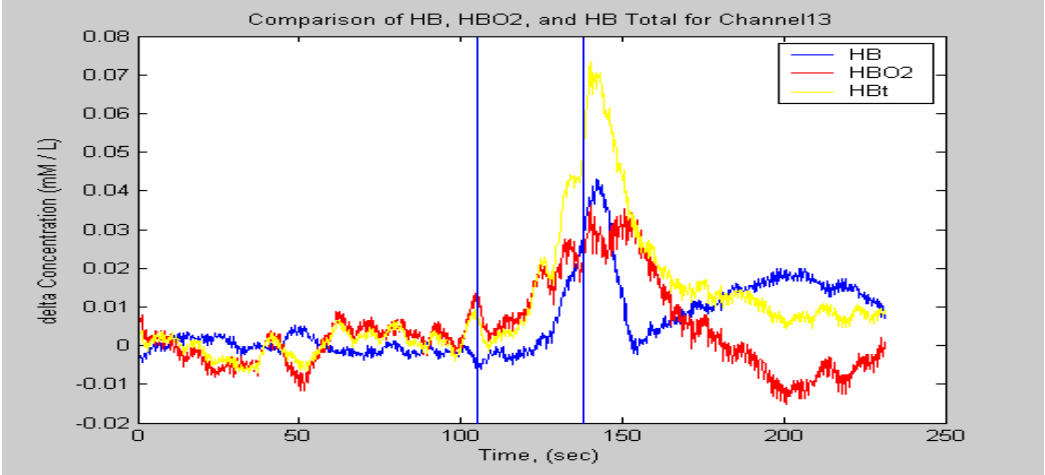

Figure 2.17 Participant 1- Plot of Hb, HbO2 and Hbt for Channel 13

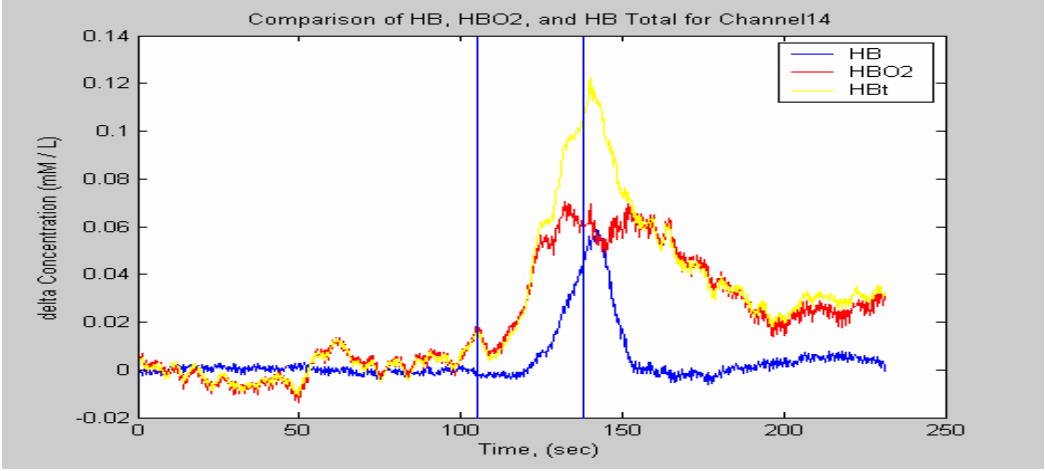

Figure 2.18 Participant 1- Plot of Hb, HbO2 and Hbt for Channel 14

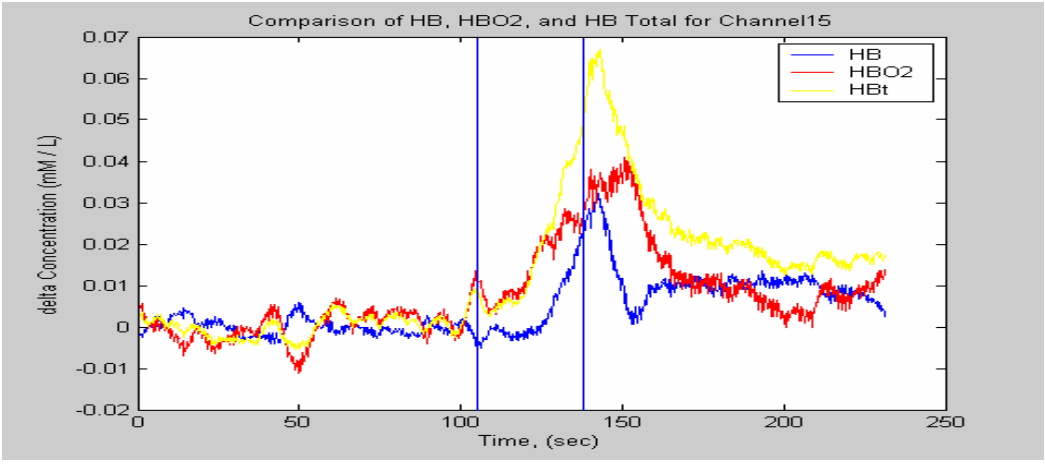

Figure 2.19 Participant 1- Plot of Hb, HbO2 and Hbt for Channel 15

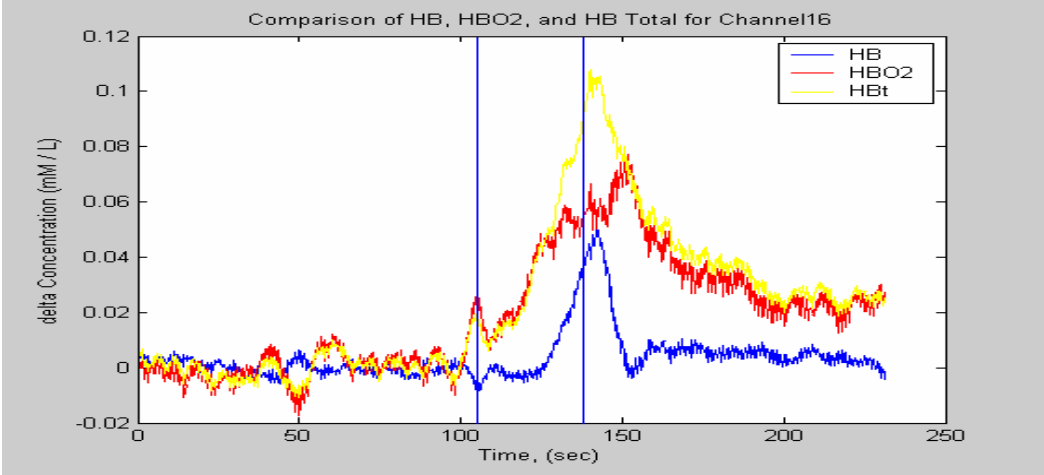

Figure 2.20 Participant 1- Plot of Hb, HbO_2 and Hbt for Channel 16

Figures 2.21, 2.22 and 2.23 show individual plots of Hb_{total}, Hb, HbO_2, for all 16 channels respectively. It can be easily observed that the changes in all 16 channels with respect to time are consistent.

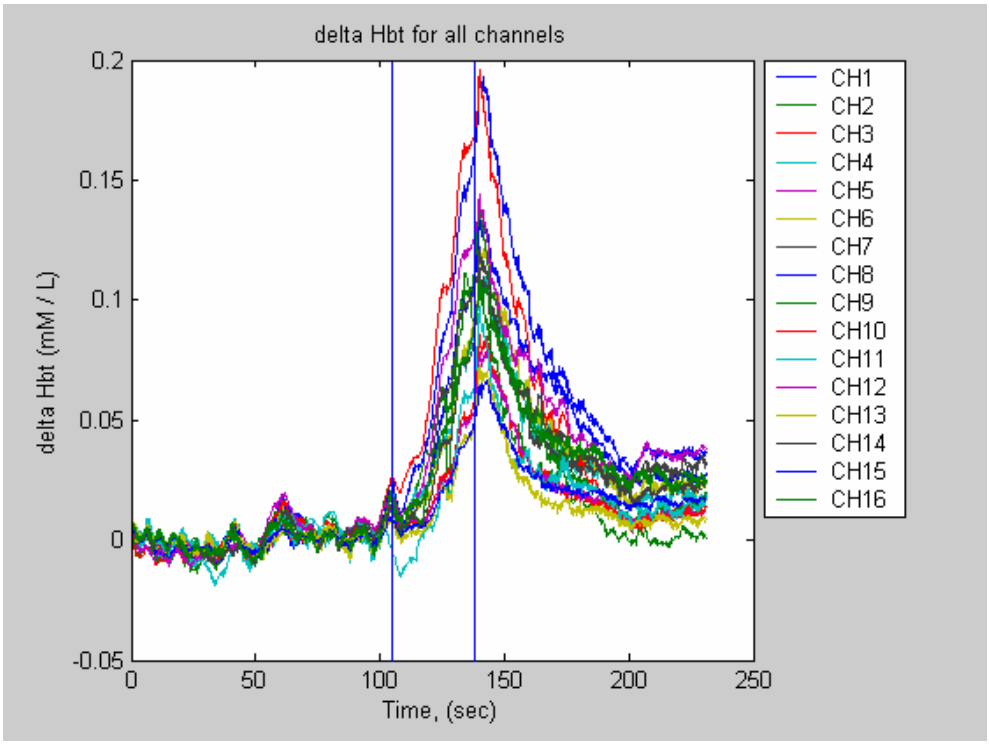

Figure 2.21 Participant 1 - Plot of Hb_{total} for all channels

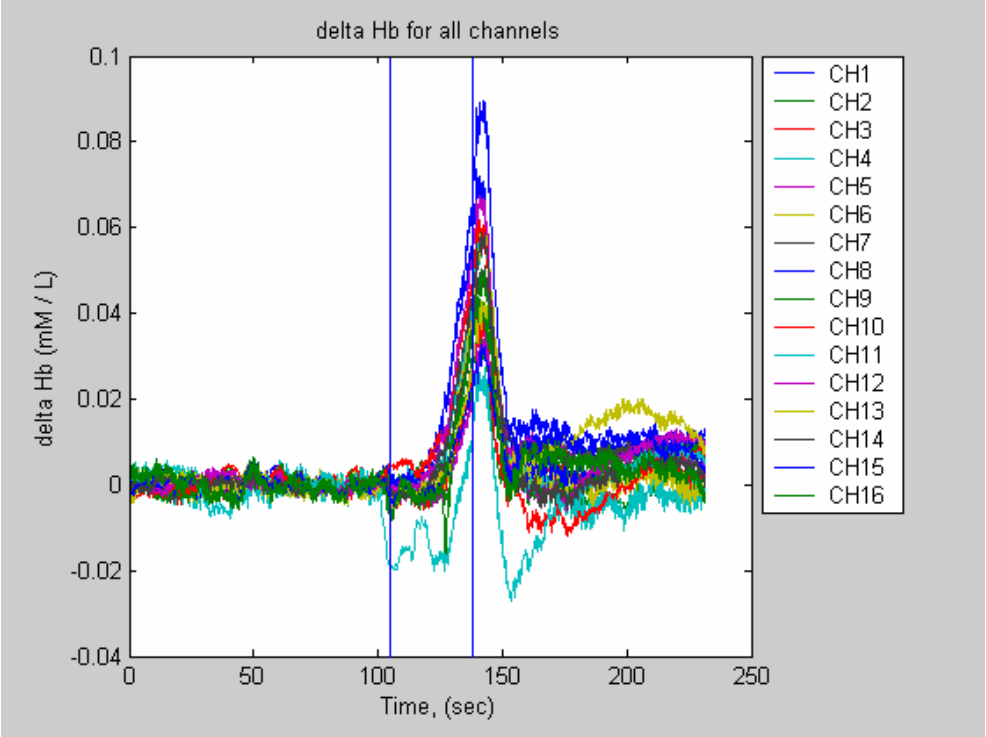

Figure 2.22 Participant 1 - Plot of Hb for all channels

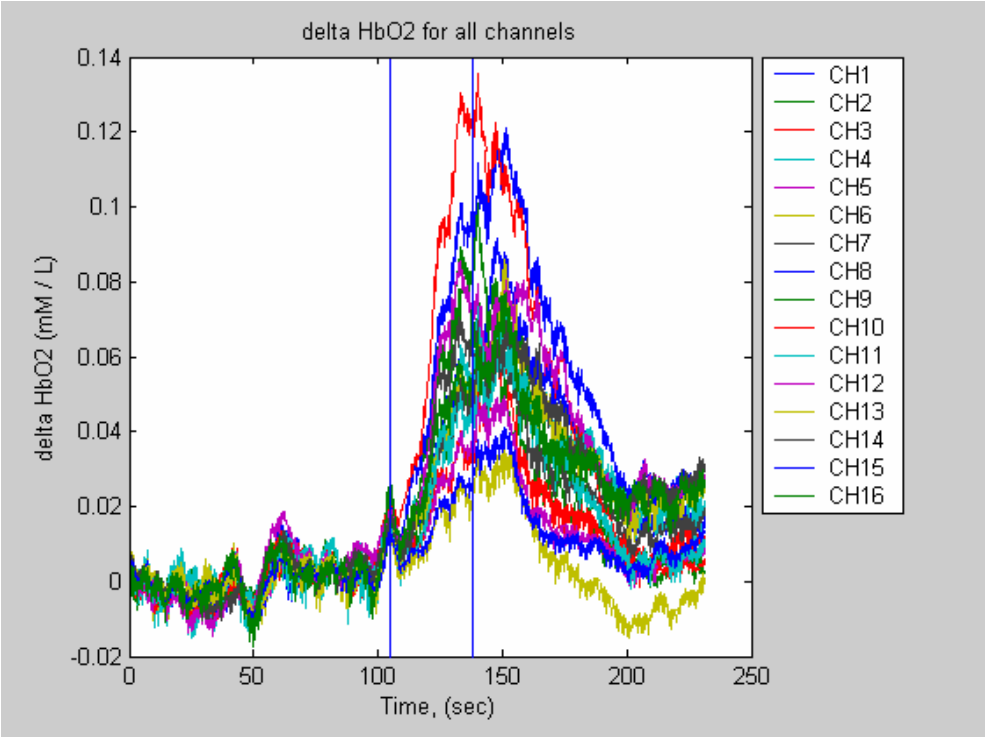

Figure 2.23 Participant 1 - Plot of HbO_2 for all channels

As these detectors are placed on the forehead, data can be interpolated at any point of time to obtain a spatial map of the changes occurring behind the forehead. Figure 2.24 demonstrates the placement of the probe on the forehead, where D1 and D10 represent detectors 1 and 10 respectively. Figures 2.25 to 2.28 show the spatial map of the forehead at different instances. The black vertical marker is the time instant at which the spatial map shown below is displayed. The two blue markers represent the breath hold period. The spatial map of the forehead can be seen at the lower part of these figures. Linear interpolation was done to smooth the spatial map using matlab function 'interp2', which is a two dimensional interpolation function. The rectangular image represents the topographic area of the brain behind the probe, which has an approximate dimension of 4 cm x 14.5 cm. A 2 x 8 array representing the sixteen channels is interpolated to generate a (41 x 141) array so that a smooth image of the forehead is obtained.

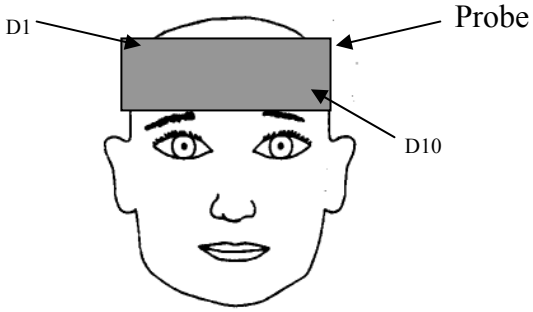

Figure 2.24 Demonstration of probe placement over the forehead

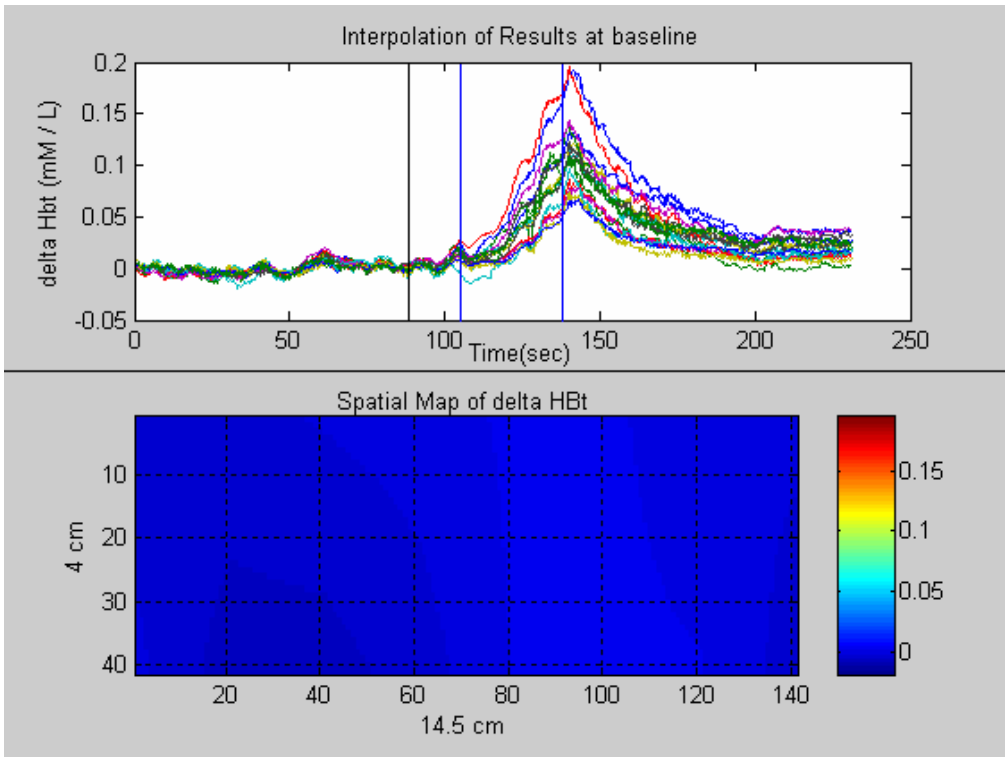

Figure 2.25 Spatial map of ΔHbt on the forehead at baseline.

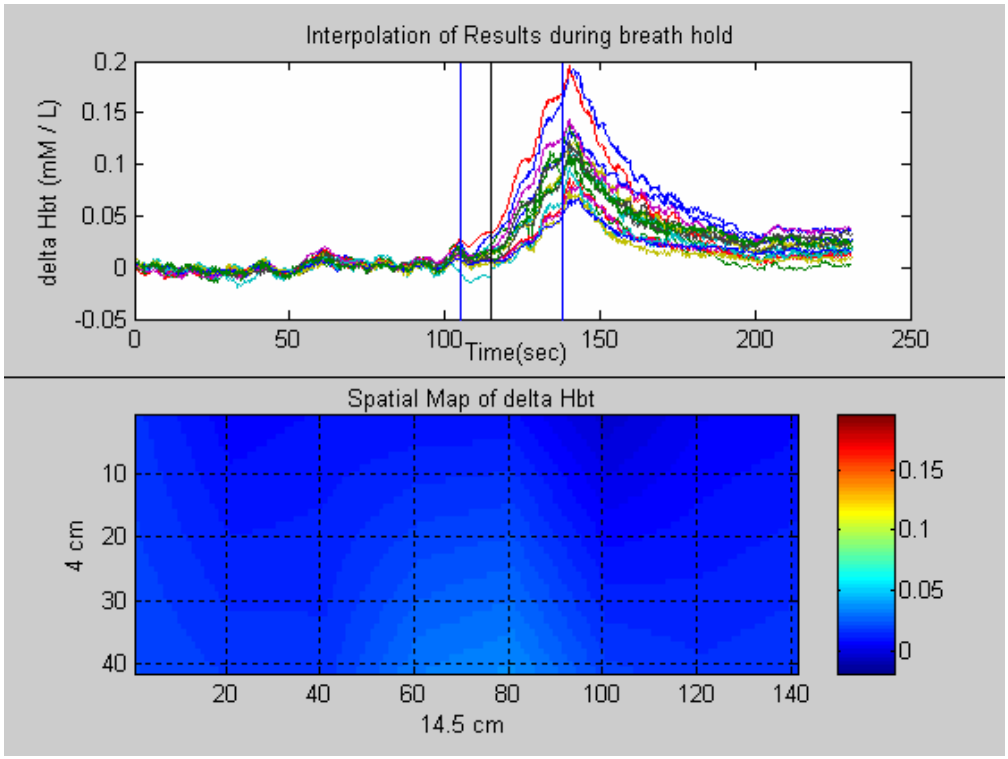

Figure 2.26 Spatial map of ΔHbt on the forehead during breath hold

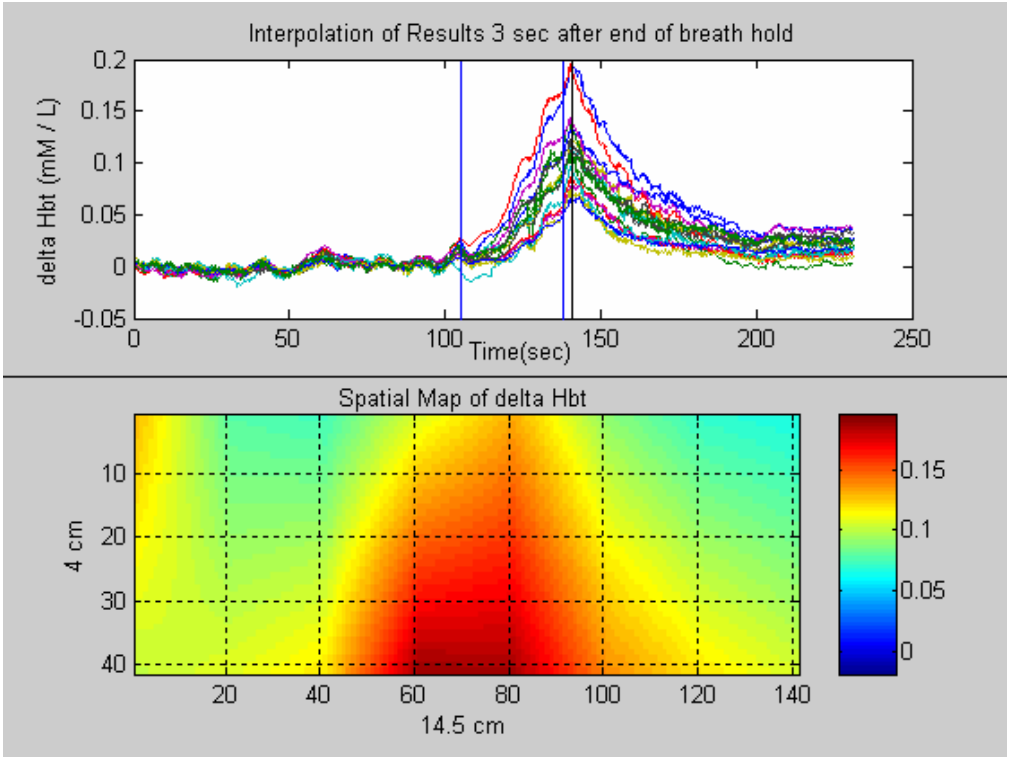

Figure 2.27 Spatial map of ΔHbt on the forehead, 3 sec after breath hold

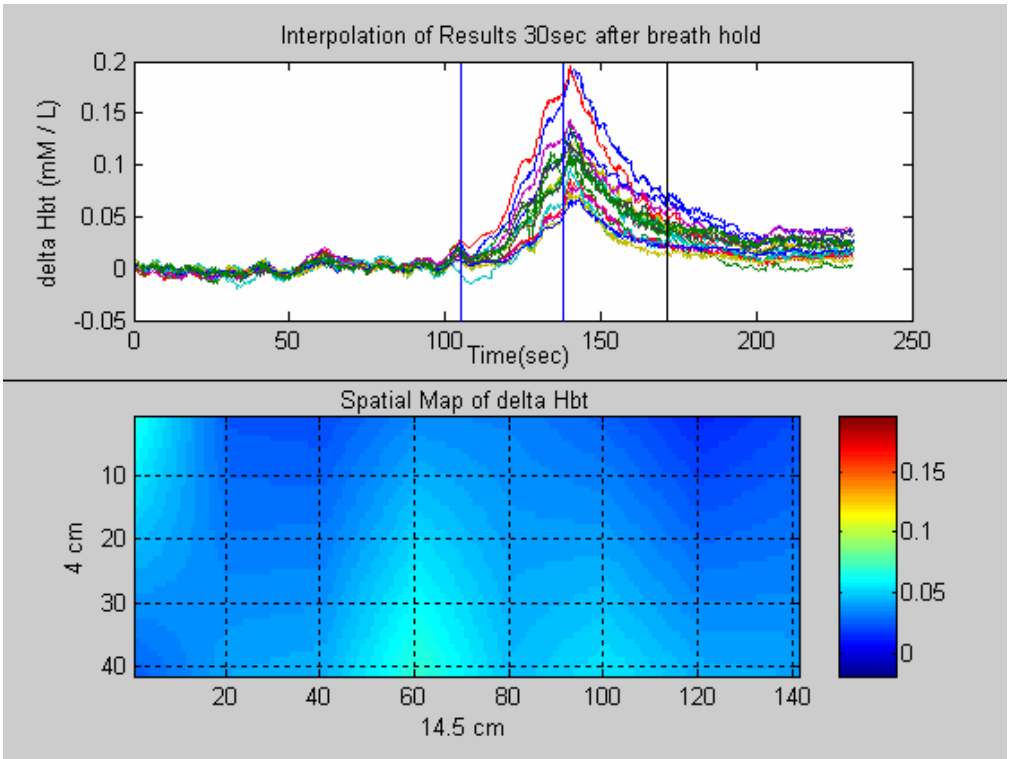

Figure 2.28 Spatial map of ΔHbt on the forehead, 30sec after breath hold

Figures 2.26, 2.27 and 2.28 show three characteristic spatial maps of ΔHbt on the forehead during, immediately after, and 30 sec after the breath hold respectively. Such kind of maps display clearly that the forehead have strong and heterogeneous responses, and that the central region of the forehead has larger responses to the breath holding.

Tables 2.1 and 2.2 summarize the results from all the subjects. In table 2.1, 'BH time' is the time during which the breath was held. 'Hbtbase' and 'Hbtmax' are the baseline and maximum values of ΔHb_{total} which were calculated for every subject by taking an average of all the 16 channels. 'T3' is the time at which the maximum level of ΔHb_{total} occurs after re-breathing. Since the size of probe is quite big, some of the detectors were on the hair instead of the forehead in a few subjects who had a smaller forehead. In such cases, bad readings from those detectors were not included in the analysis. In table 2.2, 'HbO_2base', 'HbO_2max', 'HbO_2min', and 'Hbbase', 'Hbmax', 'Hbmin' represent the baseline, maximum, and minimum values of ΔHbO_2 and ΔHb, respectively, and they were calculated in the same manner as for ΔHb_{total}. Figure 2.29 shows a plot of Hbtmax vs. breath hold time. Figure 2.30 shows a plot of T3 vs. breath hold time.

As the person starts holding breath, there is an increase in ΔHb_{total}, which represents the blood volume. This change was found to be same for all the participants. However there were differences in ΔHb and ΔHbO_2 between the participants. For some participants, there was an increase in both ΔHb and ΔHbO_2 and for some there was an

increase in ΔHbO_2 and a decrease in ΔHb and for some there was a decrease in ΔHbO_2 and an increase in ΔHb.

Table 2.1 Breath hold time, baseline Hbt, maximum Hbt, T3 for all subjects

Participant #	Gender	BH time (sec)	Hbtbase (mM)	Hbtmax (mM)	T3 (sec)
1	Male	33.048	3.24E-05	1.19E-01	2.446
2	Male	29.403	1.12E-04	4.82E-02	2.871
3	Male	23.464	1.46E-04	4.77E-02	6.322
4	Male	54.528	2.37E-05	2.26E-02	1.332
5	Male	20.159	5.40E-05	8.44E-02	4.443
6	Male	41.97	3.31E-05	3.69E-02	3.755
7	Male	43.623	2.04E-05	4.35E-02	1.724
8	Male	33.378	7.47E-05	9.73E-02	5.075
9	Male	66.095	1.07E-04	8.60E-02	2.108
10	Female	29.082	3.01E-05	3.97E-02	8.571
11	Female	38.005	1.09E-05	4.18E-02	1.212
12	Male	89.559	5.32E-05	9.46E-02	4.737
13	Female	18.837	9.60E-06	1.84E-02	3.371
14	Male	31.726	1.37E-05	4.97E-02	2.458
15	Male	37.674	5.98E-05	1.79E-01	5.824

Table 2.2 Baseline, Maximum and Minimum Hb and HbO_2 for all Participants

Participant #	HbO2base (mM)	HbO2max (mM)	HbO2min (mM)	Hbbase (mM)	Hbmax (mM)	Hbmin (mM)
1	3.71E-05	7.77E-02	3.00E-02	-4.77E-06	5.27E-02	-2.96E-03
2	1.40E-04	3.03E-02	2.31E-03	-2.82E-05	3.23E-02	-8.81E-04
3	1.44E-04	3.14E-02	9.25E-04	2.19E-06	2.90E-02	-6.70E-03
4	2.74E-05	-2.66E-03	-3.49E-02	-3.63E-06	3.02E-02	7.74E-03
5	3.99E-05	6.15E-02	1.25E-02	1.41E-05	6.16E-02	-1.93E-02
6	3.36E-05	4.45E-02	2.43E-02	-4.53E-07	-3.16E-03	-2.34E-02
7	1.81E-05	4.30E-02	7.90E-03	2.32E-06	5.40E-03	-1.31E-02
8	8.20E-05	7.80E-02	2.78E-02	-7.32E-06	2.70E-02	-7.44E-03
9	9.71E-05	1.11E-02	-4.29E-02	1.02E-05	1.05E-01	7.14E-03
10	3.00E-05	4.77E-02	2.53E-02	1.29E-07	2.15E-03	-1.57E-02
11	7.47E-06	6.79E-02	2.28E-02	3.39E-06	-1.92E-02	-3.16E-02
12	4.39E-05	1.86E-02	-2.97E-02	9.25E-06	1.06E-01	3.23E-02
13	9.02E-06	2.29E-02	7.30E-03	5.76E-07	-1.88E-03	-1.23E-02
14	1.09E-05	3.68E-02	4.09E-03	2.82E-06	1.63E-02	-8.03E-03
15	7.15E-05	1.66E-01	8.65E-02	-1.17E-05	6.09E-02	-1.07E-02

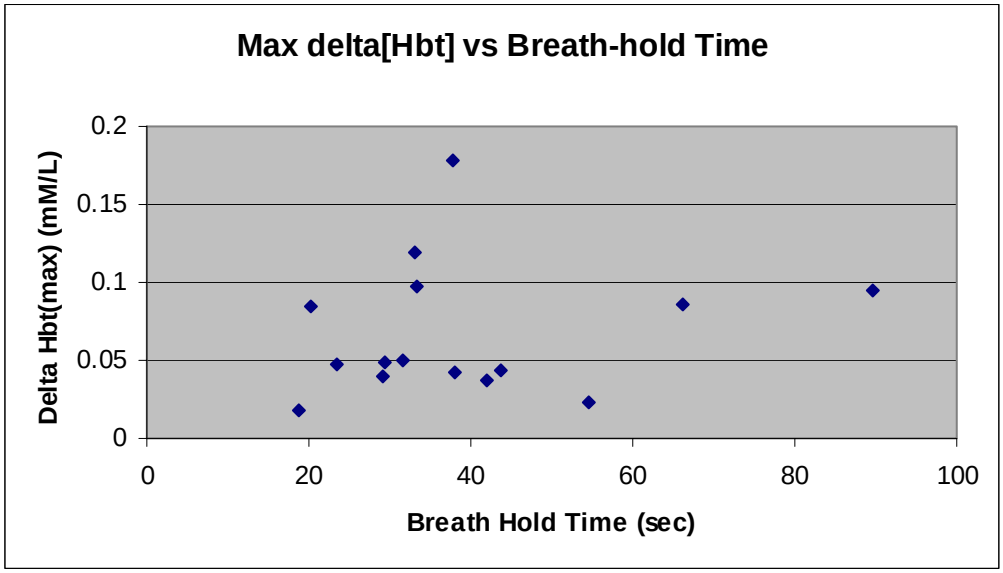

Figure 2.29 Max delta [Hbt] vs. Breath hold Time

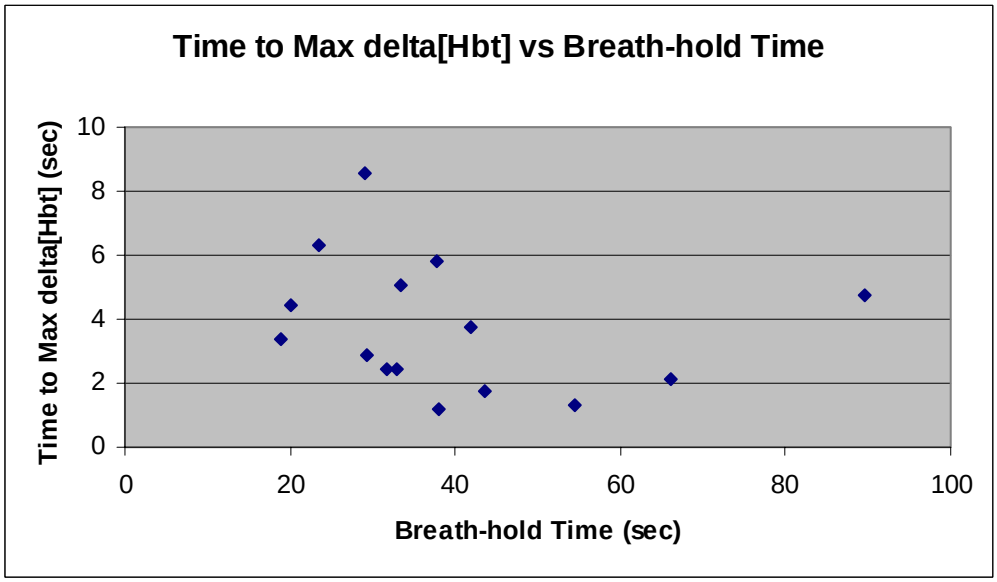

Figure 2.30 Time to Max delta [Hbt] vs. Breath hold time

2.6 Discussion

This study is to measure cerebral hemodynamics during breath holding using the NIRS. While similar work has been done by other research groups previously to study hemodynamics with functional MRI and other NIRS systems, it was performed for the first time using LED-based NIR system.

In principle, during breath holding, the oxygen supply to the whole body is obstructed. This causes an increase in pCO_2 and a decrease in pO_2. As the brain cells are sensitive to pCO_2 change, an increased level of pCO_2 causes vasodilation and an increase in global CBF (cerebral blood flow) [13, 14]. This explains a global increase in ΔHbt, which is correctly recorded for all participants in my study. ΔHbO_2 and ΔHb were found to vary among some participants. For most (n=12) of the participants, there was an increase in ΔHbO_2 during the breath hold, and sometimes this increase was persistent a few more seconds after re-breathing. But it was found that for 3 participants, there was opposite behavior in ΔHbO_2, i.e., a decrease in ΔHbO_2 during the entire period of breath hold. The breath hold time for these individuals was found to be much longer than the others. Moreover, during the breath hold period, all participants but one had an increase in ΔHb.

Statistical analysis was done to find out relationship between breath holding time and the amount of hemodynamic changes occurring inside the skull. There was no evident correlation between the time during which the breath was held and the maximum levels of changes in ΔHbt (Figure 2.29). Similarly, no relationship was found between the breath holding time and the time after re-breathing at which maximum

change in ΔHbt occurs (Figure 2.30). Furthermore, student T-test was done to verify that there was a significant difference between the average baseline readings (temporally and spatially) and the average maximum values (spatially) of ΔHbt, ΔHb, and ΔHbO_2. Alpha value was chosen to be 0.01, and the p-values were 2.88E-05 for ΔHbt, 0.003825 for ΔHb, and 0.00032 for ΔHbO_2, respectively. The fact that the p-values are much less than the alpha value indicates that there is a significant difference between the baseline reading and the maximum values of respective parameters.

2.7 Conclusion and Future Scope

It was concluded from the results that an LED based continuous wave system (LEDI) is capable of measuring hemodynamic changes occurring inside the human skull, on the pre-frontal lobe, during breath holding. This provides us with confidence to apply the LEDI for brain activity studies, such as monitoring brain functions during mental cognitive tasks, even during physical exercises. Other clinical applications include the use of this system for sleep apnea detection, where a similar condition to breath hold takes place. Indeed, an NIR frequency-domain system has been applied to sleep apnea study earlier [15]. Another possible clinical application is the use of this system to monitor syncope, which is temporary loss of consciousness and posture, described as "fainting" or "passing out." It is usually related to temporary insufficient blood flow to the brain. This neurological disorder is a common problem, accounting for 3 percent of emergency room visits and 6 percent of hospital admissions [16].

After being confident about the LEDI system, we have made effort to explore a new application of NIRS, i.e., an attempt to use a continuous wave NIR system to measure hot flash condition in women. As the second stage of my research, I will describe the phenomenon of “Hot Flashes” and the feasibility measurement using the LEDI NIR system.

CHAPTER 3

HOT FLASHES

3.1 Background

Hot flashes (also known as vasomotor, menopausal or climacteric symptoms) are the most reported symptom of menopausal transition [17]. A hot flash can be defined as subjective and transient sensation of heat, most commonly felt in upper chest and head [18]. It causes cutaneous vasodilatation and a subsequent drop in the temperature set point in hypothalamus. Hot flashes may be accompanied by sweating, flushing, palpitations, anxiety, irritability, and may even cause panic [19]. Though there is a sensation of heat during the occurrence of hot flashes, body temperature actually falls due to sweating and vasodilation, thus they are often followed by chills [22]. All the above symptoms, when occurring during the night, can lead to frequent disturbances in the sleep resulting in discomfort and irritability throughout the day and can affect the work efficiency and behavior of a person. Hot flashes thus are a major reason for medical advice in menopausal women [22].

Studies have shown that up to 80% of the women may experience this symptom [18]. Another study showed that almost two third of postmenopausal women have hot flashes, and 10-20% of them find it nearly intolerable [19]. It is estimated that during the next five decades, 27 to 37 million American women may experience menopausal

hot flashes [21]. Although hot flashes are a frequently discussed problem, there is not much known about the pathophysiology of hot flashes.

3.2 Occurrence of Hot Flashes

The hot flashes are randomly occurring phenomena. The duration, intensity, or frequency of occurrence may vary between any of two subjects or from one subject over time [20, 22]. Hot flashes can last from a few seconds to up to an hour. They can be very mild to very intense, though the quantification of severity is very subjective. The average duration of one hot flash is about 4 minutes. They may occur several times a day, once a day, once a week, or they may never occur after one or two times. In some women, hot flashes may keep occurring for up to ten years [20, 22].

In women, hot flashes can begin during early perimenopause or late premenopausal years, but they become more severe and frequent during early postmenopausal years [19]. Apart from menopausal women, those who have undergone ovariectomy and some women during pregnancy and immediately postpartum also report hot flashes [24]. Hot flashes are also a common problem in men with prostate cancer who undergo androgen deprivation therapy (ADT) [27].

There are external factors like psychological stress, hot and humid whether, being in a confining space, consuming caffeine, alcohol, or spicy foods which are reported by some women to trigger hot flashes [23, 24].

3.3 Physiology of Hot Flashes

The core body temperature is regulated to meet the temperature set point of our body. In case the core temperature increases, there is stimulation of heat loss by sweating and cutaneous vasodilation. When the core temperature decreases, heat conservation is stimulated which causes cutaneous vasoconstriction and shivering [25]. It is believed that hot flashes result from a sudden perturbation of the body's temperature set point in hypothalamus. This transient change causes heat loss responses to be stimulated. As a result, there is a sensation of intense heat, cutaneous vasodilation, and sweating. Other physiological changes that are accompanied are drop in skin resistance, increase in heart rate and peripheral (skin) blood flow. When the set point returns back to normal, the body temperature has already fallen down due to the heat loss responses. Thus there is a sensation of chill or shivering to bring body temperature back to normal [24].

Though there is a change in the temperature set point followed by the thermoregulatory response as explained above, the exact pathophysiology of why it happens has not been explained as yet. Several independent studies have shown the dependence of hot flashes on various factors such as hormones (like estrogen) and neurotransmitters (like norepinephrine). During menopause, there is a decreased secretion of gonadal steroids. Gonadal steroid replacement therapies like estrogen replacement therapy (ERT) have proved to be the most effective treatment for hot flashes. Testosterone presence in sufficient levels also reduces the hot flashes [26]. But the levels of estrogen are low in women who are not suffering from hot flashes, thus

level of estrogen alone does not indicate the trigger for hot flashes. A change in the concentration rather than the absolute concentration of estrogen is believed to be more important [23].

Hot flashes are also associated with increased levels of norepinephrine level in the brain. Animal studies have shown that injection of norepinephrine in the brain (hypothalamus) induces conditions similar to hot flashes. There is also an established relation of glucose levels to the hot flashes. Hypoglycemia induction in rat showed symptoms similar to hot flashes. A study conducted on post menopausal women also suggested that an increase in blood glucose level helped reducing hot flashes significantly in post menopausal women. Hot flashes are also thought to have an effect on neuronal degeneration and subsequently cognition [26].

As stated above, there are multiple complex changes occurring during the hot flashes, but more research is needed to understand the exact mechanisms causing them.

3.4 Measurement of Hot Flashes

Hot flashes can be measured using either subjective measurements or objective measurements or both. Subjective measurements are self reported data which are collected using surveys which include daily diaries or electronic monitoring devices. There have been different kinds of surveys which have been used for different hot flash studies, but not all of them have been validated. Some of them are Blatt-Kupperman index, Women's Health Questionnaire (WHQ), Menopause-specific Quality of Life (MENQOL) questionnaire etc [17, 21]. Objective measurements are done by measuring

certain physiological factors which may indicate the occurrence of a hot flash event. There are different parameters that can be measured for hot flashes, such as sternal skin conductance, respiratory exchange ratio, skin temperature, core body temperature, sweat rate, and etc. All of them involve different sensor technologies and have varying degrees of flexibility and complexity [27]. An ideal objective measurement for hot flash would be preferably non-invasive (for subject's comfort), be correlating well with the subjective measurement, should be specific to hot flashes so that there are no false readings, and should be suitable for long term ambulatory measurements. An objective method used which is close to the above stated properties is the sternal skin conductance monitoring device, the Biolog instrument, which measures sternal skin conductance using skin electrodes [17].

There are certain limitations of both objective and subjective measurements which need to be overcome. Objective measurements available so far can provide the instance of occurrence of hot flashes but cannot provide information about the duration of the hot flash experience, intensity of the event, and effect on the activity of daily living [17]. Also, subjective measurements are influenced by the external factors like mood and level of stress, which may affect the assessment of severity of the event. In the experiments where both the subjective and objective measures are used for hot flash studies, it was found that there was a significant underreporting of the frequency of hot flashes from self reported data [18].

Thus there is a need of an objective instrument that can give information about frequency, amplitude, and duration of hot flashes and is less susceptible to noise or false reading from external factors in laboratory as well as ambulatory settings.

3.5 Measurement Using NIR Spectroscopy

As discussed in section 3.1, blood rushes through the upper part of the body during a hot flash. Since the rush of blood is cutaneous, a good change in blood flow on the upper chest surface can be expected. Thus, measuring blood flow over the chest could provide useful information about hot flashes. Here, we proposed to measure hot flashes using a continuous wave NIRS system that is capable of measuring relative changes in the oxy and deoxy hemoglobin levels. As explained in chapter 2, we can also estimate changes in blood flow (or volume) using these two factors. The penetration depth of the continuous wave NIRS system is a little more than a centimeter if the source and detector separation is about 2 cm. Since the changes occur at the surface level, which is comparable to the penetration depth of the NIRS system, we expect to capture the changes occurring during a hot flash episode. Based on the above discussion, we tried to measure hot flashes with the existing LEDI system which is described in chapter 2.

In order to prove the hypothesis that a continuous wave NIRS system is capable of measuring hot flashes, four menopausal women experiencing hot flashes were recruited and tested with our device at the Institute for Aging and Alzheimer's Disease at the University of North Texas Heath Science Center, Fort Worth. The probe was

placed on the upper chest (sternal region) of the female subjects. Two women did not report any hot flashes during the measurement period of one hour. One woman had a very mild hot flash (as reported by the subject), and one reported a moderate hot flash.

3.5.1 Results and analysis

The data obtained were analyzed using a MATLAB program (Appendix A). Data was acquired for duration of about one hour, but it was clipped for the period of 14 minutes during which the hot flash event occurred. A fourth order low pass butterworth filter (available in the MATLAB) was used to remove high frequency noise which could be due to heart rate or transient motion. The cut off frequency was chosen with trial and error method and was selected to be 0.03 Hz. Figures 3.1 through 3.16 shows the data from all 16 channels. The blue marker represents the time at which the subject reported hot flash.

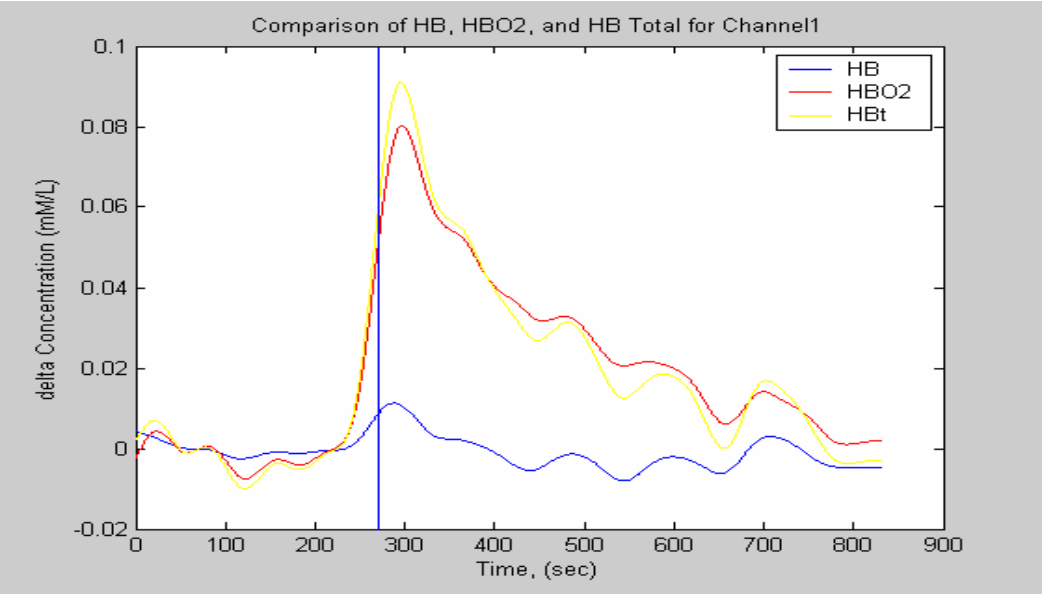

Figure 3.1 Plot of Hb, HbO2 and Hbt for Channel 1

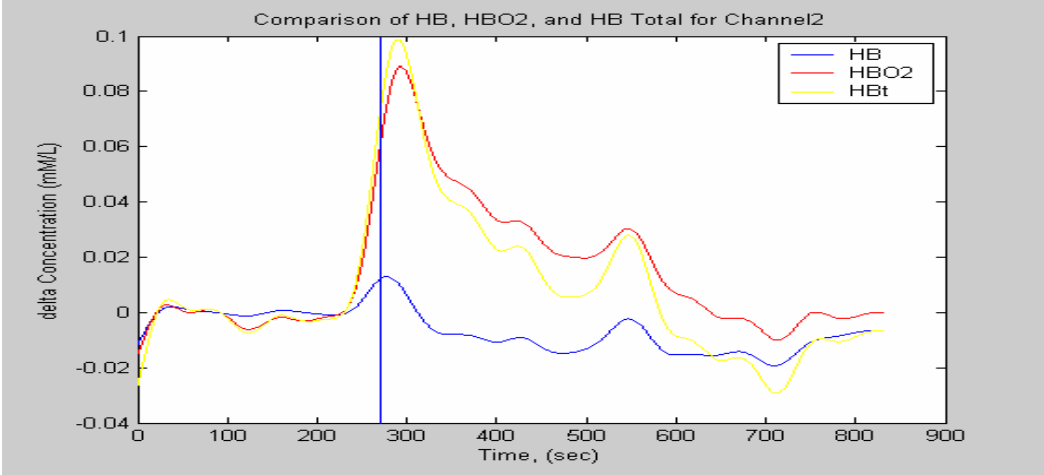

Figure 3.2 Plot of Hb, HbO2 and Hbt for Channel 2

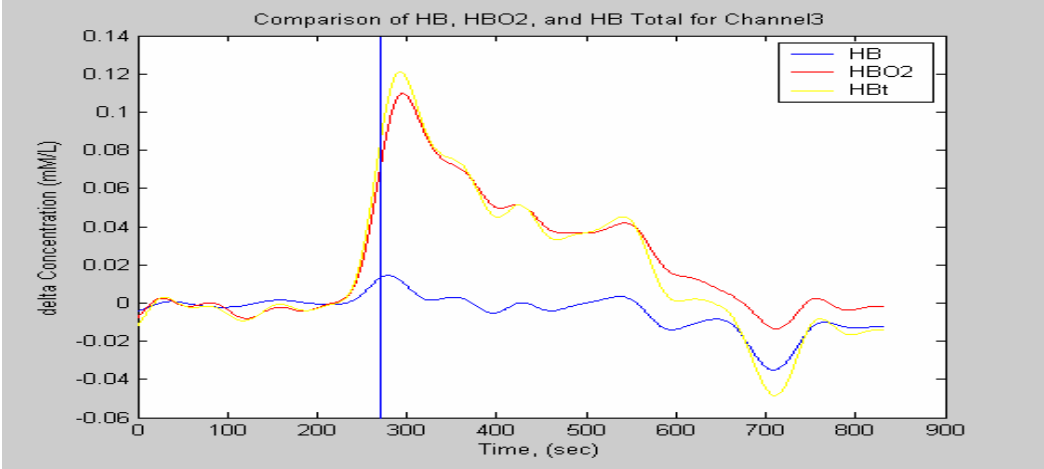

Figure 3.3 Plot of Hb, HbO2 and Hbt for Channel 3

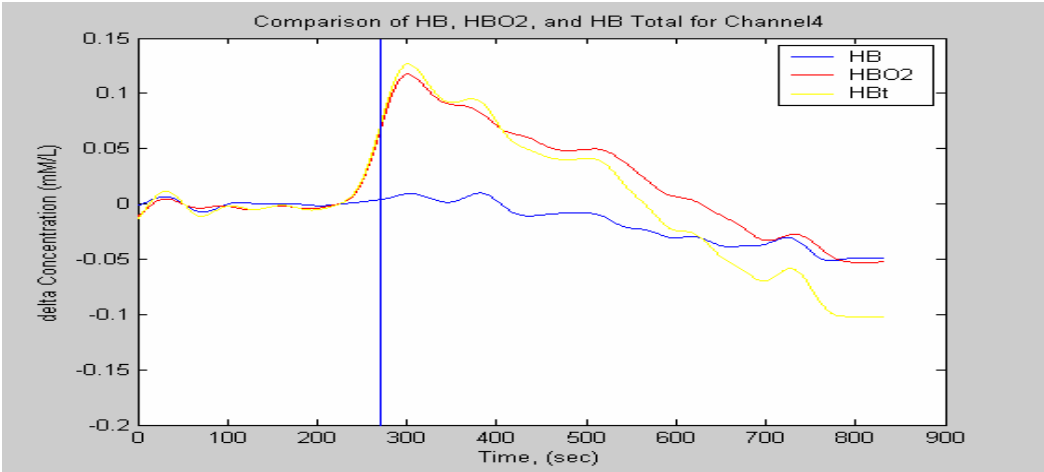

Figure 3.4 Plot of Hb, HbO2 and Hbt for Channel 4

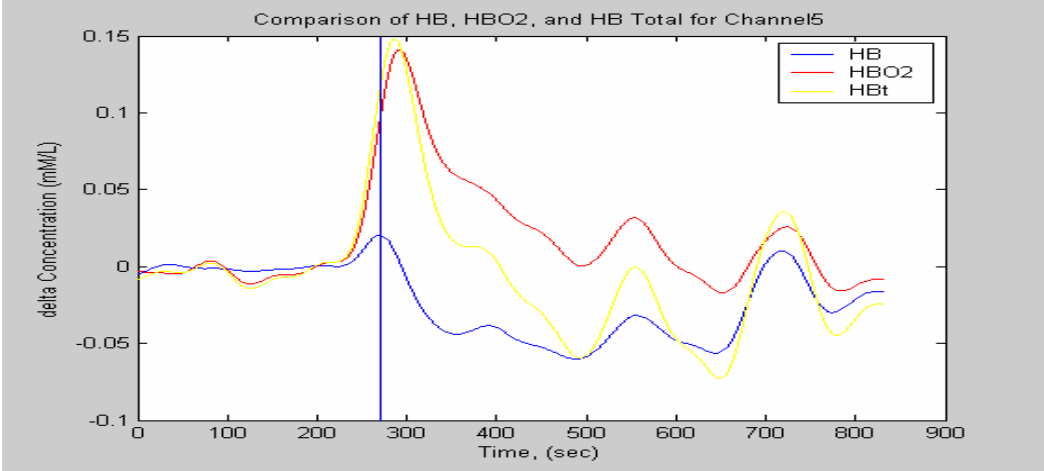

Figure 3.5 Plot of Hb, HbO2 and Hbt for Channel 5

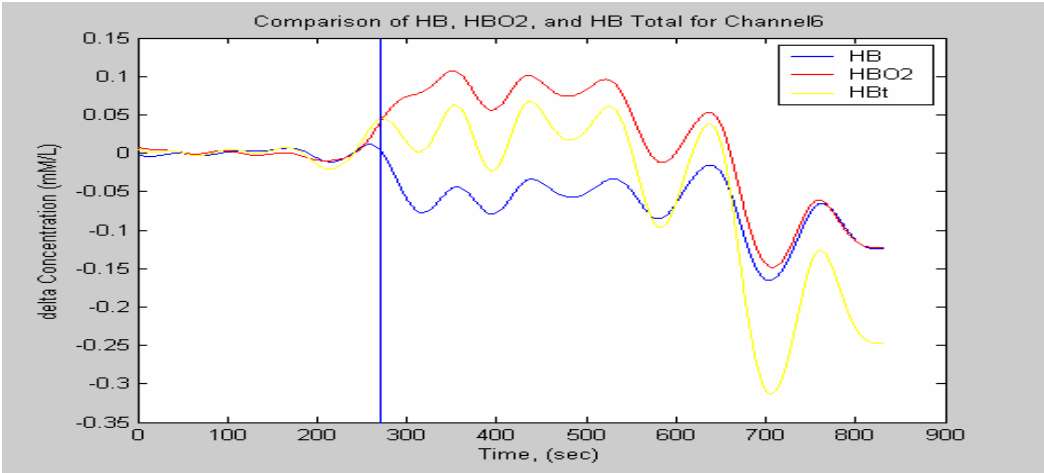

Figure 3.6 Plot of Hb, HbO2 and Hbt for Channel 6

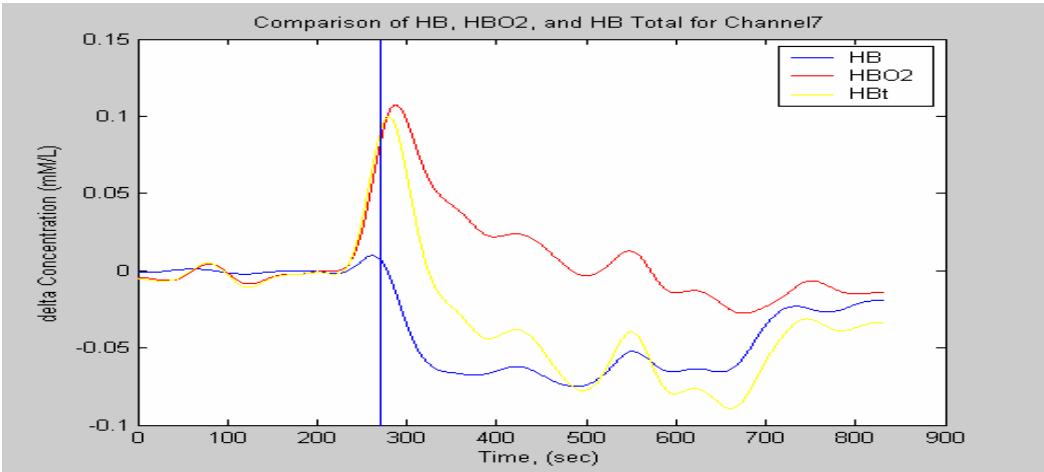

Figure 3.7 Plot of Hb, HbO2 and Hbt for Channel 7

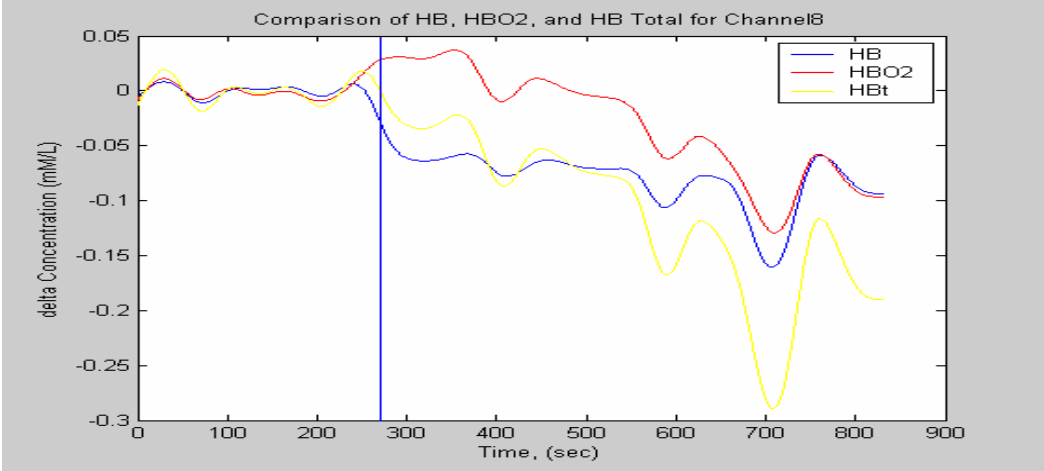

Figure 3.8 Plot of Hb, HbO2 and Hbt for Channel 8

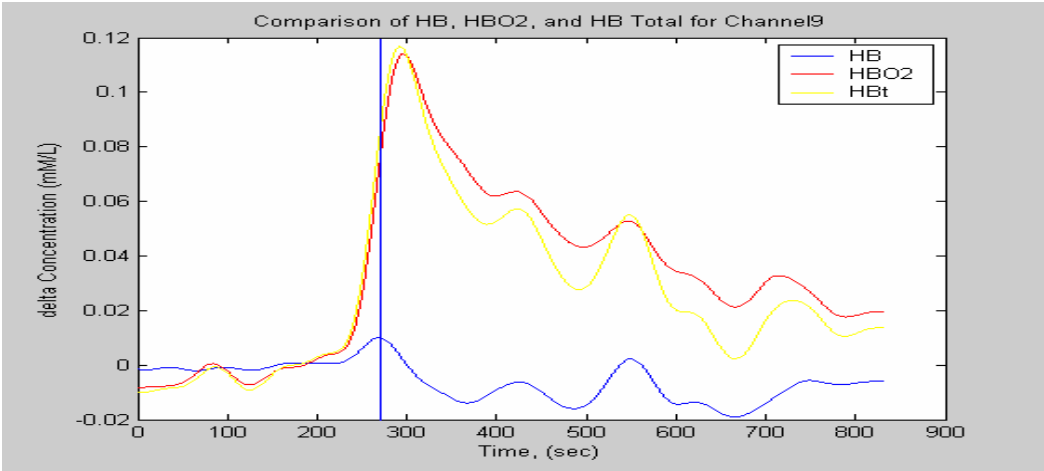

Figure 3.9 Plot of Hb, HbO2 and Hbt for Channel 9

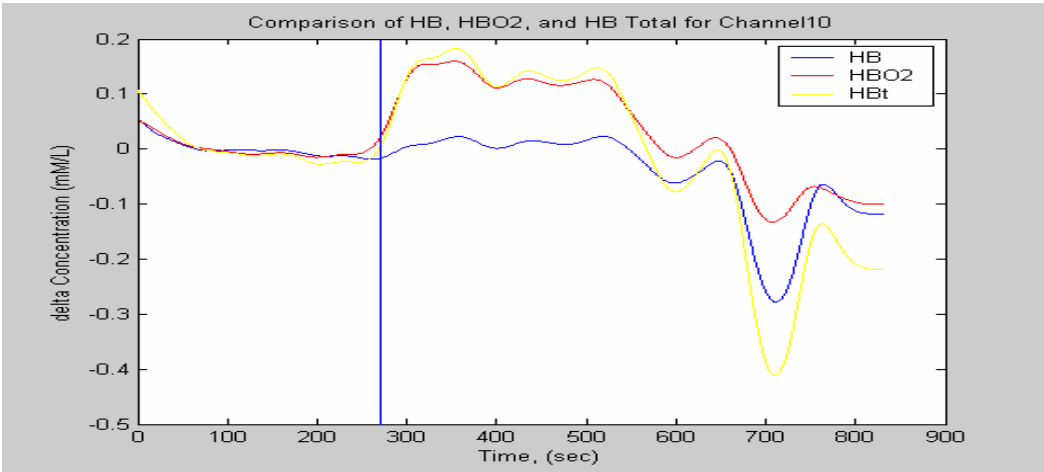

Figure 3.10 Plot of Hb, HbO2 and Hbt for Channel 10

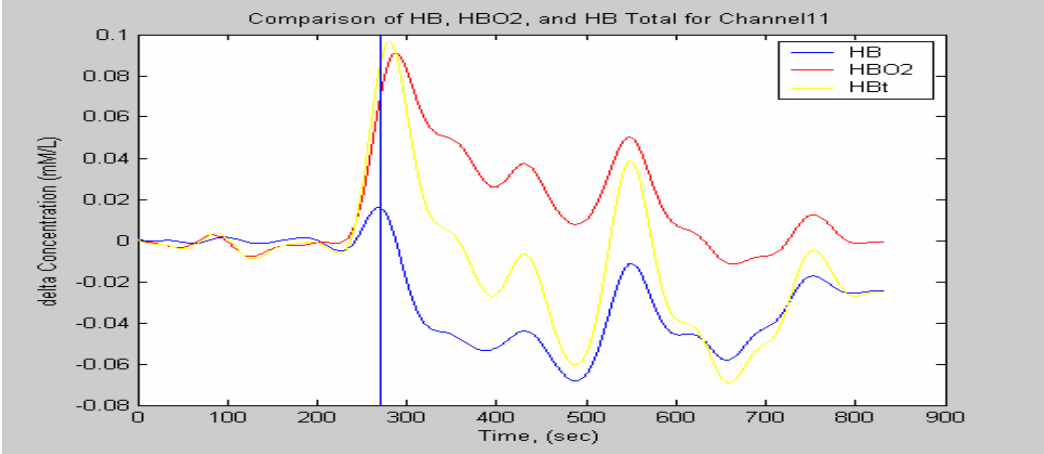

Figure 3.11 Plot of Hb, HbO2 and Hbt for Channel 11

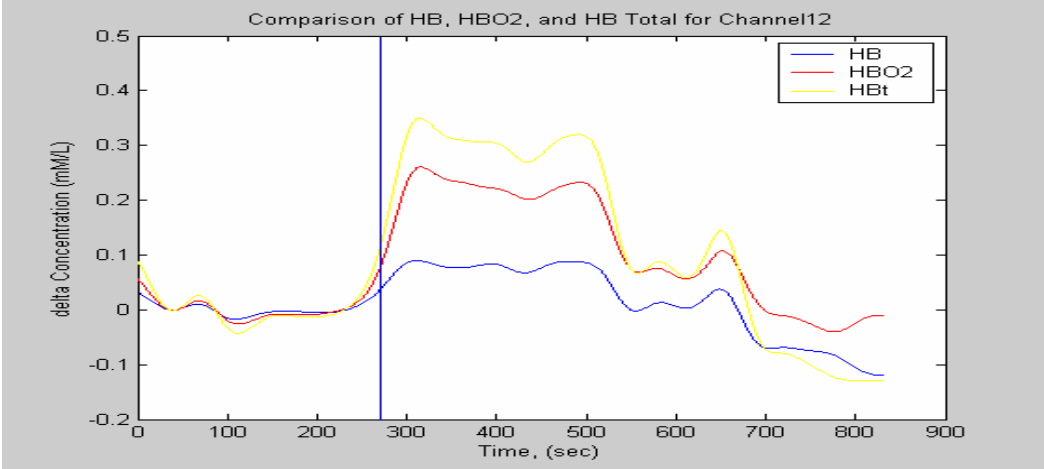

Figure 3.12 Plot of Hb, HbO2 and Hbt for Channel 12

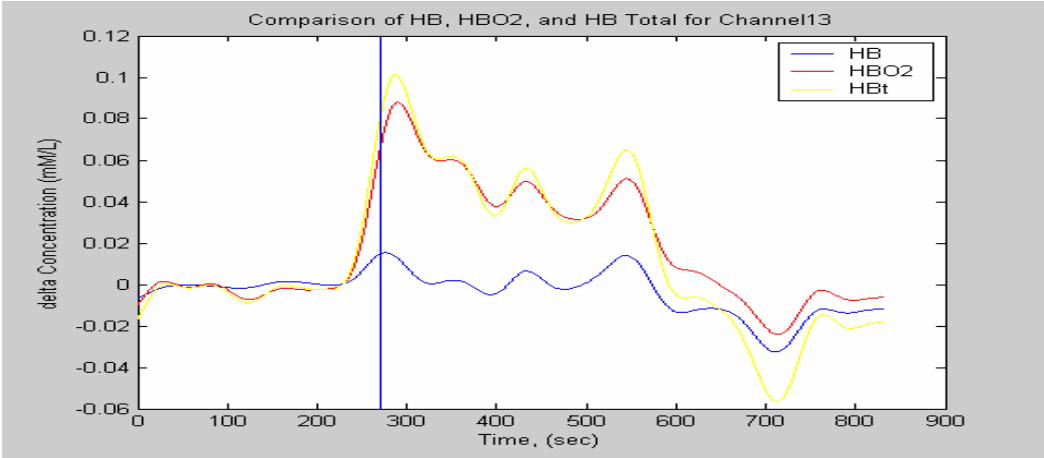

Figure 3.13 Plot of Hb, HbO2 and Hbt for Channel 13

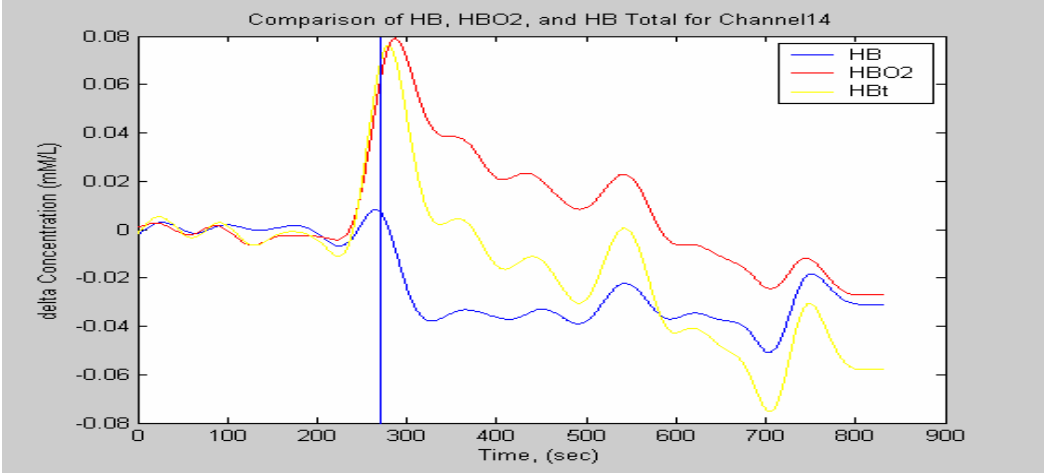

Figure 3.14 Plot of Hb, HbO2 and Hbt for Channel 14

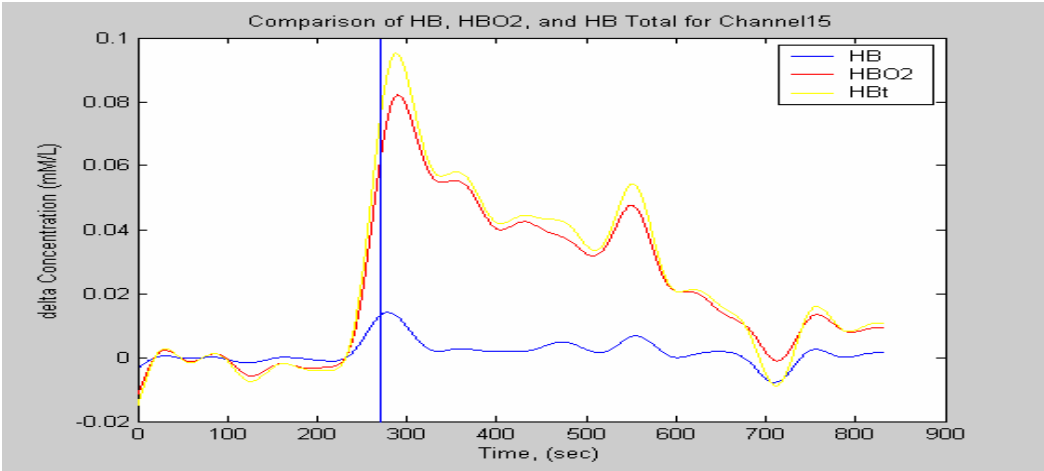

Figure 3.15 Plot of Hb, HbO2 and Hbt for Channel 15

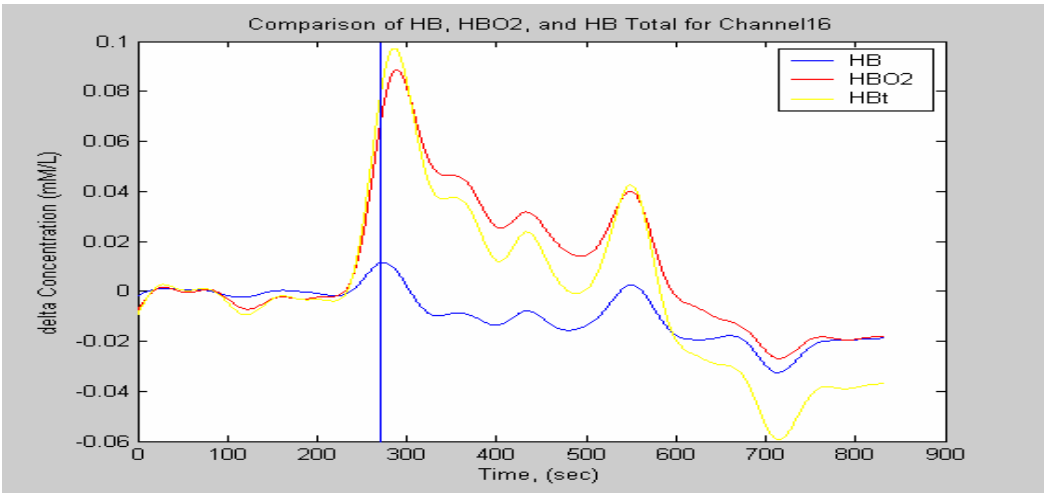

Figure 3.16 Plot of Hb, HbO2 and Hbt for Channel 16

As seen in Figures 3.1 to 3.16, all the channels except channels 6, 8, 10 and 12 recorded very similar patterns, showing a sudden increase in blood volume as soon as the hot flash is reported. After a few minutes, the increased signals slowly come back to the baseline, and they even go below the baseline at around 720 sec (about 9 minutes after the hot flash was reported). This is very much consistent with the hot flash symptoms that heat triggered vasodilation to give rise to blood volume increase, followed by a feeling of chill caused by vasoconstriction (leading to blood volume decrease).

The inconsistency in data for some channels such as 6, 8, 10 and 12 can be attributed to the fact that the length of the probe is large, even enough to cover the whole chest. Since the surface of the large probe is not perfectly flat and stationary, any body motion may cause artifacts and distortion of the detected signals. This effect mostly occurred for the probes located in the center of the upper chest, as the places near channels 8, 10, and 12. The LEDI probe used is not particularly designed for such kind of the measurements taken from the chest area, but the attempt here is to explore the ability and feasibility of a continuous wave NIRS system to capture hot flashes, which is achieved successfully.

From the above discussion and the presentation of data, it can be concluded that it is possible to measure hot flashes using a continuous wave NIRS system. To carry on further research, in particular for a long term monitoring purpose, there is a great need to develop a flexible and compact probe that can be applied to the sternal area without much discomfort and be able to capture data continuously and in ambulatory conditions.

As a first step towards the application of NIRS for hot flash measurements, an in-house, low-cost, compact NIR (LCC-NIR) system was built with a probe having a single source chip and four detectors, as the last part of my research work. The new probe developed through the LCC-NIR system can be placed anywhere in the upper chest area. The complete prototype would be capable of measuring hot flashes in laboratory conditions and has a potential to be made wirelessly in the future. The development of the LCC-NIR system is going to be described in chapter 4.

CHAPTER 4

IN-HOUSE SYSTEM DEVELOPMENT

4.1 Need for the System

In Chapter 2, an existing system, LEDI, was used for the brain study. Certain limitations of the system led us to the idea of designing our own system for broader applications. The design of the LEDI probe limits the use to mainly the forehead. If we have our own system, we can design probes for a particular region of body using a variable number of detectors and light sources to target a specific application. In this way, we will have more flexibility to conduct experiments in different set-ups for different biomedical applications. Also, the LEDI system is relatively costly, and it could cost more to have the custom probes made. After I looked at the requirements of the hardware and software, I believed that it is possible to build our independent system at a relatively low cost. This is why I built a LCC-NIR system as a major part of my thesis work.

4.2 System Requirements

The probe for our present design consists of 4 photo-detectors and one light source. The source is a tri-wavelength LED, emitting light at 730 nm, 805 nm, and 850 nm. Both detected signals at 730 nm and 850 nm can be used for the calculation of Hb and HbO_2 using the equations described in Chapter 2. The wavelength of 805 nm is

considered to be the isobestic point at which the absorption by both kind of molecules (Hb & HbO_2) is same [27]. Thus by taking measurement at this wavelength, we can get a direct approximation of changes in blood volume. The probe was designed keeping in mind the "Hot Flash Application", which was discussed in detail in Chapter 3.

The aim of the design for the new probe was to acquire the data from multiple (four) channels while the LED light source switching between the three wavelengths, two NIR light and one background without light. The frequency of acquisition was kept as 5 Hz for one set of data, which consisted of 12 data points for each LED source (three data points from three wavelengths at four detectors, 3x4=12). Actually, I started the development of a system with a single wavelength LED (at 850 nm) and later extended to the three wavelengths LED. Figure 4.1 shows a block diagram of the LCC-NIR system.

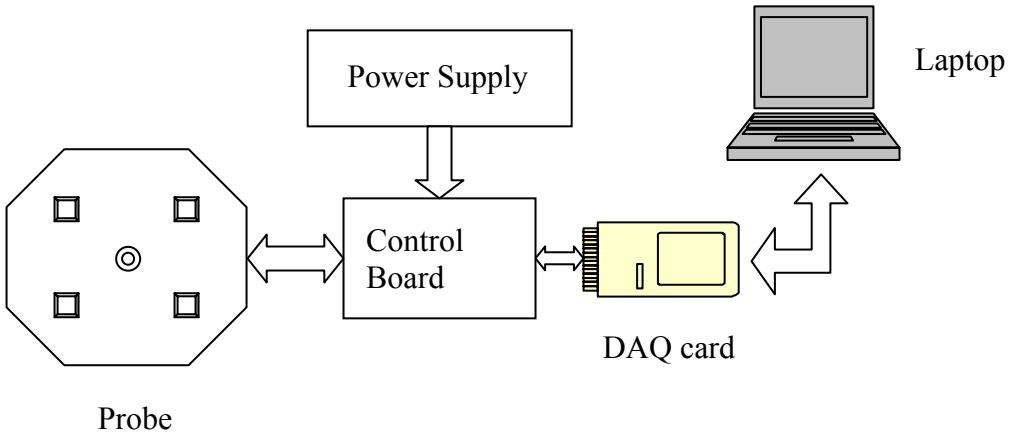

Figure 4.1 Block Diagram of the system

4.3 Hardware

The Hardware of the LCC-NIR system consists of four components (see figure 4.1): 1) a probe which has one light source and four detectors, 2) a control board that contains the control circuit for the LED and gain control for the detectors, 3) an NIDAQ card 6036-E used for data acquisition and triggering of the LED control circuit, 4) a power supply which provides ± 5V for the detectors and other components and 8V for the LED. Figure 4.2 shows pictures of the system.

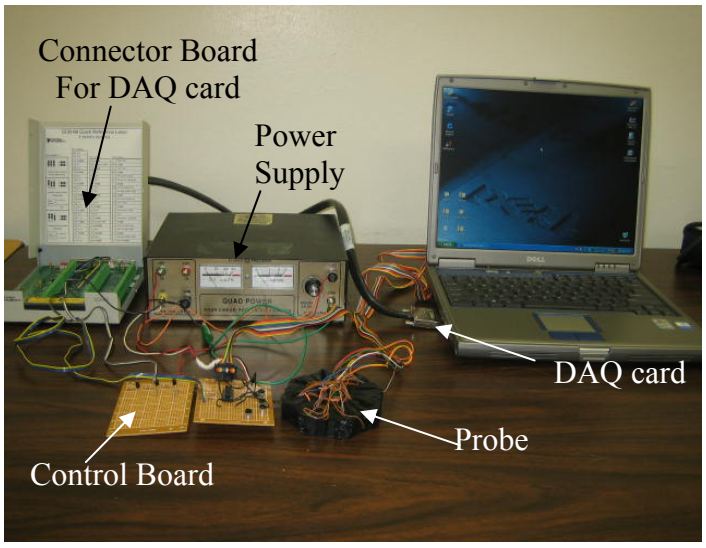

(a)

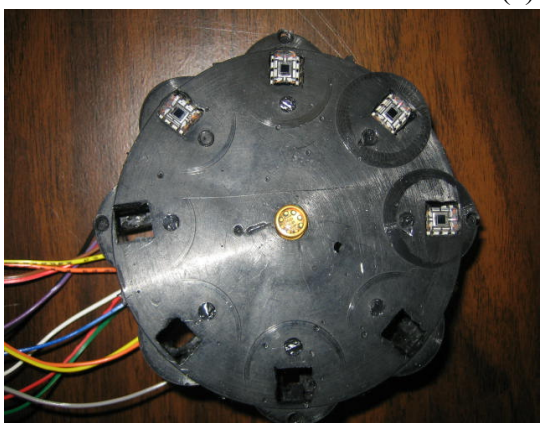

(b)

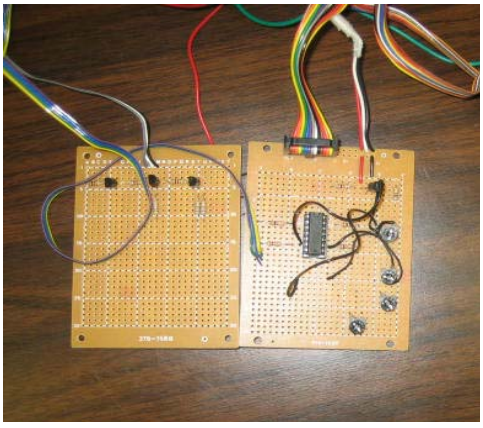

(c)

Figure 4.2 A picture of (a) the entire LCC-NIR system; closer look at (b) the probe and (c) the control board.

4.3.1 Probe

The application that is targeted here is for 'Hot Flash Measurement'. In order to measure the hot flashes, we need to place the probe on the upper chest (sternal area), where a change in blood hemodynamics is more significantly expected. The one-source and four-detector arrangement seems to be quite suitable for this kind of measurement.

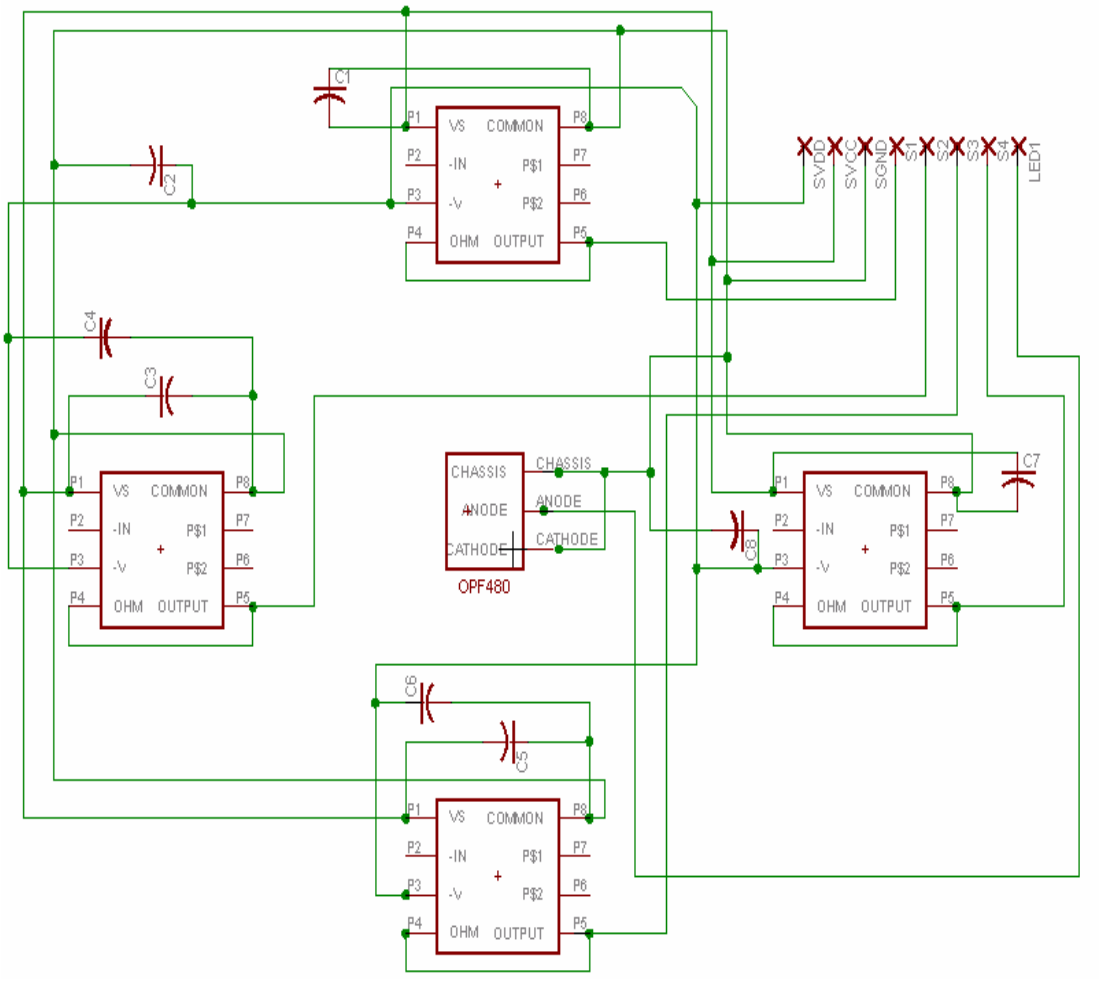

Figure 4.3 The Single-Wavelength Probe

Initially a probe was designed using a single wavelength LED OPF370A (Optek technologies), emitting at 850 nm and four detectors. Figure 4.3 shows a circuit diagram of the single-wavelength, four-detector probe.

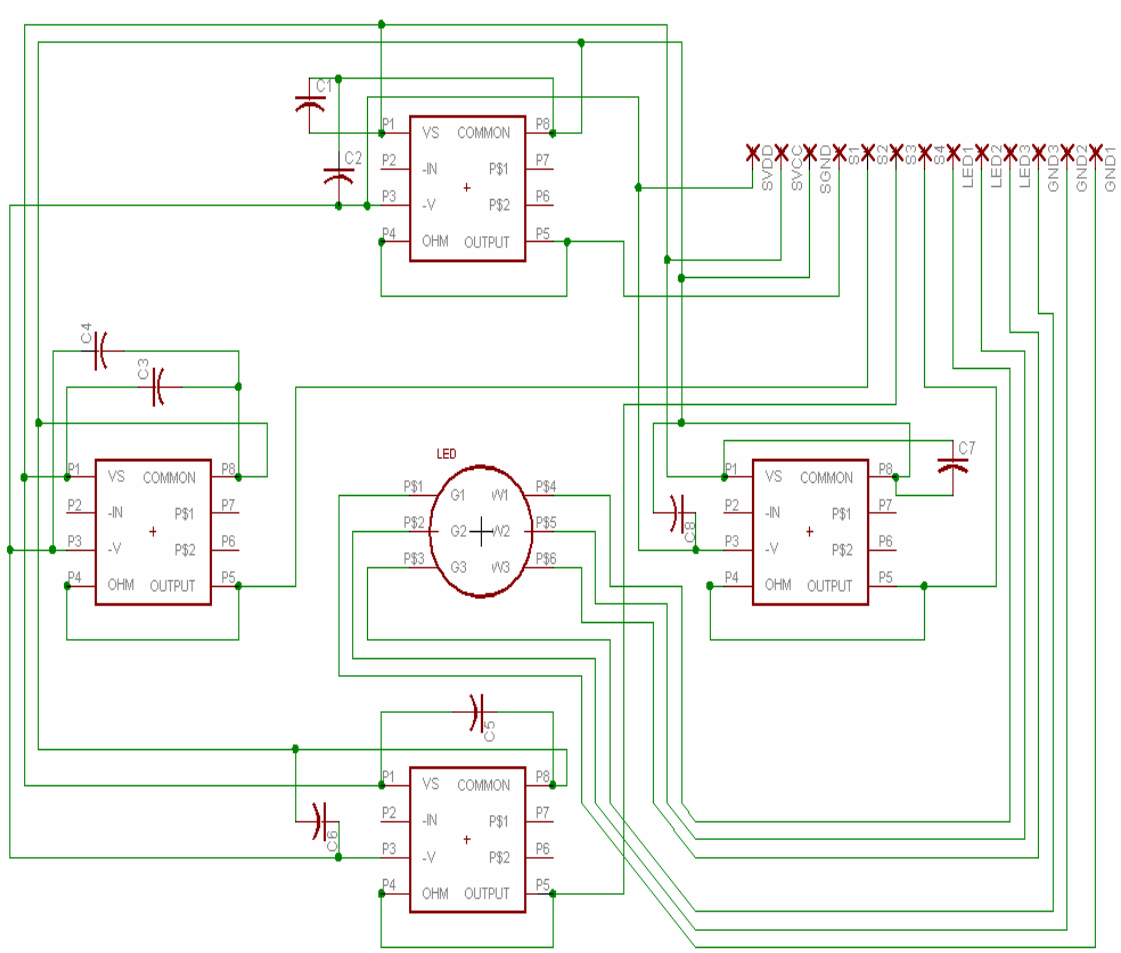

Figure 4.4 The Three-Wavelength Probe

As shown in Figure 4.4, the probe consists of one single wavelength LED in the center and four photo detectors on the side. The probe is connected to the control board which is explained later in detail. Only difference between the single-wavelength probe

and three-wavelength probe is the LED. For the three-wavelength probe, the LED used emits at three wavelengths (730 nm, 805 nm, 850 nm) (L4*730/4*805/4*850-40Q96-I Epitex Inc.). This kind of LEDs contains four chips made of AlGaAs for each wavelength. The detectors used for both of the probes are same and are connected in the same configuration. Figure 4.4 shows the circuit for the three-wavelength probe.

The detectors used were OPT101, which is a monolithic photodiode with on-chip transimpedance amplifier manufactured by Burr-Brown. The detectors provide a gain of 10^6 through an internal 1MΩ feedback resistor. The photodiode was connected in a bipolar power supply operation mode as shown below in Figure 4.5. A negative bias voltage to pin 3 improves the dynamic performance with capacitive loads. Also, the JFET connected between pins 5 and 3 allows the output to sink current which can be useful for driving capacitive inputs of some A/D converters [28]. ± 5 Volts were used to operate the detectors in this mode.

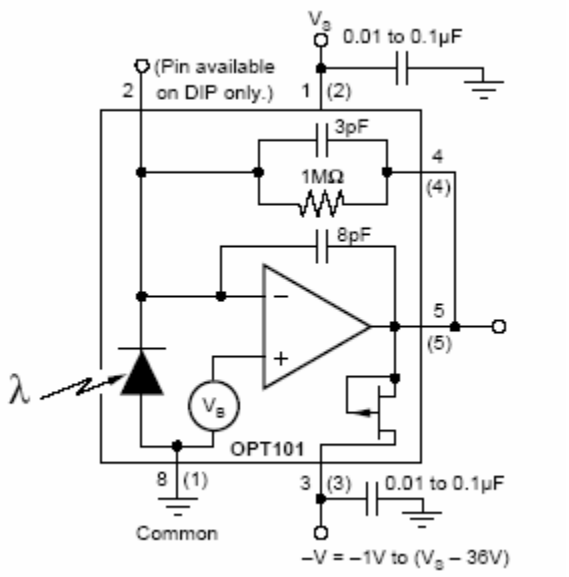

Fig. 4.5 Bipolar power supply circuit connections for OPT101

4.3.2 Control Board

The control board has two primary functions: firstly, to further amplify the pre-amplified signals from the photodetectors on the probe; secondly, to control the switch the LED on and off using the 5V input from the DAQ card.

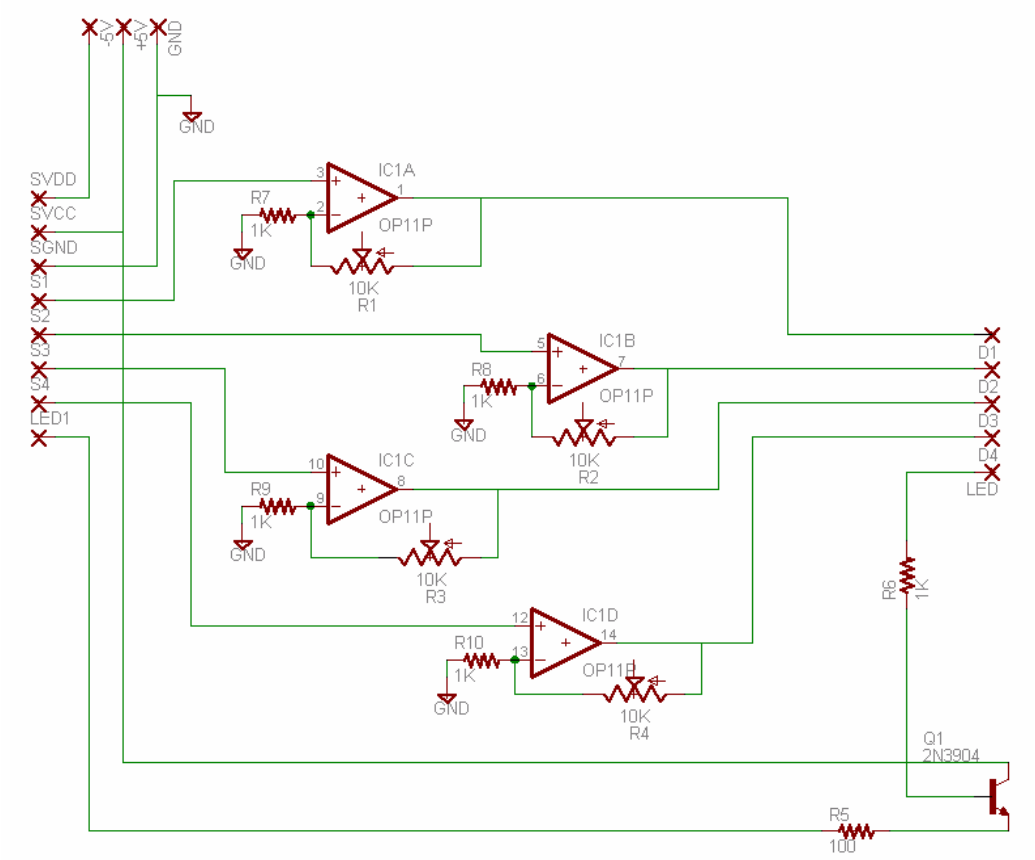

Figure 4.6 Control Circuit for the Single-Wavelength System

4.3.2.1 Amplification (Gain)

A TLC274 quad operation amplifier was used in the non-inverting mode to amplify the signals from the four photodetectors. The gain of the amplifier is kept

variable from 1 to 11 through a 10K potentiometer. In the non-inverting mode, gain of an amplifier is given by:

$$GAIN = 1 + R_2 / R_1$$

Therefore, if we have R_2 ranging from 0 to 10 KΩ, and if R_1 is 1 KΩ, we can have the gain adjustable from 1 to 11. The amplification circuit is the same for the single-wavelength as well as the three-wavelength probe, as seen in Figures 4.6 and 4.7.

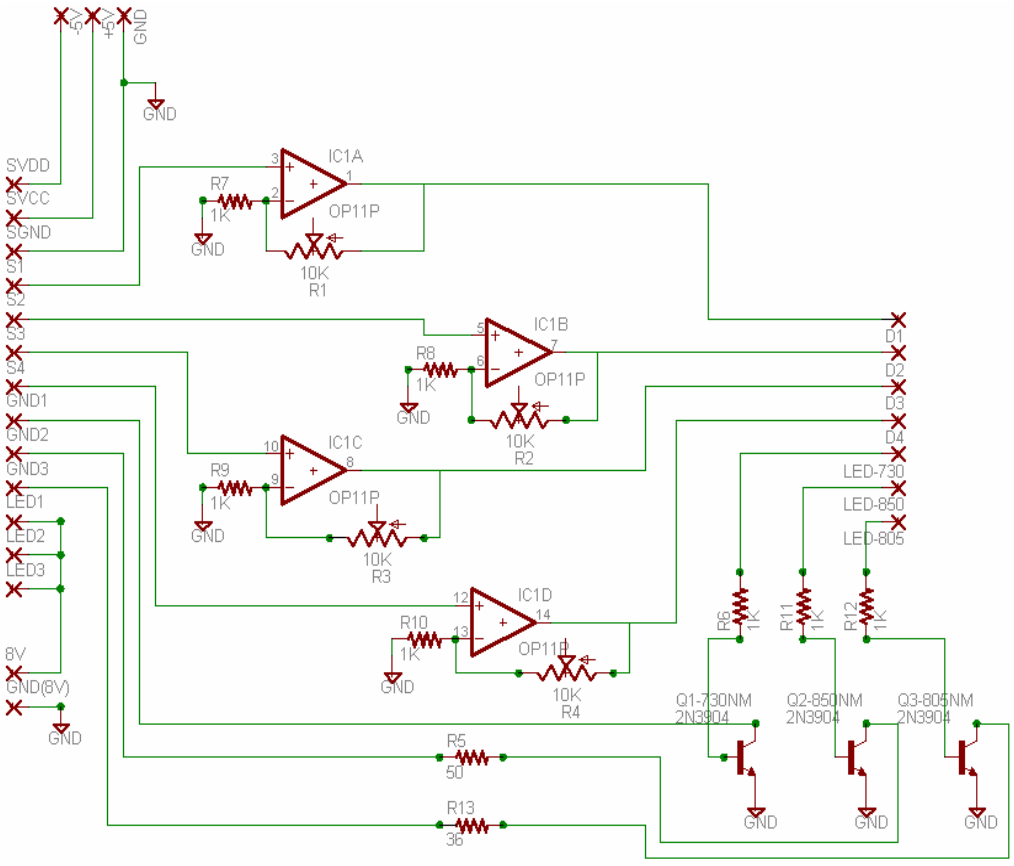

Figure 4.7 Control Circuit for the Three-Wavelength System

4.3.2.2 LED Control

In case of using single wavelength, only one LED (OPF370A) is to be controlled, and it is done using a BJT (bipolar junction transistor) as a switch as shown in figure 4.6. A 5V bias voltage is given by a line from digital port of the DAQ card through 1KΩ resistor to the base of NPN transistor 2N3904 to switch on the transistor. The LED is powered through the current flowing through the emitter when the transistor is switched on. A 100 Ω resistor is used to limit current to the LED.

For the three wavelengths, three switches are required which are controlled using three lines of the digital port on the DAQ card. The three NPN transistors are used as switches, and the 5V bias is given from the DAQ card through a 1 KΩ resistor. The anode of each LED is connected to 8V power supply as shown in Figure 4.7, and the cathode (ground) is connected to the collector of the transistor (please refer to Figure 4.4 if needed). When the transistor is switched on, the cathode of the LED is grounded through the emitter. For 850 nm and 805 nm, 50 Ω and 36 Ω resistors are added respectively to limit current through the LED's. Switching of the LED is software controlled through the DAQ card and LABVIEW.

4.3.3 DAQ Card

An NI DAQ card 6036-E is used for acquisition of the data after A/D conversion and for controlling the switching of the LED. The dynamic range of the DAQ card is 16-bit, so its resolution is $1/2^{16}$, leading to a signal to noise ratio of ~96 dB

(=20*log [2^{16}/1] dB). The DAQ card is controlled using a software code written in LABVIEW. The code is explained in the next section.

4.4 Software

National Instruments software LABVIEW 7.1 was used to program the DAQ card for data acquisition from the four detectors and to control the switching on and off of the LED.

4.4.1 Program for the Single-Wavelength Probe System

For the single-wavelength probe, the LED control is simply an on-off control that can be set through a line of digital out port. Data acquisition is taken at a rate of 5 points per second (5 Hz) per data set (from the four detectors), i.e. one data set is acquired every 200 ms. Note that one data set consists of 4 data points read from the four detectors for the single-wavelength probe. A flow chart for this code is shown in figure 4.8.

4.4.1.1 Front panel

Figure 4.9 shows the front panel for the program. The four graphs display the data for each of the four channels. “STORE DATA” button allows saving the acquired data in a spreadsheet file and then ends the acquisition. The LED control is for switching the LED on and off, when triggered through the digital out line selectable through the drop down menu. The “Chart Length” is a control that allows user to select

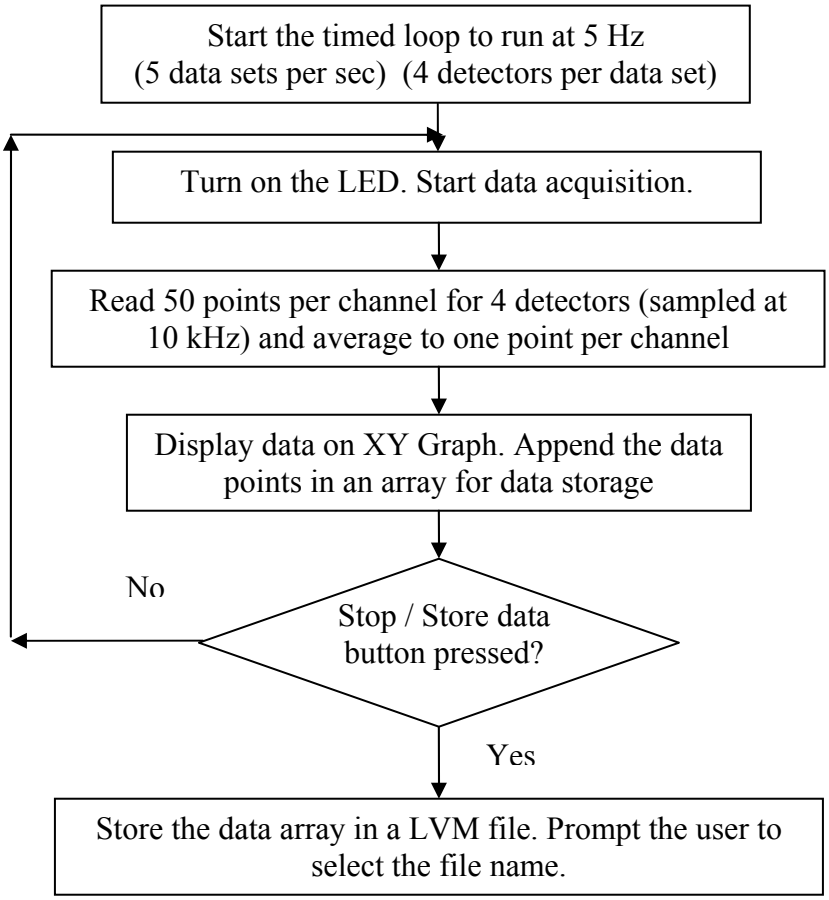

Figure 4.8 Flow Chart of interface code for the single-wavelength probe

the number of points to be displayed on each graph at a time. Time elapsed is an indicator to show elapsed time in seconds as the program is running. “STOP” button stops the program without storing the data. “Finished Late” indicates if there is a lag in data acquisition, i.e., if it takes more than usual 200 ms to acquire one data set (4 readings from the four detectors).

4.4.1.2 Block Diagram

The block diagram for the above front panel is displayed in two parts in figures 4.10 & 4.11. The diagram is labeled from step 1 to step 9 to make the explanation easy. Each step is explained as follows:

1. The 'Waveform Chart' variable is initialized using initialize array command, which will later be used for data storage. The timing loop is used, which uses a 1kHz source, and the period is selected to be 200 ms, i.e., the loop repeats every 200 ms.
2. Finished late indicator turns on the led indicator on the front panel in case the loop takes more than 200 ms to finish.
3. A voltage read task 'DATA_ACQUISITION' is used to create four analog input voltage channels connected in differential configuration. The task is set to acquire 50 samples per channel with a sampling rate of 10,000 Hz. Read data, which is 50 points for each channel, is then averaged out using a 'for' loop to give one point per channel per iteration.
4. A millisecond timer is used to calculate the x-axis for XY graph. Time elapsed in seconds is calculated by multiplying number of iterations with 0.2 (200 ms) and is displayed on the front panel.
5. Data obtained from step 3 is appended in each iteration to the array stored in variable 'waveform chart' which was initialized in step 1.

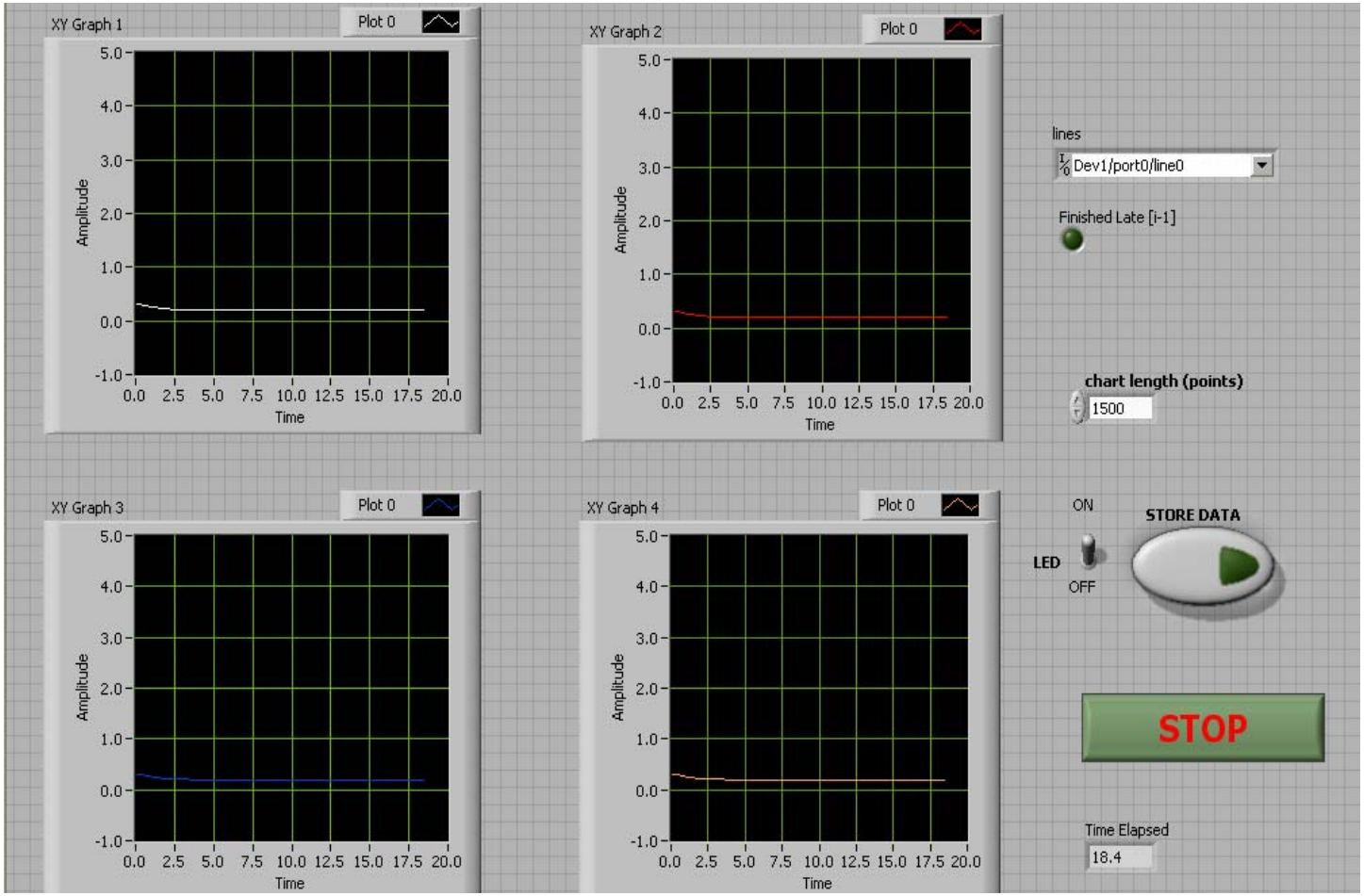

Figure 4.9 Front panel for Single wavelength code

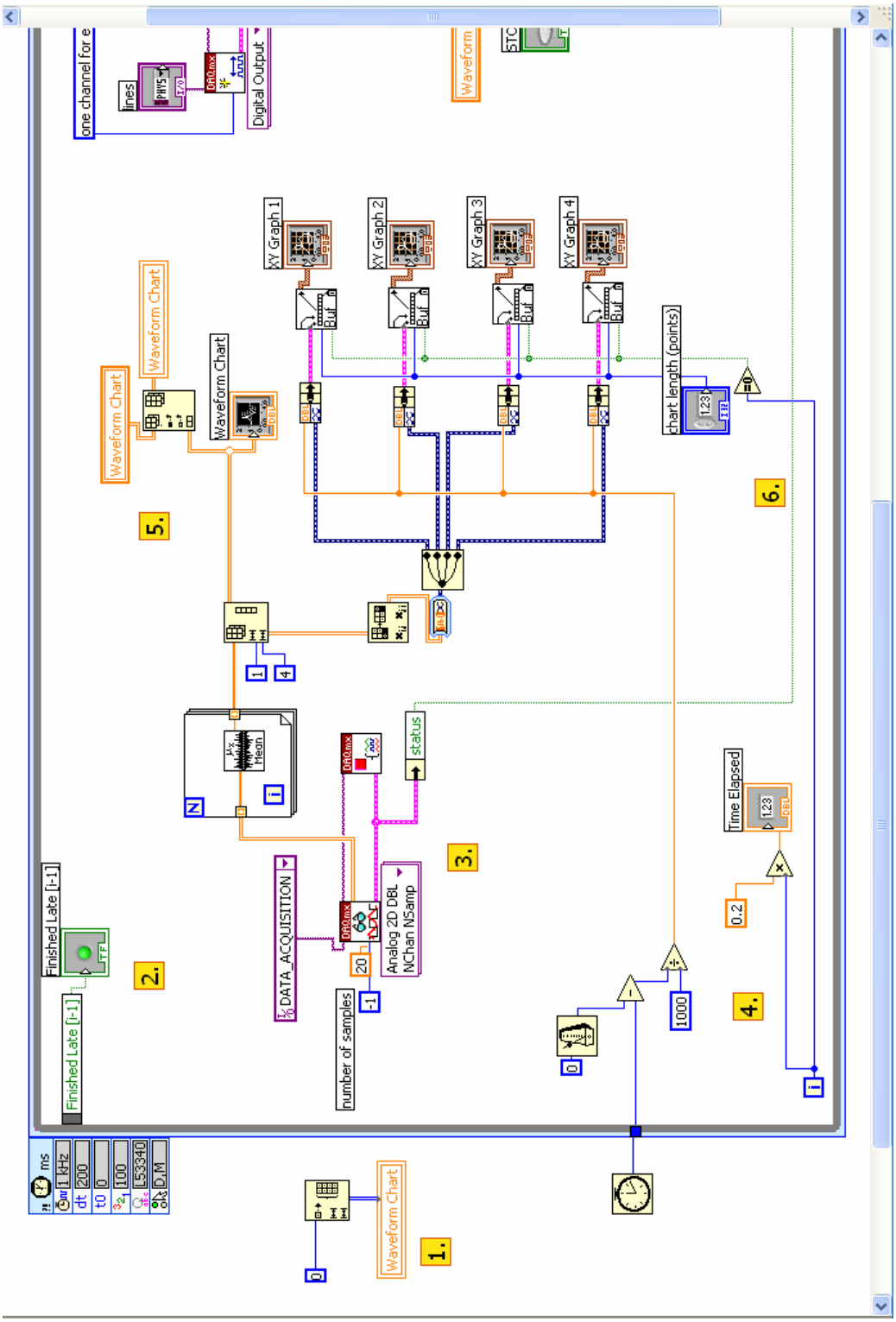

Figure 4.10 Block Diagram for Single wavelength code part 1

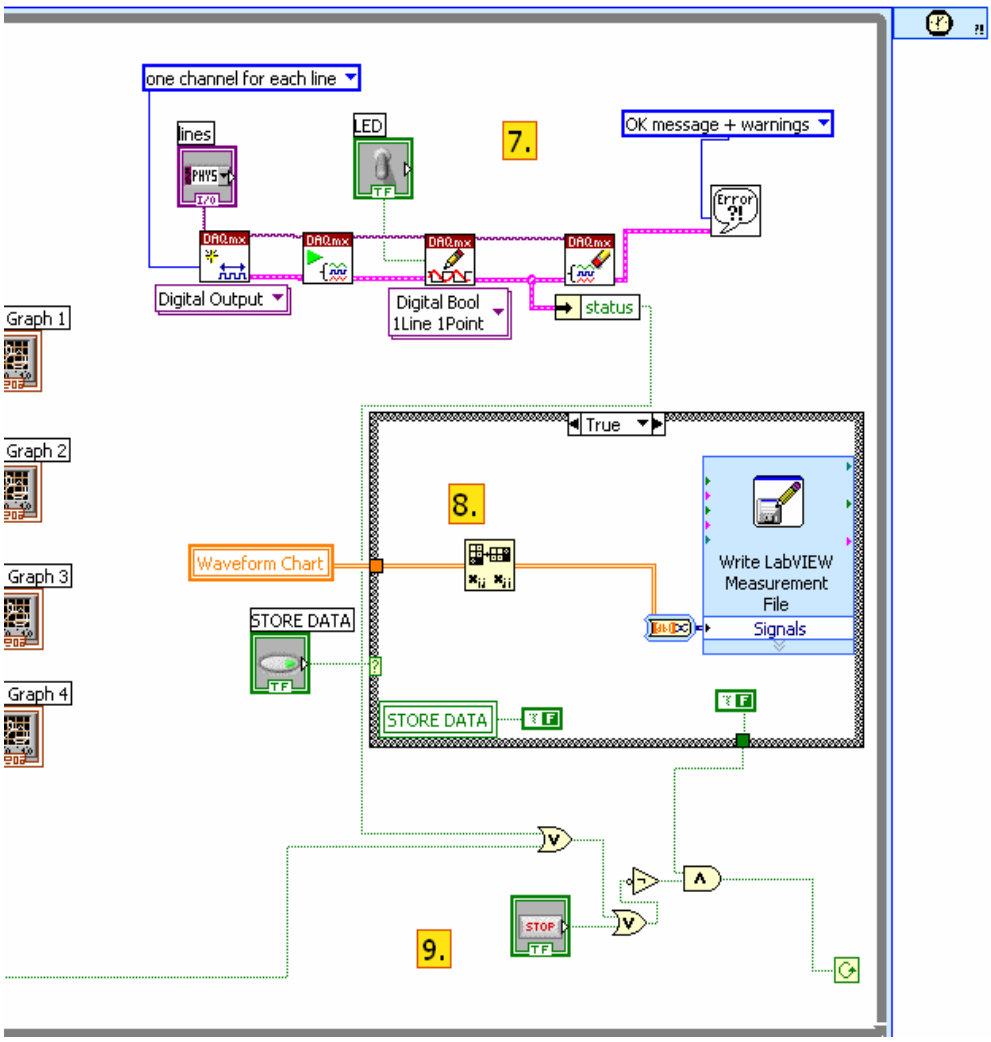

Figure 4.11 Block Diagram for Single wavelength code part 2

6. Four XY graphs are used to display the averaged out data on the front panel in real time for the readings taken at the four detectors. This step is parallel with step 5.
7. A digital output channel is created to switch on the LED, and the output line can be selected on the front panel by the user.

8. When “STORE DATA” control on the front panel is pressed, the case structure condition is true and data from ‘waveform chart’ is formatted and written into a spreadsheet file and the program stops execution.
9. The program stops in three conditions, if there is any error, or if the STOP button or STORE DATA button is pressed on the front panel.

4.4.2 Program for the Three-Wavelength Probe System

As explained in hardware (Section 4.2), in the three-wavelength probe system, we need to switch on the three wavelengths (730 nm, 805 nm and 850 nm) in sequence when each set of data (read from the four detectors) is acquired. In the three-wavelength probe case, one data set consists of 12 points, i.e. 4(detectors) X 3(sources). Data is acquired at a frequency of 5 Hz, i.e. one data set (12 data points) is acquired every 200 ms, but this frequency can be changed from the front panel. A flow chart for the three-wavelength code is shown in figure 4.12.

4.4.2.1 Front Panel

Figure 4.13 shows the front panel for the three-wavelength probe system. The program allows the flexibility to enter the frequency of acquisition and the duration of acquisition, which can be set through the controls of ‘Number of data sets per second’ and ‘Number of seconds to acquire’.

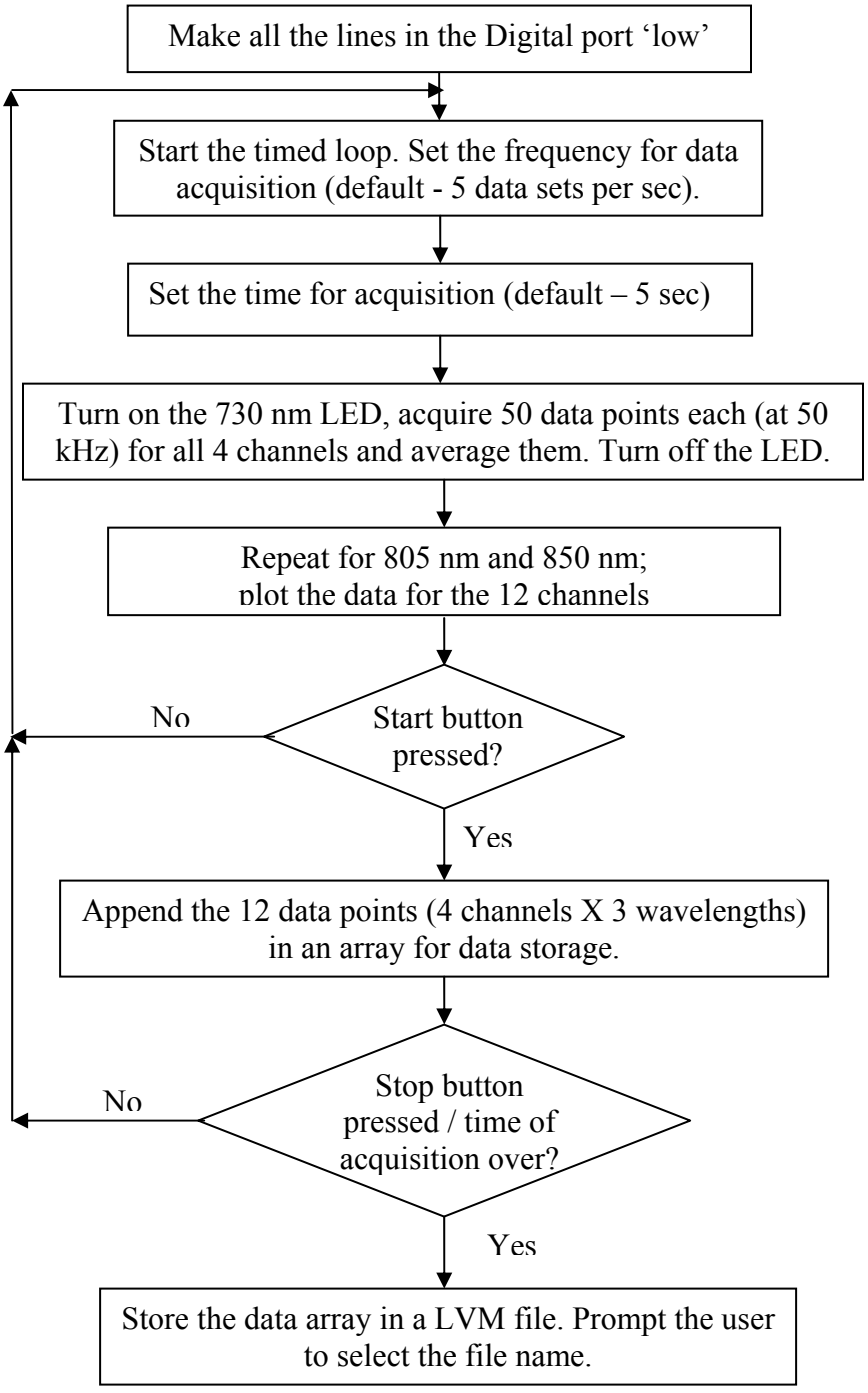

Figure 4.12 Flow Chart of interface code for the three-wavelength probe

The first graph ‘Mean data from four channels’ displays the mean data from four channels (detectors) as it is acquired, i.e. without separating the data for each wavelength. This gives an idea of the voltage levels before the acquisition so that the gain can be adjusted. When ‘START’ button is pressed, the data acquisition starts and the ‘Seconds Elapsed’ and ‘Number of Samples Acquired’ indicators start counting. On pressing the ‘STOP’ button, the program stops running, and there is prompt to save the acquired data. The second graph ‘Data after separating the wavelengths’ starts running only after the ‘START’ button is pressed and it shows all the 12 (4 X 3) channels of data.

4.4.2.2 Block Diagram

The block diagram is divided in two parts, Figures 4.14 and 4.15. The diagram has been labeled from step 1 to 11 to make the explanation easy. Each step is explained as follows:

1. Timing loop is used to set the frequency of acquisition of one data set (12 points). Period can be set by the user on the front panel using ‘Number of data sets per second,’ which is converted to milliseconds and fed to the timing loop.
2. All the pins on the digital port are high by default. Before start of the acquisition, all lines of port ‘0’ are made low by writing zero to all the lines using DAQmx write VI (virtual instrument).
3. Variables are initialized. ‘Means of a single set (12 x 1)’ stores the acquired data, and ‘Number of samples’ stores the number of samples acquired.

4. Three digital output tasks are created to write to lines 0, 1 and 2 of the digital port '0' of the DAQ card. The tasks are fed to the 'for' loop one by one so the LED's are switched on in a sequence.
5. The program stops running in two cases: if the 'STOP' button is pressed, or the time specified in the 'Number of seconds to acquire' expires.
6. In the 'for' loop specified in step 4, a sequence structure is created which runs three tasks in a sequence. The first step in the sequence is to make the line of port '0' corresponding to the task specified by the 'for' loop high.
7. The second step in the sequence is to read the data from the four analog inputs connected to the detector outputs. A task called 'LambdaCapture' is created, which configures the pins ai0 to ai3 of the DAQ card as the analog inputs. 50 data points per channel are acquired at a rate of 50 kHz. After collecting 50 samples per channel, they are averaged out to give one mean reading per channel per wavelength in a single iteration. There are 4 output channels for the 4 detectors per iteration.
8. The third step in the sequence is to switch off the LED (at one specific wavelength) that was turned on in the first step in the sequence (step 6 here).
9. In every iteration of the timed loop, a data set of 4x3 points comes out of the 'for' loop (in step 8), where one data point records an averaged output per detector per wavelength. The collective data per detector is displayed on the first graph on the front panel but is not being stored until the 'START' button is pressed. When the start button is pressed, the data enters the case structure

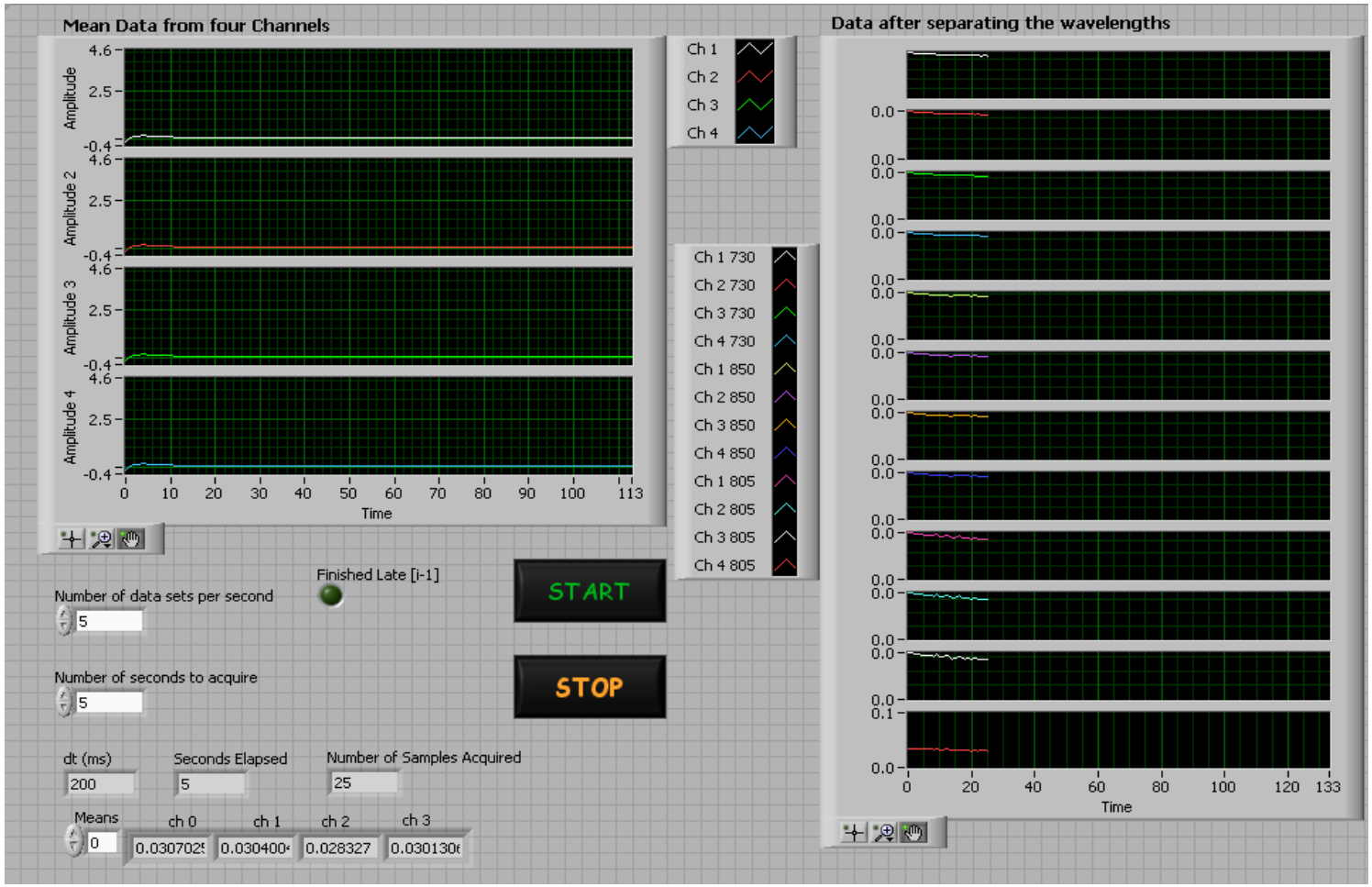

Figure 4.13 Front panel for Three wavelength code

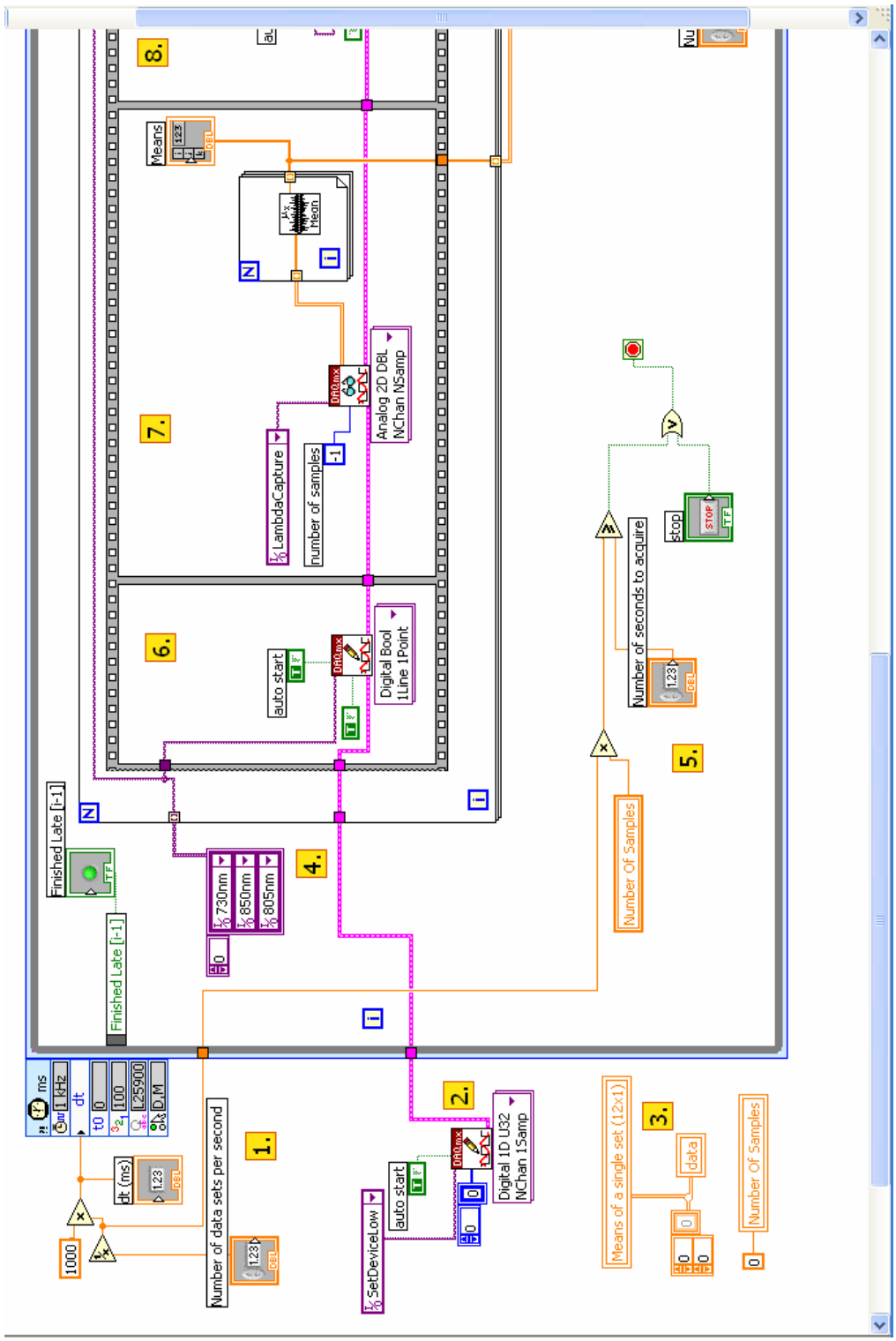

Figure 4.14 Block Diagram for Three wavelength code part 1

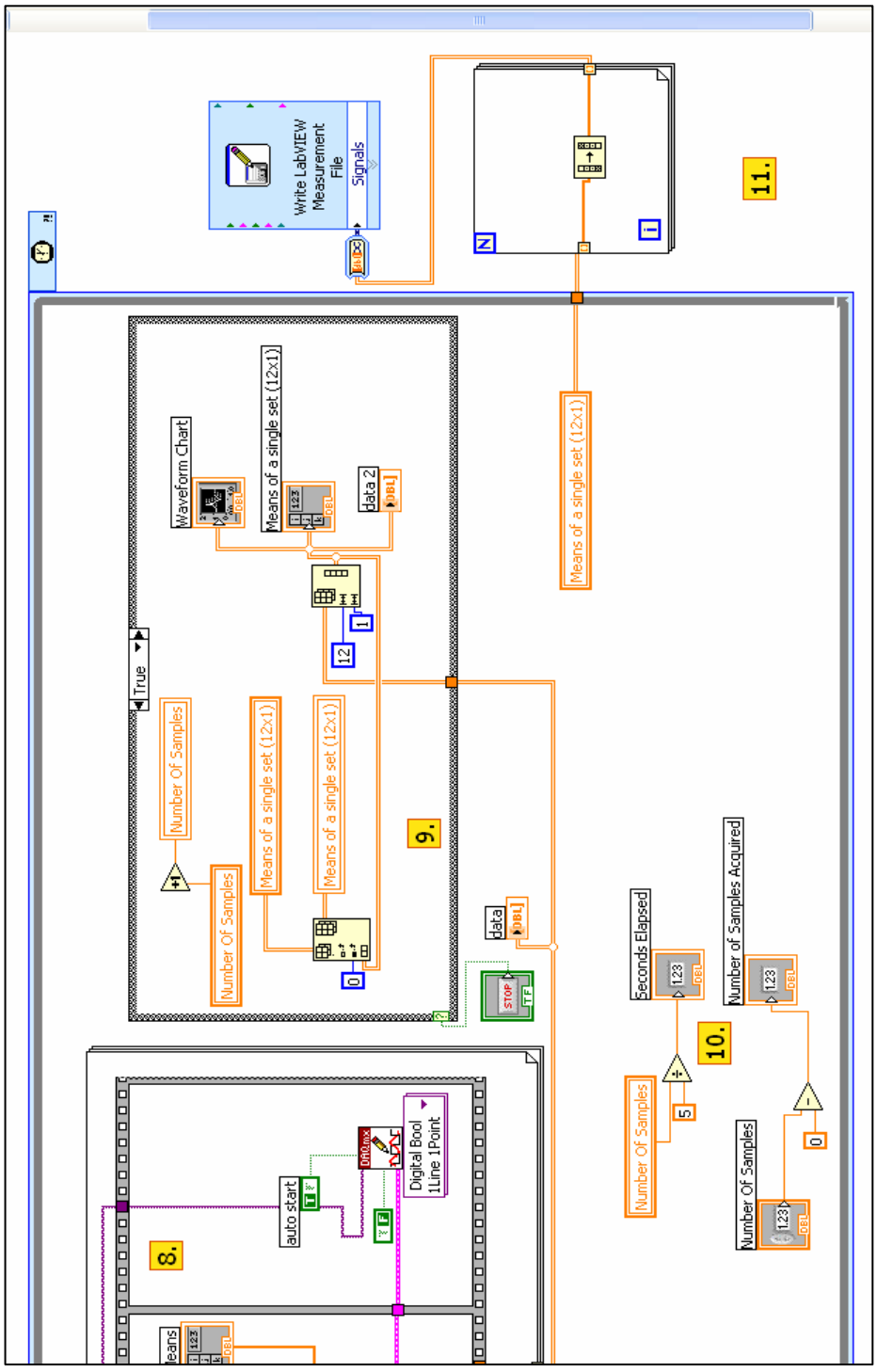

Figure 4.15 Block Diagram for Three wavelength code part 2

where is reshaped to 12x1 form and is stored in the variable 'Means of a single set (12x1)'. Also the 'Number of samples' variable is incremented each time when the loop runs.

10. This step shows the calculation of number of seconds elapsed and number of samples acquired.
11. When the 'STOP' button is pressed, or the time to acquire is over, timed loop stops, and the data in the variable 'Means of a single set (12x1)' can be stored in a user selectable file

.4.4.3 Data Analysis

The output data was analyzed using MATLAB program (Appendix A). The calculation algorithm used here was the same as the one used for the breath holding experiment analysis. The program was modified for four channels instead of 16 channels. Since the LABVIEW program does not allow putting markers during the experiment, the marker locations (in seconds) need to be specified before running the calculation program.

4.5 LED Wavelength Adjustment

The spectrum of the three-wavelength LED was measured using a miniature fiber optic spectrometer (USB2000, Ocean Optics Inc., FL, USA). It was found that the source peaks were centered at 739 nm, 794 nm, and 845 nm instead of 730 nm, 805 nm, and 850 nm respectively, as shown in Figures 4.16 to 4.18. The spectra were measured

at room temperature. These three figures show that during the data analysis, the values of extinction coefficients due to absorption may need to be adjusted based on the measured spectral peaks in order to obtain improved accuracy for Hb and HbO_2 calculations. Also, it is worthwhile to note that the bandwidths (FWHM: full width at half maximum) of the LED spectra at these three wavelengths are quite broad, in the range of ~30 nm. Such a broad bandwidth may affect the accuracy of hemodynamic calculations if only the peak wavelengths are used. Further studies are needed to find possible solutions and alternatives to take into account the spectral broadness.

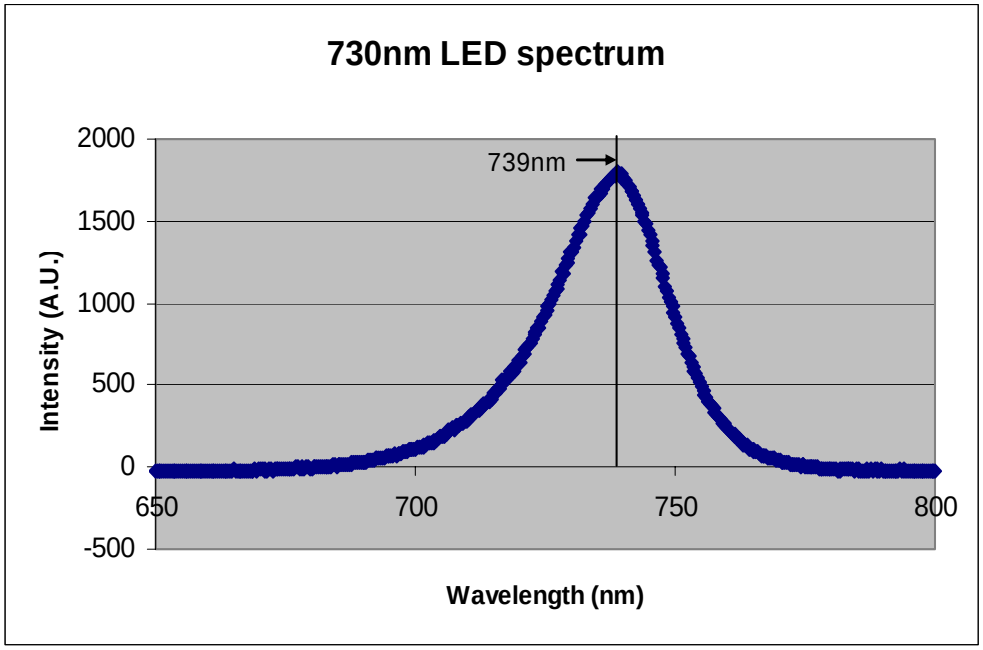

Figure 4.16 Spectrum of 730 nm LED

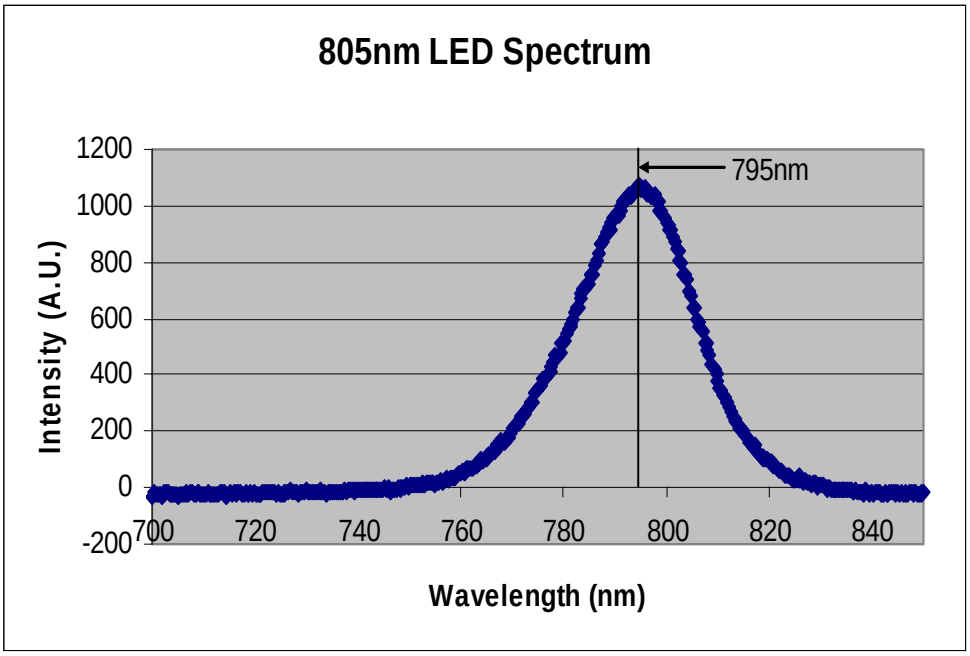

Figure 4.17 Spectrum of 805 nm LED

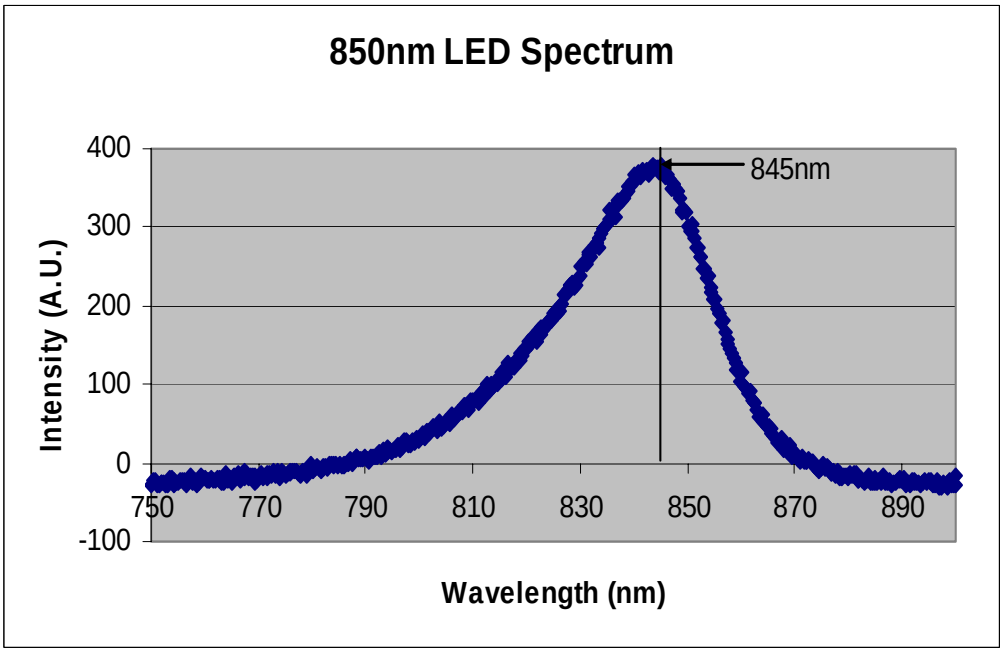

Figure 4.18 Spectrum of 850 nm LED

4.6 Testing

To validate the functionality of the LCC-NIR system, it was required to conduct laboratory phantom experiments, which could prove the capability of the system to measure oxy-hemoglobin and deoxy-hemoglobin changes occurring inside the tissue. Two experiments were conducted for this purpose using horse blood mixed with intralipid solutions as tissue phantoms. The first experiment was done using a static phantom, and the second was done using a dynamic phantom. The LCC-NIR three-wavelength probe was in good contact to the phantom, and the measurements were taken while the blood was oxygenated and deoxygenated.

4.6.1 Static Blood Phantom Measurement

The experimental set up used for this experiment is shown in Figure 4.19. A beaker filled with a 1500-ml, 1% Intralipid solution mixed with 15 ml of pure horse blood was used as the static tissue phantom. The probe was wrapped on the side of the beaker, and the top of the beaker was covered to prevent air from contacting the surface of the solution. The blood was initially deoxygenated by bubbling nitrogen gas into the solution. Figures 4.20 to 4.23 show the results obtained from the four detector channels.

At first, the blood was fully deoxygenated by bubbling nitrogen gas for 4 hours, and then the measurement was started. Thus, the baseline represents the case of deoxygenated blood in the solution. After 260 seconds (~4.3 min), bubbling of nitrogen was stopped, and the gas was switched to oxygen with a slow bubbling rate (to prevent the solution from forming too many bubbles).

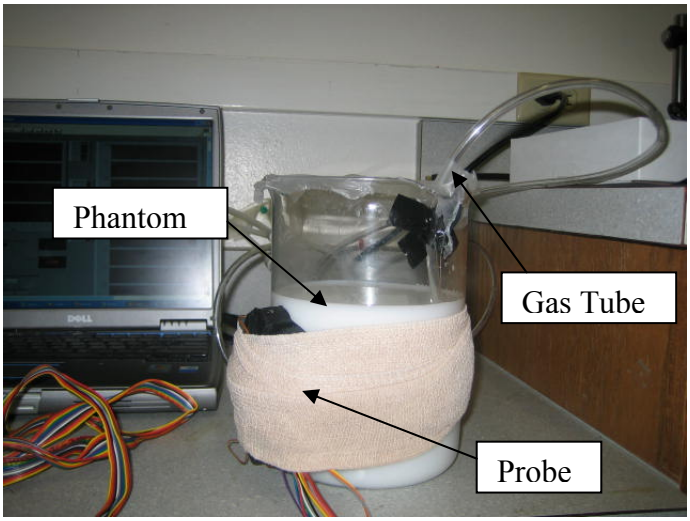

Figure 4.19 Set up for Static Phantom Measurement

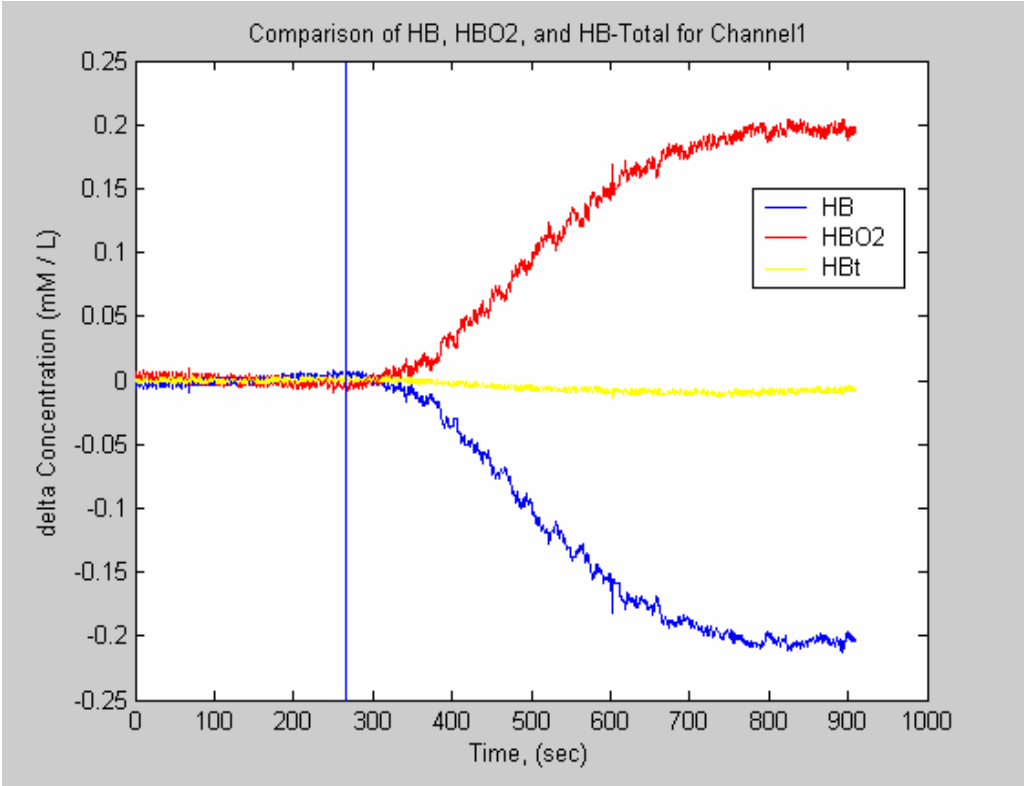

Figure 4.20 Static Blood Phantom data for Channel 1

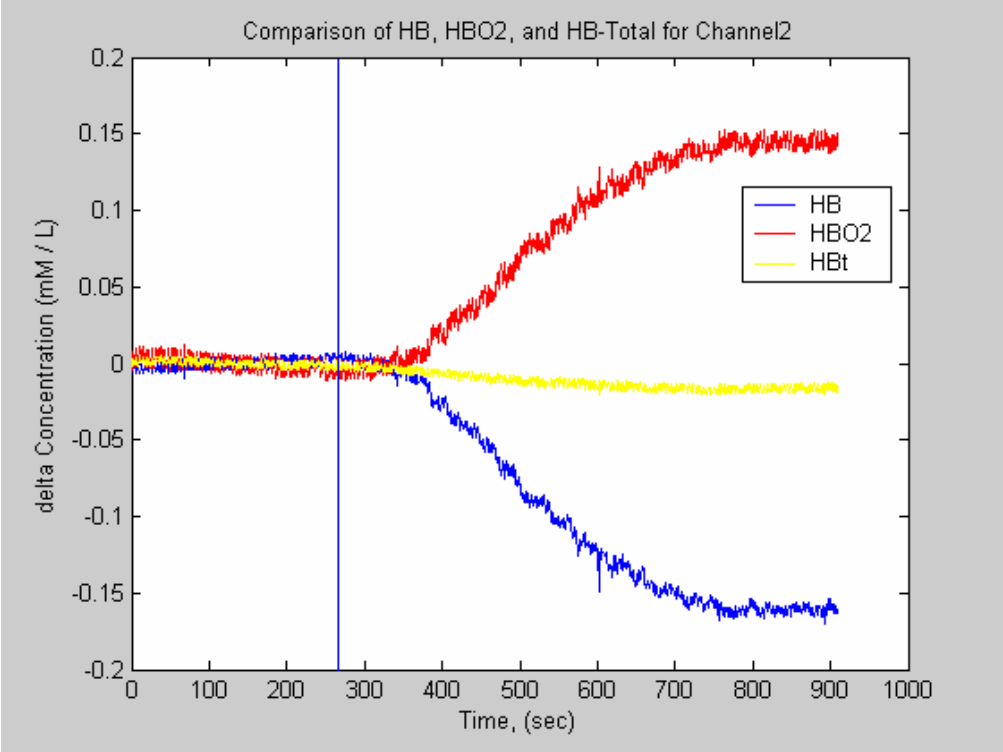

Figure 4.21 Static Blood Phantom data for Channel 2

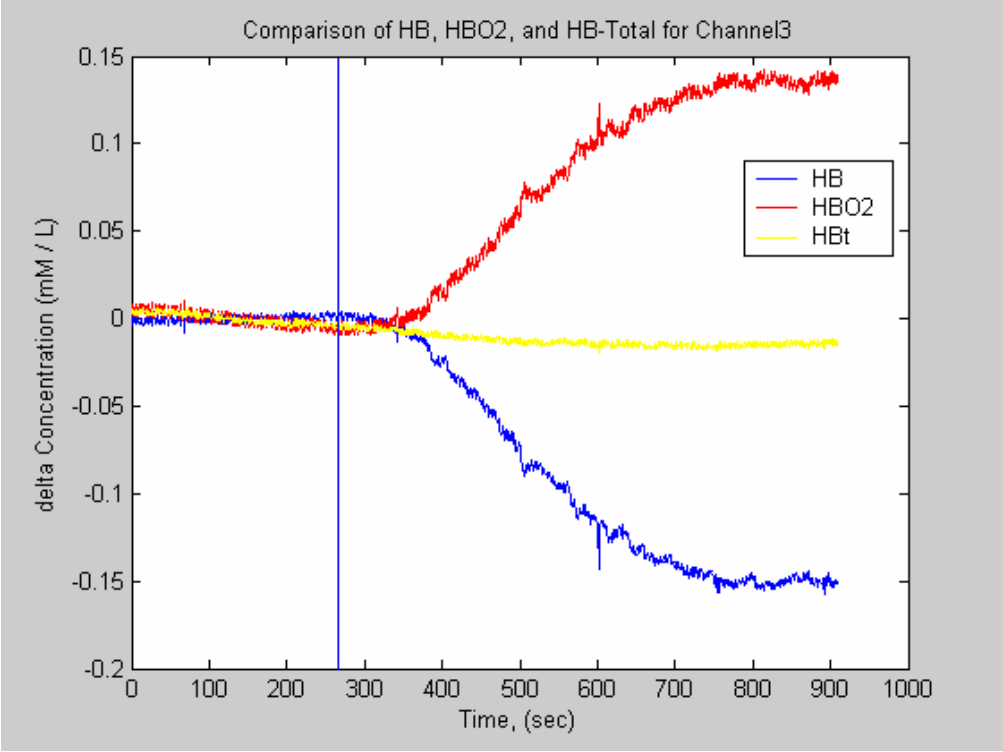

Figure 4.22 Static Blood Phantom data for Channel 3

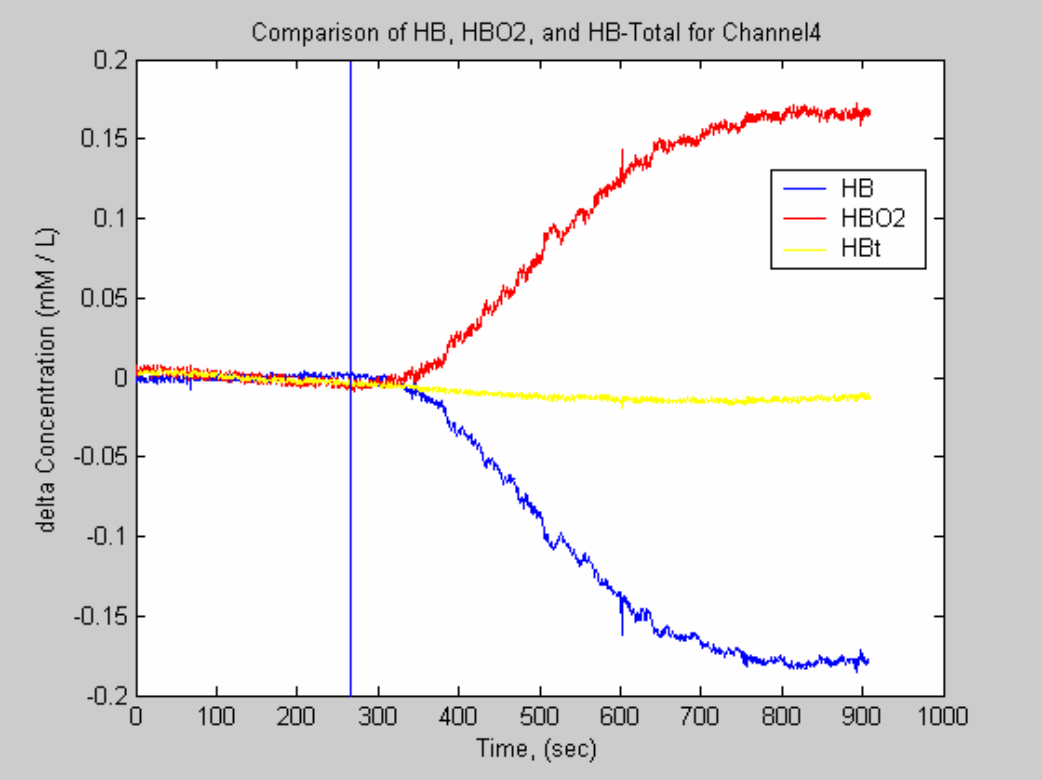

Figure 4.23 Static Blood Phantom data for Channel 4

The vertical blues line in the above figures represent the time at which nitrogen was switched to oxygen. By close inspection on the plots, it can be seen that HbO_2 concentration starts increasing and Hb concentration starts decreasing soon after the blood-Intralipid solution is oxygenated. The fact that the total hemoglobin concentration remains almost constant throughout the oxygenation is clearly evident for all channels, and this is what we expect to see if the NIR system operates and functions correctly.

4.6.2 Dynamic Blood Phantom Measurement

To observe a relative change in oxy- and deoxy- hemoglobin concentrations, a dynamic multi-tube phantom was used, which could simulate the blood vessels inside a

tissue [28]. The set-up of such a dynamic phantom is shown in Figure 4.24(a). The phantom consists of a big cylindrical glass tube which has small transparent tygon tubes going through, simulating the blood vessels inside the tissue (see Figure 4.24(b)). The tygon tubes were surrounded by 0.5% Intralipid solution filled in the glass tube (Figure 4.24(c)). There were two manifolds on each side of the glass tube to channel the multi tygon tubes into a single big plastic tube. The blood was pumped through the big plastic tube from the bottom of phantom using a peristaltic pump and was collected from the top of phantom in a beaker.

4.6.2.2 Results and Discussion

Figures 4.25 to 4.27 show the plots for Channels 1, 2, and 4 respectively. The detector for Channel 3 could not be placed properly because of small size of the dynamic phantom. Plots for all the three channels show the changes in Hb, HbO_2 and Hbt with time. The data was filtered using a fourth order low pass butterworth filter with a cutoff frequency of 0.15 Hz. The two blue vertical lines are the markers for switching gases. Initially, from time zero to the first marker, there was oxygenated blood in the phantom, i.e., within the tygon tubes. The first marker represents the time when the peristaltic pump was started, and the deoxygenated blood was pumped completely through the tygon tubes. The incoming blood was de-oxygenated using the nitrogen gas, and the newly entered deoxygenated blood was left within the phantom till the time marked by the second marker.

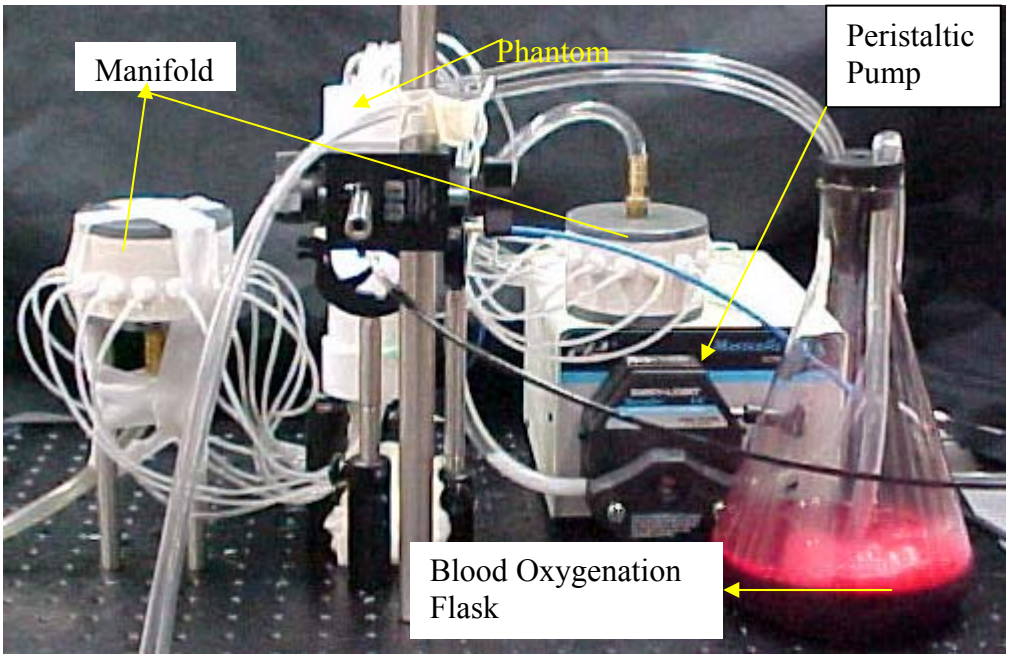

(a)

(b)

(c)

Figure 4.24 (a) Set up for dynamic measurement; (b) Dynamic phantom filled with blood without the surrounding Intralipid solution; (c) Probe attached to the phantom.

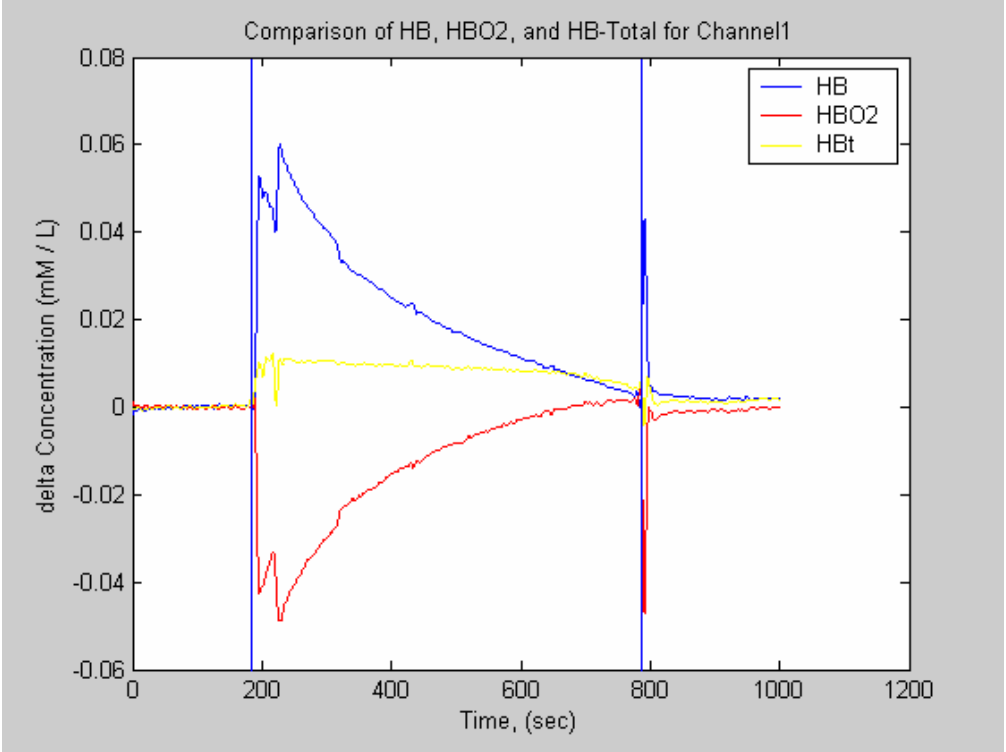

Figure 4.25 Dynamic Blood Phantom data for Channel 1

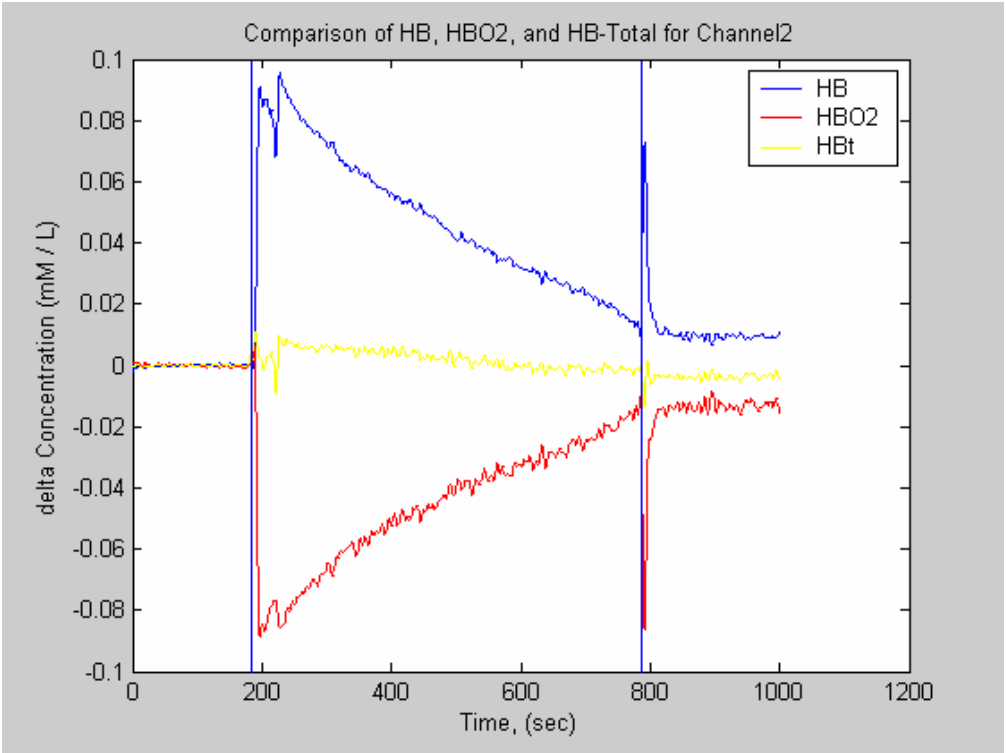

Figure 4.26 Dynamic Blood Phantom data for Channel 2

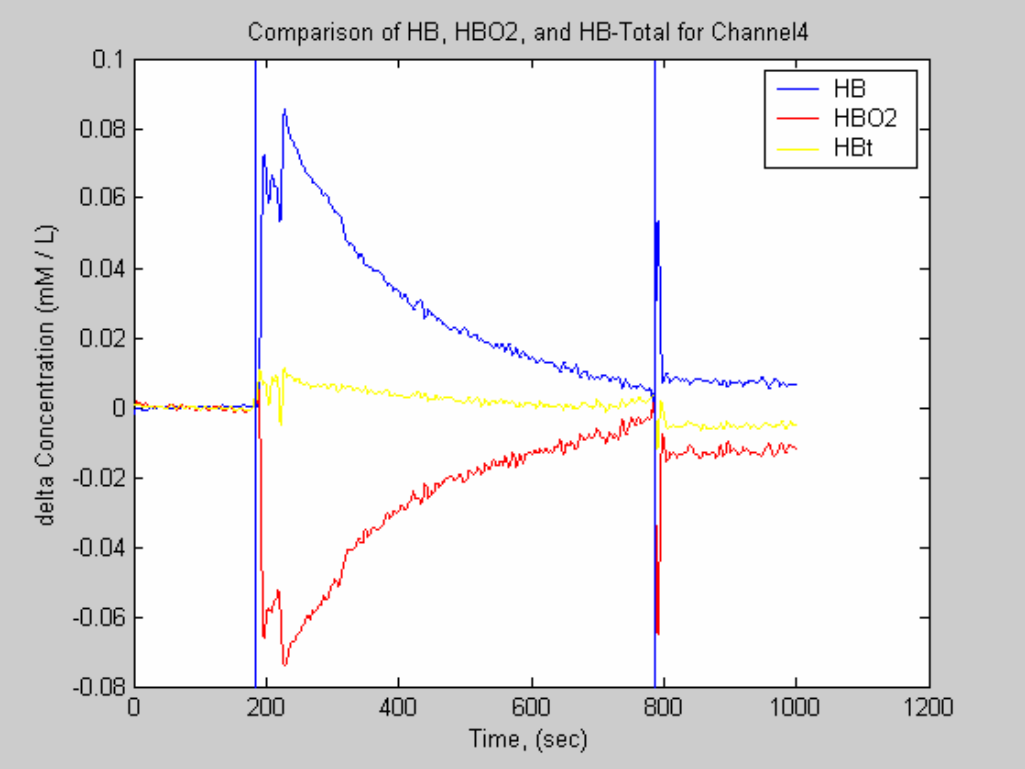

Figure 4.27 Dynamic Blood Phantom data for Channel 4

It can be observed that there is a sudden increase in Hb concentration and a decrease in HbO_2 as the deoxygenated blood rushes in the tube. As the time passes, the blood which is held in the tube starts to oxygenate since the surrounding Intralipid solution contains much oxygen, leading to oxygen diffusion process into the blood through oxygen-permeable tubes. Thus, there is a gradual decrease in Hb concentration and an increase in HbO_2. We notice that at around 220 seconds, there is an irregularity (dip) shown in the data. This is due to the fact that during the experiment, the tube on the input side was out of blood for few seconds, and thus a little air was pumped in during that time. But soon the tube was filled with the blood. During the oxygenation cycle, Hbt as expected remains almost constant throughout the measurement. In all

three channels, we observe that there is a sudden increase in Hbt after marker 1. Our interpretation for this is that as the blood was pumped initially, some empty spaces may exist in the tygon tubes of phantom and could be filled, giving rise to a little extra hemoglobin concentration. For the rest of the measurement, Hbt remains almost constant.

The second marker (at 788 sec = 13.3 min) represents the time when oxygenated blood was pumped through the phantom. The peaks (upward for Hb and downward for HbO_2) are due to the incoming rush of deoxygenated blood which was stored in the manifold but is quickly replaced by oxygenated blood. The level of Hbt is very close to the original baseline, while HbO_2 is a little higher with respect to the baseline, possibly due to freshly oxygenated blood just coming into the tygon tubes.

4.6.3 Conclusion

From the results obtained by the two laboratory phantom experiments, it can be concluded that the LCC-NIRS system is capable of measuring hemodynamic changes. The first prototype of the system is nearly ready to be used for hot flash measurement in a laboratory environment. Since it is the first prototype, there are number of modifications that can be done on this design to make it more compact and suitable for clinical uses. A few suggestions that could be addressed in near future are discussed in chapter 5.

CHAPTER 5

SUMMARY AND FUTURE SCOPE

For my thesis research, I have focused on the continuous-wave, LED-based NIR system so as to calculate changes in Hb, HbO_2 and Hb_{total}. The project consisted of three sections: 1) using a commercial system, LEDI, I have mapped temporal cerebral hemodynamics and tested the ability of the system to be able to measure cerebral oxygenation changes induced by breath holding. The study was successfully completed with 15 human subjects. 2) In order to explore a new application of NIRS, I have also conducted a preliminary study to apply the LEDI for hot flash measurement in women. While the results are positive showing the feasibility to use NIRS for hot flash identification and monitoring, it seemed that the probe of the existing LEDI system was not appropriate for sternal measurements. Thus, I decided to develop a low-cost, compact, NIR (LCC-NIR) system to provide flexibility for hot flash measurements. 3) I designed and built a prototype of LCC-NIR system with a single-wavelength and three-wavelength source and four detector chips. Then the newly built LCC-NIR system was tested using laboratory phantoms, and the results are satisfactory, showing correct functionality of the system.

A first prototype of a low-cost, LED-based, continuous-wave, near infrared system was built. After testing, it was concluded that the system works well to show

hemodynamic changes using the standard blood-tissue phantoms. However, since it is the first prototype, there are certain improvements that can be done on the system to make it more compact and ready to use in ambulatory conditions. The suggestions for the future work are as follows:

1. The control board and the probe can be combined by building a PCB (printed circuit board) and using circuit mount devices.
2. The power supply unit can be eliminated by using batteries in the circuit.
3. A shielded cable from the probe PCB to the DAQ card would reduce the pick up of electrical noise.
4. The LABVIEW software can include a program for data processing to provide real time changes in Hb and HbO_2.
5. An ideal system for hot-flash measurement would be wireless. An RF circuitry can be used to make the system wireless, and then it can be used for ambulatory measurements.

All the above features, when added, will make an ideal system for hot flash measurements. Apart from this application, there are other applications where such a LCC-NIR system would be very valuable. For example, one of the applications is to monitor syncope, which was mentioned in chapter 2. Syncope can be defined as a transient loss of consciousness and posture, also described as "fainting" or "passing out." It is usually caused by temporary insufficient blood flow to the brain [29]. So, the future wire-less, LCC-NIR system can be used to measure changes in cerebral

oxygenation and, if measured in ambulatory conditions, could provide valuable information.

Moreover, the probe may be modified for certain applications by adding more number of sources and detectors. The changes required in hardware and software for new applications are not very difficult to implement, and thus this system may have multi probes available for different applications.

APPENDIX A

MATLAB CODES

1. Code for Breath holding data analysis

```
clc;
clear all;
close all;

%load the data and identify the markers

A = load('C:\Documents and Settings\Vikrant\My Documents\Breathholding
research\Raw Data\Filename.dat');
a = A(:, 48)<5000;
b = A(:, 48)>4000;
bindex = find(b);
beginsample = bindex(1);
breathsample = bindex(2);
endsample = breathsample + 80;
baselinesample = beginsample - 25;
A730 = A(a,[1 4 7 10 13 16 19 22 25 28 31 34 37 40 43 46]);
A850 = A(a,[3 6 9 12 15 18 21 24 27 30 33 36 39 42 45 48]);
time = A(a,49);

%Calculate HB & HBO2 & HBt

baseline730 = mean(A730(1:baselinesample,:));
baseline850 = mean(A850(1:baselinesample,:));
compare730 = ones(size(A730,1),1)*baseline730./A730;
compare850 = ones(size(A850,1),1)*baseline850./A850;
HB = (0.994*log10(compare730) - 0.3578*log10(compare850));
HBO2 = (-0.674*log10(compare730) + 1.1171*log10(compare850));
HBt = HB + HBO2;

% Calculate T1, T2, T3, HBmax, HBO2max & HBtmax

[HBmax, Imax] = max(HB(breathsample+1:endsample,:));
HBmax=HBmax'
[HBmin, Imin] = min(HB(breathsample+1:endsample,:));
HBmin=HBmin'
[HBO2max, Jmax] = max(HBO2(breathsample+1:breathsample+120,:));
HBO2max=HBO2max'
[HBO2min, Jmin] = min(HBO2(breathsample+1:breathsample+120,:));
HBO2min=HBO2min'
[HBtmax, Kmax] = max(HBt(breathsample+1:breathsample+120,:));
HBtmax=HBtmax'
```

```
T1 = time(breathsample) - time(beginsample);
T1 = T1
TimeJmax = time(Jmax + breathsample) - time(breathsample);
T2 = TimeJmax
TimeKmax = time(Kmax + breathsample) - time(breathsample);
T3 = TimeKmax

% baseline HB HBO2 ant HBt

HBbase = mean(HB(1:baselinesample,:));
HBObase = mean(HBO2(1:baselinesample,:));
HBtbase = mean(HBt(1:baselinesample,:));
HBbase = mean(HBbase)
HBObase = mean(HBObase)
HBtbase = mean(HBtbase)

% plot HB

figure;
plot(time, HB);
v = axis;
hold on; line([time(beginsample) time(beginsample)], [v(3) v(4)]);
line([time(breathsample) time(breathsample)], [v(3) v(4)]); hold off;
xlabel('Time, (sec)');
ylabel('delta HB');
title('delta HB');
legend('CH1', 'CH2', 'CH3','CH4', 'CH5', 'CH6', 'CH7', 'CH8', 'CH9', 'CH10', 'CH11',
'CH12', 'CH13', 'CH14', 'CH15', 'CH16', -1);
saveas(gcf,'c:/data/Subjectname/HB','fig');

% plot HBO2

figure;
plot(time, HBO2);
v = axis;
hold on; line([time(beginsample) time(beginsample)], [v(3) v(4)]);
line([time(breathsample) time(breathsample)], [v(3) v(4)]); hold off;
xlabel('Time, (sec)');
ylabel('delta HBO2');
title('delta HBO2');
legend('CH1', 'CH2', 'CH3','CH4', 'CH5', 'CH6', 'CH7', 'CH8', 'CH9', 'CH10', 'CH11',
'CH12', 'CH13', 'CH14', 'CH15', 'CH16', -1);
saveas(gcf,'c:/data/Subjectname/HBO2','fig');
```

```
% plot HBt

figure;
plot(time, HBt);
v = axis;
hold on; line([time(beginsample) time(beginsample)], [v(3) v(4)]);
line([time(breathsample) time(breathsample)], [v(3) v(4)]); hold off;
xlabel('Time, (sec)');
ylabel('delta HBt');
title('delta HBt');
legend('CH1', 'CH2', 'CH3','CH4', 'CH5', 'CH6', 'CH7', 'CH8', 'CH9', 'CH10', 'CH11',
'CH12', 'CH13', 'CH14', 'CH15', 'CH16', -1);
saveas(gcf,'c:/data/Subjectname/HBt','fig');

% Plot HB, HBO2 and HBt for all channels

for i=1:16
figure ; plot(time, HB(:, i), 'b');
hold on; plot(time, HBO2(:,i), 'r');
plot(time, HBt(:, i), 'y'); hold off;
v = axis;
hold on; line([time(beginsample) time(beginsample)], [v(3) v(4)]);
line([time(breathsample) time(breathsample)], [v(3) v(4)]); hold off;
xlabel('Time, (sec)');
ylabel('delta Concentration');
cntr = num2str (i);
Mystring = strcat ('Comparison of HB, HBO2, and HB Total for Channel',cntr);
title(Mystring);
legend('HB', 'HBO2', 'HBt');
Mypath = strcat('c:/data/Subjectname/',cntr);
saveas(gcf,Mypath,'fig');
end
```

2. Code for Hot Flash Analysis

```
clc;
clear all;
close all;

% Load the file and select the data segment for analysis

A = load('C:\Documents and Settings\Vikrant\My Documents\Breathholding
research\Raw Data\filename.dat');
A = A(5500:8000,:);
X = A(1:2500,:);
A = [X' (A(2800:end,:))'];
A=A';
a = A(:, 48)<5000;
b = A(:, 48)>5000;
T = A(a,49);

bindex = find(b);
beginsample = bindex(1);
endsample = bindex(2);
baselinesample = beginsample - 25;
A730 = A(a,[1 4 7 10 13 16 19 22 25 28 31 34 37 40 43 46]);
[d,c] = butter(4,0.01);     %filter the data
A730 = filtfilt(d,c,A730);
A850 = A(a,[3 6 9 12 15 18 21 24 27 30 33 36 39 42 45 48]);
[d,c] = butter(4,0.01);     %filter the data
A850 = filtfilt(d,c,A850);
time = 1:1:size(T);
time = time/3;

%Calculate HB & HBO2 & HBt
baseline730 = mean(A730(1:baselinesample,:));
baseline850 = mean(A850(1:baselinesample,:));
compare730 = ones(size(A730,1),1)*baseline730./A730;
compare850 = ones(size(A850,1),1)*baseline850./A850;
HB = (0.994*log10(compare730) - 0.3578*log10(compare850));
HBO2 = (-0.674*log10(compare730) + 1.1171*log10(compare850));
HBt = HB + HBO2;

% plot HB
figure;
plot(time, HB);
v = axis;
```

```
hold on; line([time(beginsample) time(beginsample)], [v(3) v(4)]);
line([time(endsample) time(endsample)], [v(3) v(4)]); hold off;
xlabel('Time, (sec)');
ylabel('delta HB');
title('delta HB');
legend('CH1', 'CH2', 'CH3','CH4', 'CH5', 'CH6', 'CH7', 'CH8', 'CH9', 'CH10', 'CH11',
'CH12', 'CH13', 'CH14', 'CH15', 'CH16', -1);

% plot HBO2
figure;
plot(time, HBO2);
v = axis;
hold on; line([time(beginsample) time(beginsample)], [v(3) v(4)]);
line([time(endsample) time(endsample)], [v(3) v(4)]); hold off;
xlabel('Time, (sec)');
ylabel('delta HBO2');
title('delta HBO2');
legend('CH1', 'CH2', 'CH3','CH4', 'CH5', 'CH6', 'CH7', 'CH8', 'CH9', 'CH10', 'CH11',
'CH12', 'CH13', 'CH14', 'CH15', 'CH16', -1);

% plot HBt
figure;
plot(time, HBt);
v = axis;
hold on; line([time(beginsample) time(beginsample)], [v(3) v(4)]);
hold off;
xlabel('Time, (sec)');
ylabel('delta HBt');
title('delta HBt');
legend('CH1', 'CH2', 'CH3','CH4', 'CH5', 'CH6', 'CH7', 'CH8', 'CH9', 'CH10', 'CH11',
'CH12', 'CH13', 'CH14', 'CH15', 'CH16', -1);


for i=1:16
figure ; plot(time, HB(:, i), 'b');
hold on; plot(time, HBO2(:,i), 'r');
plot(time, HBt(:, i), 'y'); hold off;
v = axis;
hold on; line([time(beginsample) time(beginsample)], [v(3) v(4)]);
hold off;
xlabel('Time, (sec)');
ylabel('delta Concentration');
cntr = num2str (i);
Mystring = strcat ('Comparison of HB, HBO2, and HB Total for Channel',cntr);
```

```
title(Mystring);
legend('HB', 'HBO2', 'HBt');
end
```

3. Code for Data analysis of In-House instrument

```
clc;
clear all;
close all;
% Specify the location of markers (in seconds)
marker1=40;
marker2=145;

% extinction coefficients (from Mark Cope's Thesis)
eHbO_850 = 1.1596;
eHbO_730 = 0.4383;
eHb_730 = 1.3029;
eHb_850 = 0.7861;

% Load the datafile
A = load('C:\Documents and Settings\Vikrant\My Documents\LabVIEW
Data\filename.lvm');
baselinesample = (marker1-5)*5;
A730 = A(:,[2 3 4 5]);
A850 = A(:,[6 7 8 9]);
A805 = A(:,[10 11 12 13]);
time = A(:,1)/5;

%Plot Raw Data
figure;
subplot(2,2,1);
plot(time, A730);
v = axis;
hold on; line([time(marker1*5) time(marker1*5)], [v(3) v(4)]);
line([time(marker2*5) time(marker2*5)], [v(3) v(4)]); hold off;
xlabel('Time, (sec)');
ylabel('Raw Data');
title('Raw Data for 730nm');
legend('Ch1','Ch2','Ch3','Ch4',-1);

subplot(2,2,2);
plot(time, A850);
v = axis;
hold on; line([time(marker1*5) time(marker1*5)], [v(3) v(4)]);
line([time(marker2*5) time(marker2*5)], [v(3) v(4)]); hold off;
xlabel('Time, (sec)');
ylabel('Raw Data');
title('Raw Data for 850nm');
```

```
legend('Ch1','Ch2','Ch3','Ch4',-1);

subplot(2,2,3);
plot(time, A805);
v = axis;
hold on; line([time(marker1*5) time(marker1*5)], [v(3) v(4)]);
line([time(marker2*5) time(marker2*5)], [v(3) v(4)]); hold off;
xlabel('Time, (sec)');
ylabel('Raw Data');
title('Raw Data for 805nm');
legend('Ch1','Ch2','Ch3','Ch4',-1);

subplot(2,2,4);
plot(time, A850 + A730);
v = axis;
hold on; line([time(marker1*5) time(marker1*5)], [v(3) v(4)]);
line([time(marker2*5) time(marker2*5)], [v(3) v(4)]); hold off;
xlabel('Time, (sec)');
ylabel('Raw Data');
title('Raw Data for 730nm + 850nm');
legend('Ch1','Ch2','Ch3','Ch4',-1);

%Calculate HB & HBO2 & BV
baseline730 = mean(A730(1:baselinesample,:));
baseline850 = mean(A850(1:baselinesample,:));
compare730 = ones(size(A730,1),1)*baseline730./A730;
compare850 = ones(size(A850,1),1)*baseline850./A850;
HB = 1*(eHbO_730*log10(compare850) -
eHbO_850*log10(compare730))/(eHb_850*eHbO_730-eHb_730*eHbO_850);
HBO2 = 1*(eHb_850*log10(compare730) -
eHb_730*log10(compare850))/(eHb_850*eHbO_730-eHb_730*eHbO_850);
BV = HB + HBO2;
% plot the results of HB, HBO2 and HBt for all four channels
for i=1:4
   figure;
   plot(time, HB(:, i), 'b');
   hold on; plot(time, HBO2(:,i), 'r');
   plot(time, BV(:, i), 'y'); hold off;
   v = axis;
   hold on; line([time(marker1*5) time(marker1*5)], [v(3) v(4)]);
   line([time(marker2*5) time(marker2*5)], [v(3) v(4)]); hold off;
   xlabel('Time, (sec)');
   ylabel('delta Concentration');
   cntr = num2str (i);
```

```
    Mystring = strcat ('Comparison of HB, HBO2, and HB Total for Channel',cntr);
    title(Mystring);
    legend('HB', 'HBO2', 'HBt');
end
```

APPENDIX B

IRB APPROVAL FORMS

THE UNIVERSITY OF TEXAS AT ARLINGTON

SCHOOL OF NURSING

Date: May 2, 2005

To: Dr. Hanli Liu
Biomedical Engineering
19138

Re: **Protocol 05.349** *A Study of Cerebral Hemodynamics during Breath Holding Task Using Near Infrared Spectroscopy*

The Institutional Review Board (IRB) has reviewed and approved this research protocol under an expedited review in accordance with Title 45 CFR 46.110. Continuing review is scheduled for one year from the above approval date.

The Office for Human Research Protections (OHRP) requires you to submit annual and final reports for review and approval by the IRB. The annual report must be on file with the IRB before the anniversary date of your initial approval. OHRP does not allow for a grace period on the continual review requirement. If the annual report is not received by the IRB by the anniversary date, the IRB will be forced to terminate the approval of your protocol and if your study is federally funded, the IRB will have to report the termination to OHRP as required by Title 45 CFR 46.103(b) 5.

If you require modifications to this proposal in the method of use of human subjects in this study, change in the Principal Investigator (PI) or Co- Investigator(s), or any change in the subject pool, you are required to obtain prior approval from the IRB before implementing the modification as required by Title 45 CFR 46.103(b) 4iii.

The IRB approved consent form that is stamped by the IRB with the expiration date of the approval must be used for all informed consent procedures on all human subjects in this study. The signed consent forms must be under lock and key on UTA campus for the duration of the study plus three years. These consent forms are subject to inspection during this time period by the IRB, Research Compliance staff and / or federal agents.

All investigators listed in this protocol must have documented Human Subjects Involved in Research (Tier II) training on file with the Office of Research Compliance. Please call the Office of Research Compliance if you have not taken the training course within the last year.

If you have any questions related to this research or to the IRB, you may contact me at (817) 272-4840 or the Office of Research Compliance at (817) 272-3723.

Sincerely,

Dr. Jennifer Gray

Dr. Jennifer Gray
Assistant Professor
IRB Chair

BOX 19407 411 S.NEDDERMAN DR. ARLINGTON, TEXAS 76019-0407 T 817.272.2776 F 817.272.5006 http://www.uta.edu/nursing

IRB Protocol #_____
FUNDED GRANT #_____
CONTRACT #_____

Office . . Research Compliance
Phone (817) 272-3723
Fax (817) 303-1111

THE UNIVERSITY OF TEXAS AT ARLINGTON

SUBJECT CONSENT FORM

I have been asked to participate as a subject in the research project entitled *A study of cerebral Hemodynamics during breath holding task using near infrared spectroscopy*
under the direction of *Dr. Hanli Liu*

PURPOSE OF THE STUDY

I understand that the purpose of this study is to *Measure oxygen levels in the brain during specific task*

PROCEDURES

There is an experiment designed to study the effects of breath holding on the cerebral heamodynamics. A non-invasive probe will be attached to the forehead of the subject. The subject will be asked to hold the breath after a baseline (2 minute) and release the breath after the maximum possible hold. There will be a wait period (5 minutes) to obtain the baseline again. The experiment lasts for less than 10 minutes.

NUMBER OF SUBJECTS PARTICIPATING
Approximately 20 healthy subjects will participate in the experiment.

The approximate number of subjects involved in the study should be stated in the consent form.

RISKS OF PARTICIPATION

I understand that the potential risks from participation in the study are *none*

BENEFITS TO THE SUBJECT

I understand that I will not benefit from my participation in the research project.

ALTERNATIVE TREATMENT

The alternative is not to participate in the study

APR 2 9 2005

APPROVED BY THE UTA-IRB
The IRB approval for this consent document will expire on

APR 2 8 2006

IRB Protocol #_____
FUNDED GRANT #_____
CONTRACT #_____

Office of Research Compliance
Phone (817) 272-3723
Fax (817) 303-1111

I voluntarily agree to participate as a subject in the above named project. I understand that I will be given a copy of the consent form I have signed.

Date	Signature of Subject

Using language that is understandable and appropriate, I have discussed this project and the items listed above with the subject and/or his/her authorized representatives.

Date	Signature of Principal Investigator

APR 2 9 2005

APPROVED BY THE UTA-IRB
The IRB approval for this consent document will expire on

APR 2 8 2006

IRB Protocol #_____
FUNDED GRANT #_____
CONTRACT #_____

Office of Research Compliance
Phone (817) 272-3723
Fax (817) 303-1111

ADDENDUM TO SAMPLE SUBJECT CONSENT

OTHER INSTRUCTIONS AND CLAUSES THAT MAY BE REQUIRED

PREGNANT SUBJECTS:

A. In protocols where risk is minimal and there is no medical reason to exclude pregnant subjects, then no particular reference to pregnancy is required.

B. In protocols which pose a medical risk to the pregnant subject or to the fetus there should be a sentence in the consent form which states the following:

Pregnant subjects are to be excluded from this research project. In order to qualify for inclusion in this study, all women of childbearing potential must have a negative pregnancy test.

C. In the recruitment notice for protocols in which there is a medical risk to the pregnant subject or to the fetus the following statement should be included:

Pregnant subjects are to be excluded from this research project. In order to qualify for inclusion in this study, all women of childbearing potential must have a negative pregnancy test.

REQUIREMENTS FOR ASSENT/CONSENT BY CHILDREN:

1. The assent to participate in a research protocol should be obtained in all children at and above the age of seven (7).

2. When children are being asked to assent to participate in research, the following statement should be included in the consent form as standard clause #10:

My child has had the risks and benefits of the research explained to him/her in language that he/she can understand and has agreed to participate in this research.

3. Children with at least a cognitive age of an average 2nd grader or about seven years of age should sign on an "assent" line as the "subject" of the research. This is in addition to his/her parents signature(s) on the "authorized third party" line.

4. The issue of advocates for children who need them will be determined on a case by case basis.

5. If the research procedure holds the possibility of direct benefit that is important to the well-being of the child or the capability of the child is so limited that assent/consent is not possible, the IRB can choose to waive the requirement of assent/consent.

INFORMED CONSENT PROCESS

APR 29 2005

The principal investigator has the difficult task of explaining the proposed activity to a potential

APPROVED BY THE UTA-IR
The IRB approval for this cons
document will expire on

APR 28 2006

Office of Research Compliance
Phone (817) 272-3723
Fax (817) 303-1111

subject in enough detail and in appropriate language so as to assure that the potential subject fully understands what he/she is consenting to and that the consent is an educated one.

The Institutional Review Board has the equally difficult task of determining whether or not the consent procedure proposed by the principal investigator adequately assures legally informed consent of the subject. To assist the principal investigator in better preparing subject consents, the following statements may be helpful.

The subject consent form must identify the activity to be conducted, name(s) and the phone number of the individual(s) who are to conduct the activity and state the purpose of the activity. It must describe any procedures that are deemed to be experimental in nature and indicate the risks attendant thereto. It must also refer to any prior experience gained in human use or state that no prior human use has occurred and indicate the experience that has been acquired in animal studies.

A statement should be made about expected or potential reactions resulting from all procedures to be performed that are not deemed to be experimental. The benefits, if any, that could accrue from the activity should be described and a statement made as to whether the benefit would accrue to the individual subject or to society in general. Alternative procedures that could be used in lieu of the experimental procedures must be described. An offer to answer any inquiries concerning the procedure should be made in writing. The subject should also be informed in writing that he/she may discontinue participation in the activity at any time without prejudice to the subject.

It is important that the terminology used in the subject consent form be such that it is understandable and relevant to the average lay person rather than the investigator.

It is the responsibility of the Institutional Review Board to be satisfied that the subject consent will be obtained without undue inducement or any element of force, fraud, deceit, duress or other forms of constraint or coercion.

Each subject should be given a copy of the consent form he or she has signed.

If personal data is to be acquired from surveys, questionnaires or medical records it is necessary to inform the subject of the criteria used by which he or she was selected to be a subject, describe the purpose for which the data is being collected, indicate any benefits to be gained by the subject's participation in the activity, and state what risks (physical, psychological, or social) or possible detrimental effects that may accrue to the subject. The investigator should describe the plan by which the confidentiality of personal data will be assured. Documents, discs, tabs, coded keys, etc., which contain personal data that may place the subject at risk of losing confidentiality should be stored in a locked area with access to that area limited only to the investigator or other authorized personnel. The investigator should also develop a plan for the destruction of such personal data at an appropriate time and in a specified manner.

When an activity proposes to use normal subjects, the subject should be informed that no benefit will be derived from his/her participation. The inducements offered to a normal subject should be consistent with the degree of remuneration and shall not unduly influence the subject to participate in the activity.

If randomization (by chance) is used to select a subject population, the subject must be so

APR 2 9 2005

APPROVED BY THE UTA-IRB
The IRB approval for this consent document will expire on

APR 2 8 2006

Office of Research Compliance
Phone (817) 272-3723
Fax (817) 303-1111

informed.

The investigator should incorporate into the subject consent the length of time required for participation in the activity, whether this is continuous or intermittent, any requirement for follow-up examinations or studies and whether or not there will be limitations or constraints on the physical activities of the subject after the activity is completed.

If monitoring procedures are required during the activity, the type, number and frequency of such procedures should be explained and the risks or discomforts of each should be described. If the performance of such procedures will incur additional expense to the subject, he/she should be so informed.

If the research subject or his/her insurance company will be expected to pay for any expenses incurred by participation in the research protocol, this must be explained in the consent form.

The signed consent forms must be kept under lock and key for a minimum of 3 years after the conclusion of the research. For research funded by the federal government, the signed informed consent forms for each participant must be kept for 3 years (or more depending on the funding agency) after final close-out by the Office Grant and Contract Services at UTA. All signed consent forms will be subject to quarterly monitoring by the Institutional Review Board.

APR 2 9 2005

APPROVED BY THE UTA-IRB
The IRB approval for this consent document will expire on

APR 2 8 2006

APPENDIX C

INK-INTRALIPID CALIBRATION DATA FOR THE DETECTORS

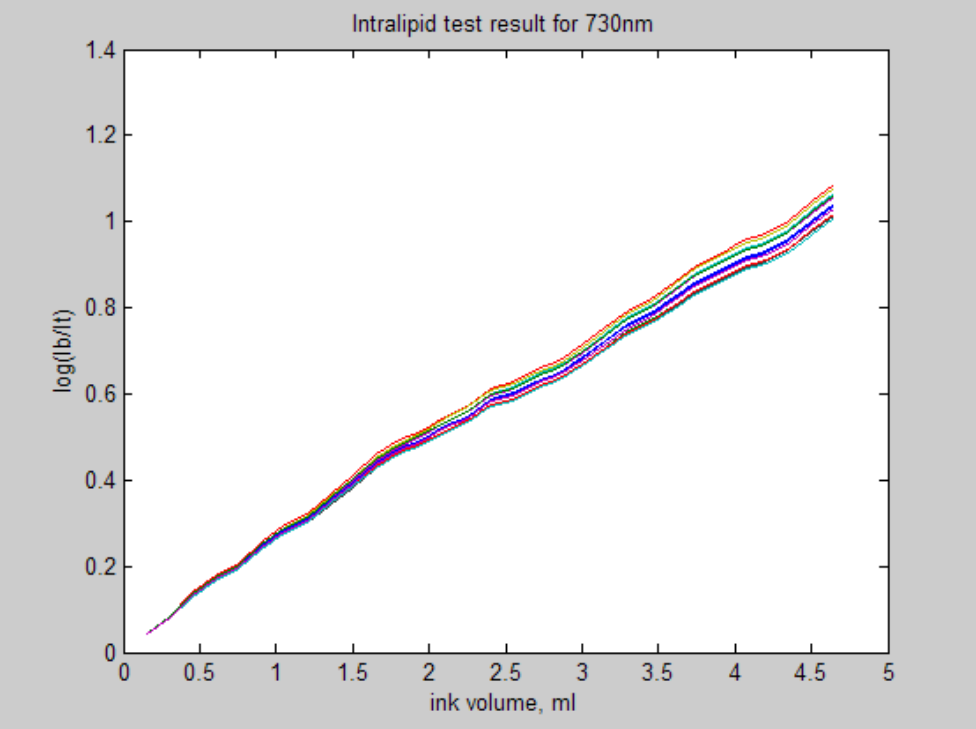

Figure C1 Optical Density plot at 730nm

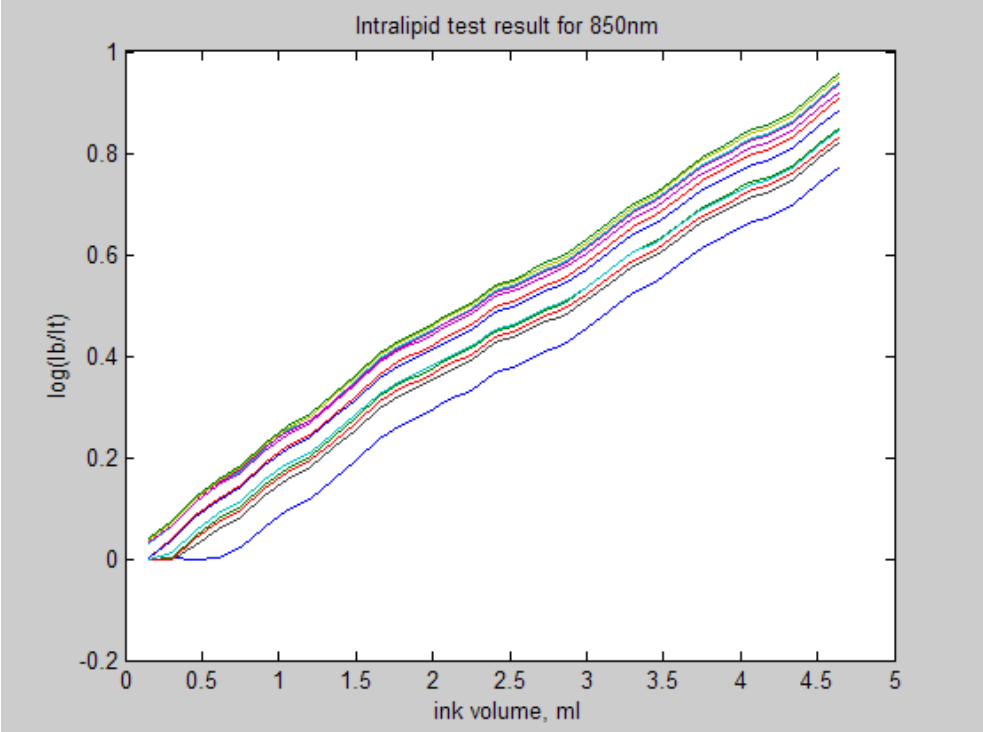

Figure C2 Optical Density plot at 850nm

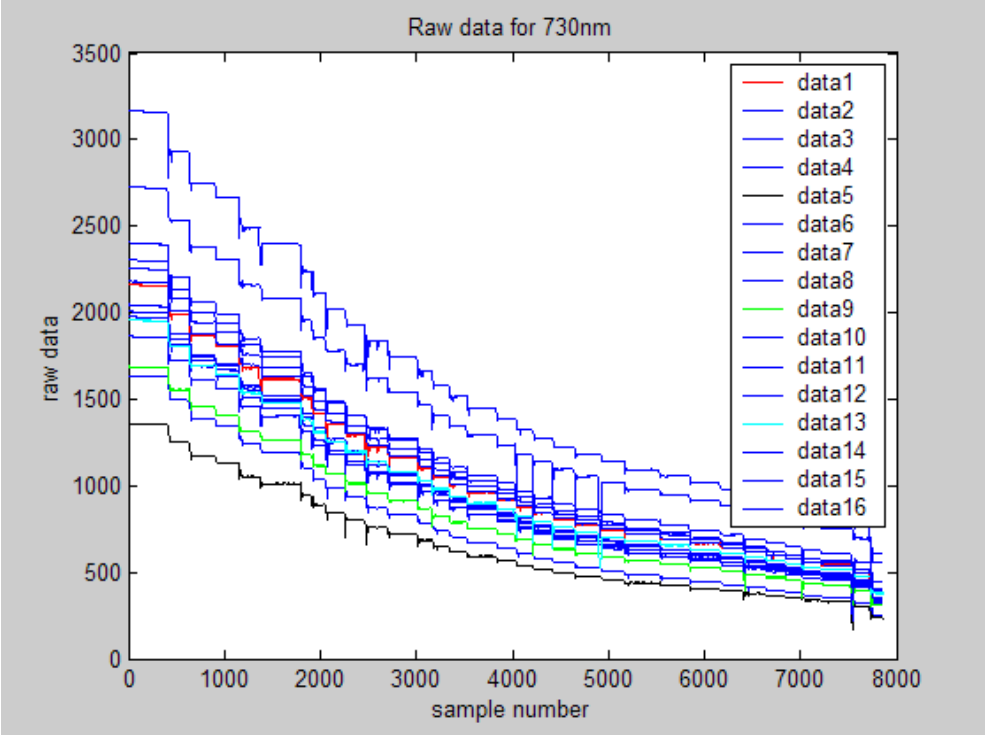

Figure C3 Raw Data (Channel 1- red, 5-black, 9-green, 13-cyan, rest-blue)

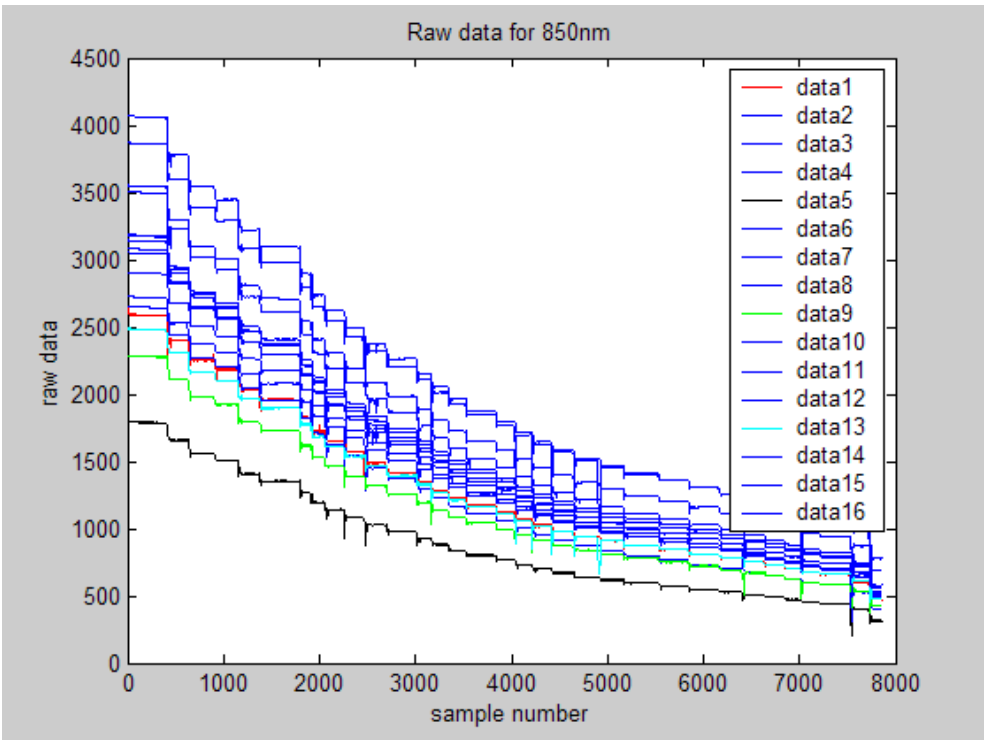

Figure C4 Raw Data (Channel 1- red, 5-black, 9-green, 13-cyan, rest-blue)

** Note:

1. Channels 1, 5, 9 and 13 in the raw data are represented differently since they were showing negative values for the background during measurement.
2. Data were processed by my colleague, Mr. Tony Chang.

REFERENCES

1. Ryer A., Light Measurement Handbook (pp. 1-8). International Light.
2. Website of Hitachi Medical, "http://www.hitachi-medical.co.jp/info/opt-e/kaisetsu-1.html".
3. Website of Photon Migration Lab at Massachusetts General Hospital, MA, "http://www.nmr.mgh.harvard.edu/DOT/home/whatis-nirs/nirs-history.htm".
4. Jobsis, F.F. "Discovery of the Near-Infrared Window into the Body and the Early Development of Near-Infrared Spectroscopy." J of Biomed Optics 4(4): 392-396. 1999.
5. Elwell, C & Hebden, J. Website of Biomedical Optics Research Laboratory at University College of London, "http://www.medphys.ucl.ac.uk/research/borl/research/NIR_topics/nirs.htm".
6. Florian E. W. Schmidt, "Development of a Time-Resolved Optical Tomography System for Neonatal Brain Imaging", Ph.D. Thesis, University College London (1999).
7. Yodh, G.A., Boas D.A. (2003). Functional Imaging with Diffusing Light. Biomedical Photonics Handbook, CRC Press LLC.
8. Hebden, J & Arridge, S. Website of Biomedical Optics Research Laboratory at University College of London, http://www.medphys.ucl.ac.uk/research/borl/research/NIR_topics/imaging_exp.htm".
9. Devaraj, A., "Signal Processing for functional near-infrared neuroimaging", M.S. Thesis, Drexel University (2005).

10. Liu, H., Y. Song, K. L. Worden, X. Jiang, A. Constantinescu & R. P. Mason (2000). "Non Invasive Investigation of blood oxygenation dynamics of tumors by near-infrared spectroscopy." Applied Optics **39**: 5231-5243
11. LEDI Manual, NIM inc., Philadelphia, PA.
12. Cope, M., "The Application of Near Infrared Spectroscopy To Non Invasive Monitoring of Cerebral Oxygenation in the Newborn Infant." Ph.D. Thesis, University of London (April 1991).
13. Kastrup, A., Kruger, G., Neumann, T., & Moseley E.M. (2001). "Assessment of cerebrovascular reactivity with functional magnetic resonance imaging: comparison of CO2 and breath holding." Magnetic Resonance Imaging **19**: 13-20.
14. Fox, S.I. (1999). Cardiac Output, Blood Flow and Blood Pressure. Human Physiology, McGraw-Hill.
15. Safonoval, L.P., Michalos, A., Wolf, U., Choil, J.H., Wolf, M., Mantulin, W., Hueber, D.M., & Gratton, E., (2003). Sleep Research on-line **5(4)** : 123-132.
16. Website of American Heart Association. "http://www.americanheart.org /presenter.jhtml?identifier=4749".
17. Miller, H. G., Maria, R., "Measuring Hot Flashes: Summary of National Institute of Health workshop," Mayo Clin Proc, Vol. 79, 777-781, (2004).
18. Carpenter, J. S., Monahan, P. O., Azzouz, F., "Accuracy of Subjective Hot Flush Reports Compared With Continuous Sternal Skin Conductance Monitoring," American College of Obstetricians and Gynecologists, Vol. 104, No.6 1322-1326, December 2004.

19. Stearns, V., Ullmer, L., Lopez, J. F., Smith, Y., Isaacs, C., Hayes, D.F., "Hot flushes," The Lancet, Vol. 360,1851-18561, December 7,2002.(URL address://http://www.thelancet.com)
20. Website of Power Surge, "http://www.power-surge.com/headlines/hotflash.htm".
21. Ratka, A., Miller, V., Brown, K., Raut, A., Cipher, D., Meczekalski, B., Simpkins, J.W. (2005) Menopausal Vasomotor Symptoms (MVS) Survey for the Assessment of Hot Flashes. (submitted to The Journal of Women's Health).
22. Kronenberg, F., "Menopausal hot flashes: Randomness or rhythmicity," Chaos Vol. 1, No.3, 271-278, (1991).
23. Kronenberg, F., "Hot Flashes: Phenomenology, Quality of Life and Search for Treatment Options," Experimental Gerontology, Vol. 29, Nos. 3/4 ,pp. 319-336, (1994).
24. Kronenberg, F., "Hot Flashes: Epidemology and Phsyiology,". Ann N Y Acad Sci. **180**: 312-16 (1990).
25. Freedman, R. R., "Biochemical, Metabolic and Vascular mechanisms in menopausal hot flashes," Fertility and Sterility, Vol. 70, No.2, 332-336, August 1998.
26. Ratka, A. (2005) Menopausal hot flashes and development of cognitive impairment. In: Estrogen and Hormone Therpay in Postmenopausal Women, Ann N Y Acad Sci, 1052: 11-26. Ed. Meharvan Singh, URL : "www.annalsnyas.org".
27. Li, Rose, "Assessing and Improving Measure of Hot Flashes," Summary of NIH Workshop (Feb 2004). Rose Li and Associates, Inc.

28. Ranga, R., “An In Vitro Hemodynamic Phantom Model For Near Infrared Spectroscopy”, M.S. Thesis, University of Texas at Arlington (May 2005).

BIOGRAPHICAL INFORMATION

Vikrant Sharma was born July 27, 1980 in Jammu and Kashmir, India. He received his Bachelor of Engineering Degree in Biomedical Engineering from Mumbai University, India in August 2001. In fall 2003 he started his graduate studies in Biomedical Engineering from Joint Program of Biomedical Engineering at the University of Texas at Arlington and University of Texas Southwestern Medical Center at Dallas, completing it by summer 2005. His research interests include medical imaging instrumentation and techniques and image processing.